THE CATHOLIC UNIVERSITY OF AMERICA
DEPARTMENT OF ELECTRICAL ENGINEERING

SEMIANNUAL PROGRESS REPORT
on
A STUDY OF SPACE-RATED CONNECTORS USING A ROBOTIC END-EFFECTOR

Research Grant NAG 5-1415

Charles C. Nguyen
Principal Investigator and Associate Professor
and
Sami S. Antrazi
Graduate Research Assistant

submitted to
Mr. Lloyd Purves
Code 714
Goddard Space Flight Center (NASA)
Greenbelt, Maryland

September 1991

REPORT SUMMARY

This semiannual report presents the results obtained from the research grant "A Study of Space-Rated Connectors Using A Robot End-Effector," sponsored by the Goddard Space Flight Center (NASA), for the period between April 1, 1991 and September 1, 1991.

ers designed by Spar interfaces, the "H" of the study and then equipped with a pas- eport then presents a ution using Newton- ons are then derived countered during the er fabrication. After study the character- of three parts. The rfaces under various the maximum allowed and interpret the ob- of recommendations

THE CATHOLIC UNIVERSITY OF AMERICA

School of Engineering and Architecture
Department of Electrical Engineering
Washington, D.C. 20064
202-319-5193

September 11, 1991

NASA Center for Aerospace Information
Baltimore/Washington International
Airport
P.O. Box 8757
Baltimore, Maryland 21240

Dear Sir:

Enclosed please find 2 copies of the semiannual technical report which [illegible] with Grant No.

Contents

1 Introduction

On-orbit maintenance of Orbit Replaceable Units (ORU) will be primarily performed through the use of telerobots [1]. ORU maintenance may also be accomplished by astronauts performing Extra Vehicular Activity (EVA). However, the astronaut is required to possess the ability to adapt to space, an environment which is not precisely controllable and fully understood *a priori* as an earth-based factory environment. Recognizing the danger of space operations, NASA has set the overall goal of the Space Station Freedom (SSF) program to minimize the number of required EVA's and to emphasize on developing robot-friendly hardwares and telerobots which will replace or assist astronauts in performing EVAs.

This report presents results obtained from the study of characteristics and feasibility of a pair of robot fingers designed by Spar Aerospace Limited. The fingers are used to grasp two types of Orbital Replaceable Interfaces:

- The "H" Handle Interface.
- The "Micro" Square Interface.

This report is organized as follows. First it presents the objectives of the study. It then describes problems encountered during the fabrication of the fingers and lists suggestions for improving the finger fabrication. After that, the report presents the results of numerous experiments conducted to study the characteristics and feasibility of the fingers. Finally it is concluded by a list of recommendations resulted from the experimental study of the fingers.

2 Study Objectives

The objectives of the study are listed below:

1. To fabricate the Spar Aerospace fingers according to its specifications given in blue prints.
2. To study the operation and seating characteristics of the fingers and the mating feasibility of the fingers with its dedicated interfaces using a robot end-effector.
3. To verify the given finger specifications including capture angles, maximum allowed translational and rotational misalignments.
4. To measure the forces, torques and passive compliance required for successful mating of the fingers with the dedicated interfaces without damaging the fingers and the interfaces.

3 Finger Fabrication Problems and Suggestions

Two sets of the Spar robot fingers were fabricated by Jackson and Tull (J & T) Chartered Engineer, according to the specifications of the blue prints provided by Spar Aerospace Limited. During the fabrication process, several problems were found by J & T engineers and are listed below. The finger fabrication was however completed by consulting with Spar Aerospace Limited designers through numerous phone conversations.

Manufacturing Problems

1. **Side View:** Missing corner lines on blue prints.
2. **Rear View:** Incorrect dimension was given and line showing angled surface was misplaced on the blue prints.
3. **Top View:** Incorrect dimension was given and corner detail was not given.

The above problems are indicated in the attached blue prints with corrections marked in red.

Design Problems

1. The selected springs are approximately 0.2 inches too long.
2. Bottom view of mid-section is missing, which leaves out important details.
3. The section that "slips" inside the "H" handle is too tight for telerobotic assembly. As a result, each of the three sides of the "H" handle was taken down about 2/1000 inches in order to manually mate the fingers with the "H" handle.

4 Test Setup and Procedures

According to Spar Aerospace Limited specifications, the grasping of the interfaces is to be performed under a relative speed of 1 inch per second with the two fingers closing simultaneously. In other words, each finger should close with a speed of 0.5 inch per second. The gripper which is currently mounted to the robot manipulator is so configured that only one finger can move. In order to achieve a relative grasping speed of 1 inch/sec with 2 fingers closing simultaneously, the first finger is controlled to close with a speed of 0.5 inch per second and the payload platform (consequently the second finger) is controlled to move with a speed of 0.5 inch per second in the direction opposite to the movement of the first finger. Before each run of the experiment, the perfect alignment between the fingers and the interface is established as follows. First the interface is mounted rigidly to the floor (Figure 4) using a vice and the payload platform pose is adjusted until no applied forces/torques are read by the force sensor. The payload pose resulting in no applied forces/torques is then recorded in the computer as the perfect alignment pose. From this pose, through proper matrix transformations, the payload platform pose can be controlled to produce arbitrary translational and rotational misalignments or the combination of both. The misalignments are produced with respect to a coordinate frame which is located at the center of the two fingers and has the same orientation as that of the UCP.

5 Test Results

In the experiments presented below, the time histories of forces/torques applied to the fingers are measured and expressed with respect to the UCP coordinate frame. The forces/torques are measured in two stages, the mating stage and demating stage. The LVDTs deflections are measured and recorded *on line* during the experiments, and are used to compute *off-line* the applied forces/torques using the force sensor forward kinematics and force computation

equations developed in Section 5 and Section 6. Numerous graphs were obtained during the experiments but only those which are representative and substantial are presented here. The graphs presented as follows can be divided into two groups. The first group consists of graphs showing forces along certain axis versus time for a particular misalignment while the second group consists of graphs showing maximum mating and demating forces along certain axis versus the misalignments either in inches or degrees.

5.1 'H' Handle Interface

Two types of misalignments considered in the testing of the fingers with the 'H' handle interface are pure rotational misalignment and pure translational misalignment about (along) a selected axis. Figure 5 shows the coordinate frame assigned to the 'H' handle interface to which the misalignments are produced.

The contents of the graphs are briefly discussed as follows:

1. **Rotational Misalignments about the Z-Axis:**
   - Figures 6-9 show the time histories of forces (in lb.) applied along the x-axis for 0, 1, 2, 3 degrees of misalignment about the z-axis, respectively with 0 degree implies perfect alignment. All graphs have similar force responses in the sense that applied forces assume zero value before the mating, are disturbed during the mating (first force transition), settle down to a constant value after the fingers are completely mated with the interface (second force transition), are disturbed again during the demating (third force transition) and finally settle down to zero value after the demating (fourth force transition)
   - Figures 10-13 present the time histories of forces (in lb.) applied along the y-axis for 0, 1, 2, 3 degrees or misalignment about the z-axis, respectively.
   - Figures 14-17 present the time histories of forces (in lb.) applied along the z-axis for 0, 1, 2, 3 degrees or misalignment about the z-axis, respectively.
2. **Translational Misalignments along the Y-Axis:**
   - The time histories of forces (in lb.) applied along the x-axis are reported in Figures 18-21 for -0.1, -0.2, -0.3, -0.4 inch of translational misalignment along the y-axis, respectively. The force transitions for this case are similar to those of the case of rotational misalignment discussed above.
   - Figures 22-25 present the time histories of forces (in lb.) applied along the y-axis for -0.1, -0.2, -0.3, -0.4 inch of translational misalignments along the y-axis inch, respectively.
   - Figures 26-29 present the time histories of forces (in lb.) applied along the z-axis for -0.1, -0.2, -0.3, -0.4 inch of translational misalignments along the y-axis, respectively.
3. **Translational Misalignments along the Z-Axis:**
   - The time histories of forces (in lb.) applied along the x-axis are reported in Figures 30-34 for 0.0, 0.1, 0.15, 0.2, 0.3 inch of translational misalignments along the y-axis, respectively.

- Figures 35-39 present the time histories of forces (in lb.) applied along the y-axis for 0.0, 0.1, 0.15, 0.2, 0.3 inch of translational misalignments along the z-axis, respectively.
- Figures 40-44 present the time histories of forces (in lb.) applied along the z-axis for 0.0, 0.1, 0.15, 0.2, 0.3 inch of translational misalignments along the y-axis, respectively.

4. **Maximum Forces for Rotational Misalignment about the X-Axis:** Figures 45-47 show the relationship between the maximum mating forces along the x-, y-, and z-axes, respectively and the misalignment degrees about the x-axis while Figures 48-50 the maximum demating forces. Except for Figure 46, the maximum mating and demating forces generally increase as the degrees of misalignment increase, as expected. The behavior of Figure 46 can be explained by the fact that the maximum mating and demating force is a function of not only the degree of misalignment but also the mating surface formed by the fingers and the 'H' handle interface.

5. **Maximum Forces for Rotational Misalignment about the Z-Axis:** Figures 51-53 show the relationship between the maximum mating forces along the x-, y-, and z-axes, respectively and the misalignment degrees about the z-axis while Figures 54-56 the maximum demating forces.

6. **Maximum Forces for Translational Misalignment along the Y-Axis:** Figures 57-59 show the relationship between the maximum mating forces along the x-, y-, and z-axes, respectively and the translational misalignment along the y-axis, while Figures 60-62 the maximum demating forces.

7. **Maximum Forces for Translational Misalignment along the Z-Axis:** Figures 63-65 present the relationship between the maximum mating forces along the x-, y-, and z-axes, respectively and the translational misalignment along the z-axis, while Figures 66-68 the maximum demating forces.

5.2 'Micro' Square Interface

We observe that in general, the 'micro' square interface is easier for the fingers to grasp than the 'H' handle interface. Therefore we think that the performed tests on the 'H' handle interface already provided us with sufficient information about the finger characteristics since the force behavior should be similar for both type of interfaces. However to see if this is the case, we perform some tests on the 'micro' square interface and consider only the translation misalignment in the y-axis. Figure 5 shows the coordinate frame assigned to the 'micro' square interface to which the translational misalignments are produced. The test results are summarized below:

- The time histories of forces (in lb.) applied along the x-axis are reported in Figures 69-70 for 0.1, 0.2 inch of translational misalignment along the y-axis, respectively. The force transitions for this case are similar to those of the case of translational misalignment for the 'H' handle interface, discussed above. The maximum mating force is about 6.7 lb while the maximum demating force is about 9.5 lb for 0.1 inch misalignment. For 0.2 inch misalignment, the maximum mating and demating forces assume a value of 9 lb and 10.5 lb, respectively.

- Figures 71-72 present the time histories of forces (in lb.) applied along the y-axis for 0.1, 0.2 inch of translational misalignment along the y-axis inch, respectively. For 0.1 inch misalignment, the maximum mating force is about 1.8 lb and the maximum demating force is about 4.4 lb. For 0.2 inch misalignment, the maximum mating and demating forces assume a value of 5 lb and 7.8 lb, respectively.

- Figures 73-74 present the time histories of forces (in lb.) applied along the z-axis for 0.1, 0.2 inch of translational misalignment along the y-axis inch, respectively. For 0.1 inch misalignment, the maximum mating force is about 10.5 lb and the maximum demating force is about 11 lb. For 0.2 inch misalignment, the maximum mating and demating forces assume a value of 8.5 lb and 9.2 lb, respectively.

5.3 Capture Ranges

The capture ranges for both interfaces were determined by increasing the misalignment (translational and rotational) and closing the fingers at very slow speed until it was impossible for the fingers to mate with the interface. The results for the capture ranges are given below:

'H' Handle Interface
x-axis rotation: $\pm 5.00^o$
y-axis rotation: $\pm 4.20^o$
z-axis rotation: $\pm 8.75^o$
y-displacement: ± 0.43 inch
z-displacement: ± 0.55 inch

'Micro' Square Interface
x-axis rotation: $\pm 4.3^o$
y-axis rotation: $\pm 5.6^o$
z-axis rotation: $\pm 12.5^o$
y-displacement: ± 0.35 inch
z-displacement: ± 0.49 inch

6 Conclusions and Recommendations

This report has considered the fabrication and testing of a pair of robot fingers designed by Spar Aerospace Limited to grasp two types of Orbital Replaceable Unit (ORU) interfaces, the "H" Handle type and the "Micro" Square type. First it presented the objectives of the study and then described the testbed to be used in the study. The report then presented a closed-form solution for the force inverse kinematics and a numerical solution using Newton-Raphson Method for the force forward kinematics. Mathematical expressions were derived to compute forces/torques applied to the finger. We then listed the manufacturing and design problems encountered during the fabrication of the fingers and gave suggestions for the improvement of the finger fabrication. After that, the report presented the results of numerous experiments conducted to study the characteristics and feasibility of the fingers. Applied forces during the

mating and demating of the fingers with the two interfaces were measured under various rotational and translational misalignments, and then graphically presented. Plots of applied forces versus misalignments showed that the forces were generally proportional to the misalignments except for some few cases in which the misalignment caused the fingers to hit different mating surfaces resulting in unexplainable force transitions. In addition, capture ranges for the two interfaces were determined empirically.

Based on the results of our study, we recommend the following:

- Correct the manufacturing and design problems pointed out in Section 3.
- Manufacturer's performance specifications need clarifications. For instance, Spar Aerospace Limited has given the capture angles of $\pm 10^o$. However, it is not clear if the capture angles has been empirically determined. Passive compliance or the use of a force controller providing active compliance during the mating and demating of the fingers with the interfaces should also be specified.
- Combinational misalignments (translational and rotational) should be considered.
- Materials (stainless steel or aluminum) used for the finger fabrication should be specified. A combination of materials such as stainless steel for finger fabrication and aluminum for interface fabrication should be considered.
- The *spring mechanism* used to reset the fingers after the demating must be redesigned. Currently the springs must be manually reset after each mating with the 'H' handle interface.

In conclusion, in order to achieve an operational set of fingers and interfaces, an iterative and cooperative development process should be adopted. Spar Aerospace Limited should modify and update their finger designs and independent laboratory should test and re-evaluate the interfaces and the fingers based on the mating performance. This process should be repeated until a satisfactory level of performance is achieved.

References

[1] Catalano, D.A., "WP-04 Orbit Replaceable Unit Robotics Maintenance Final Test Report," *Analex Corp.*, GSFC, November 1990

[2] Stewart, D., "A Platform with Six Degrees of Freedom," *Proc. Institute of Mechanical Engineering*, Vol. 180, Part 1, No. 5, pp. 371-386, 1965-1966.

[3] Dieudonne, J.E. et al, "An Actuator Extension Transformation for a Motion Simulator and an Inverse Transformation Applying Newton-Raphson's Method," *NASA Technical Report D-7067*, 1972.

[4] Hoffman, R., and McKinnon, M.C., "Vibration Modes of an Aircraft Simulator Motion System," *Proc. The Fifth World Congress for the Theory of Machines and Mechanisms, an ASME Publication*, pp. 603-606, 1979.

[5] McCallion, H., and Truong, P.D., "The Analysis of a Six-Degree-of-Freedom Work Station for Mechanised Assembly," *Proc. The Fifth World Congress for the Theory of Machines and Mechanisms, an ASME Publication*, pp. 611-616, 1979.

[6] Hunt, K. H., *Kinematic Geometry of Mechanisms*, Oxford University, London 1978.

[7] Sugimoto, K. and Duffy, J., "Application of Linear Algebra to Screw Systems," *Mech. Mach. Theory*, Vol. 17, No. 1, pp. 73-83, 1982.

[8] Hunt, K. H., "Structural Kinematics of in-parallel-actuated Robot Arms," *Trans. ASME, J. Mech., Transmis., Automa. in Des.*, Vol. 105, pp. 705-712, 1983.

[9] Premack, Timothy et al, "Design and Implementation of a Compliant Robot with Force Feedback and Strategy Planning Software," *NASA Technical Memorandum 86111*, 1984.

[10] Nguyen, C.C., Pooran, F.J., and Premack, T., "Control of Robot Manipulator Compliance," in *Recent Trends in Robotics: Modeling, Control and Education*, edited by M. Jamshidi, J.Y.S. Luh, and M. Shahinpoor, North Holland, New York, pp. 237-242, 1986.

[11] Yang, D. C. and Lee, T. W., "Feasibility Study of a Platform Type of Robotic Manipulators from a Kinematic Viewpoint," *Trans. ASME Journal of Mechanisms, Transmissions, and Automation in Design*, Vol. 106. pp. 191-198, June 1984.

[12] Mohammed, M. G. and Duffy, J., "A Direct Determination of the Instantaneous Kinematics of Fully Parallel Robotic Manipulators," *ASME Journal of Mechanisms, Transmissions, and Automation in Design*, Vol. 107 pp. 226-229, 1985.

[13] Fichter, E.F., "A Stewart Platform-Based Manipulator: General Theory and Practical Construction," *Int. Journal of Robotics Research*, pp. 157-182, Summer 1986

[14] Sugimoto, K., "Kinematic and Dynamic Analysis of Parallel Manipulators by Means of Motor Algebra," *ASME Journal of Mechanisms, Transmissions, and Automation in Design*, pp. 1-5, Dec. 1986.

[15] Lee, K. M., Chao, A., and Shah, D. K., "A Three Degrees of Freedom In-parallel Actuated Manipulator," *Proc. IASTED Int. Conf.*, pp. 134-138, 1986.

[16] Rees-Jones, J., "Cross Coordinate Control of Robotic Manipulators," in *Proceedings of the International Workshop on Nuclear Robotic Technologies and Applications, Present and Future*, University of Lancaster, UK, June 29-July 1, 1987.

[17] Behi, F., "Kinematic Analysis for a Six-Degree-of-Freedom 3-PRPS Parallel Mechanism," *IEEE Journal of Robotics and Automation*, Vol. 5, No. 5, pp. 561-565, October 1988.

[18] Sharon, A., Hogan, N., Hardt, D., "High-Bandwidth Force Regulation and Inertia Reduction Using a Macro/Micro Manipulator System," *Proc. IEEE International Conference on Robotics and Automation*, pp. 261-266, Philadelphia, PA, April 1988.

[19] Sugimoto, K., "Computational Scheme for Dynamic Analysis of Parallel Manipulators," in *Trends and Developments in Mechanisms, Machines, and Robotics-1988, ASME Proceedings of the 20th Biennial Mechanisms Conference*, 1988.

[20] Kerr, D. R., "Analysis, Properties, and Design of a Stewart-Platform Transducer,"in *Trends and Developments in Mechanisms, Machines, and Robotics-1988, ASME Proceedings of the 20th Biennial Mechanisms Conference*, 1988.

[21] Nguyen, C.C., Pooran, F.J., "Adaptive Force/Position Control of Robot Manipulators with Closed-Kinematic Chain Mechanism," in *Robotics and Manufacturing: Recent Trends in Research, Education, and Application*, edited by M. Jamshidi et al, ASME Press, New York, pp. 177-186, 1988.

[22] Griffis, M., Duffy, J., "A Forward Displacement Analysis of a Class of Stewart Platforms," *Journal of Robotic Systems*, Vol. 6, pp. 703-720, 1989.

[23] Nguyen, C.C., and Pooran, F.J., "Kinematic Analysis and Workspace Determination of A 6 DOF CKCM Robot End-Effector," *Journal of Mechanical Working Technology*, Vol. 20, pp. 283-294, 1989.

[24] Nguyen, C.C., and Pooran, F.J., "Dynamical Analysis of 6 DOF CKCM Robot End-Effector for Dual-Arm Telerobot Systems," *Journal of Robotics and Autonomous Systems*, Vol. 5, pp. 377-394, 1989.

[25] Nanua, P., Waldron, K.J., Murthy, V., "Direct Kinematic Solution of a Stewart Platform," *IEEE Trans. Robotics and Automation*, Vol. 6, No. 4, pp. 438-444, 1990.

[26] Nguyen, C.C., and Pooran, F.J., "Learning-Based Control of a Closed-Kinematic Chain Robot End-Effector Performing Repetitive Tasks," *International Journal of Microcomputer Applications*, Vol. 9, No. 1, pp. 9-15, 1990.

[27] Nguyen, C.C., Antrazi, S., Zhou, Z-L, "Trajectory Planning and Kinematic Control of a Stewart Platform-Based Manipulator," *Proc. 5th International Conference on CAD/CAM Robotics and Factories of the Future*, Norfolk, Virginia, December 1990.

[28] Nguyen, C.C., Antrazi, S., Zhou, Z-L, Campbell, Jr., C.E., "Experimental Study of Motion Control and Trajectory Planning for a Stewart Platform Robot Manipulator," *Proc. IEEE International Conference on Robotics and Automation*, Sacramento, California, April 1991.

[29] Goodman, L.E. and Warner, W.H., "Statics," *Wadsworth Publishing Company, Inc.,*, Belmont, California, 1963.

[30] Press, W.H., et al, "Numerical Recipes in C: The Art of Scientific Computing," *Cambridge University Press*, 1988.

[31] Fu, K.S. et.al., *Robotics: Control, Sensing, Vision, and Intelligence* , McGraw-Hill, New York, 1987.

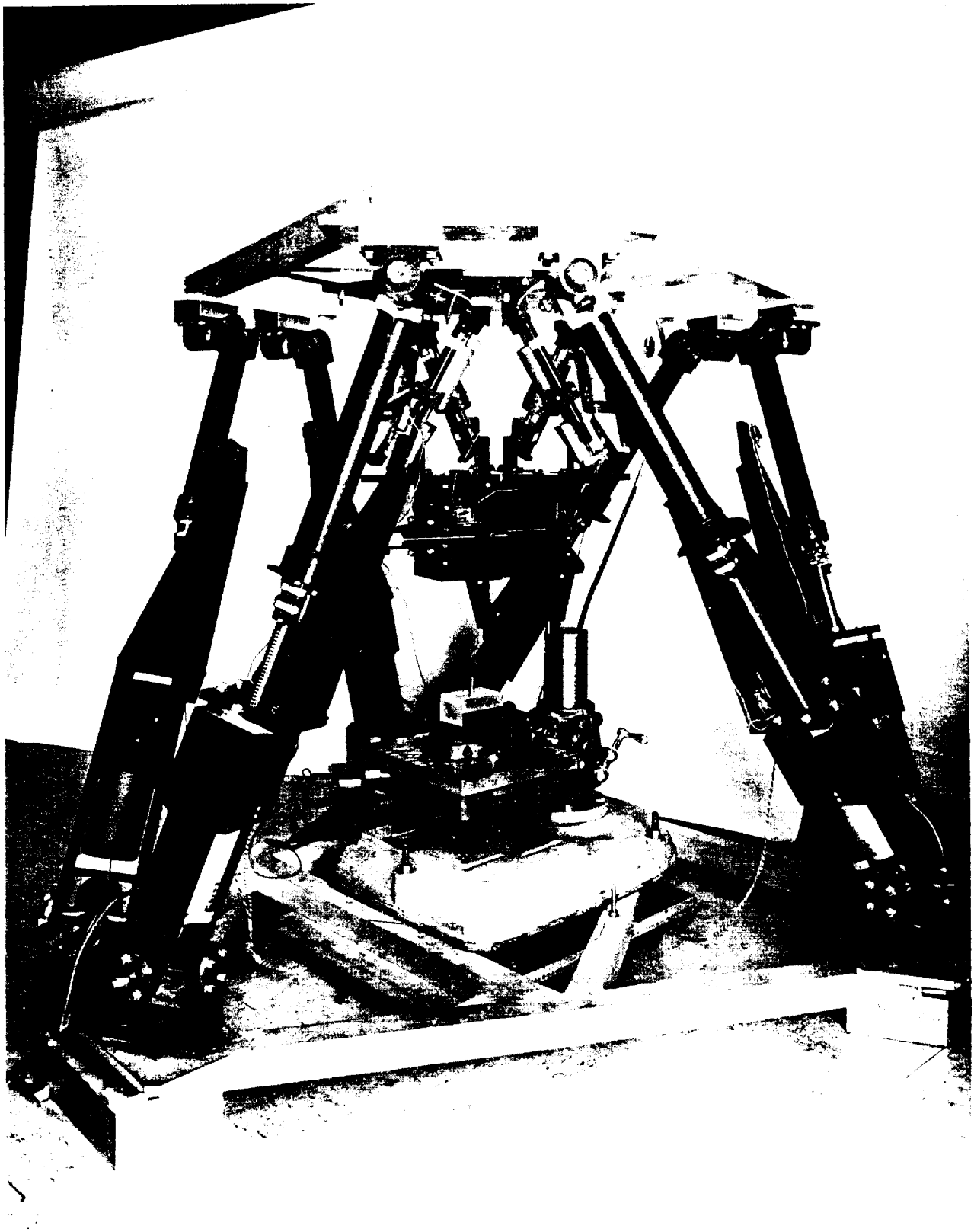

Figure 1: The robot manipulator

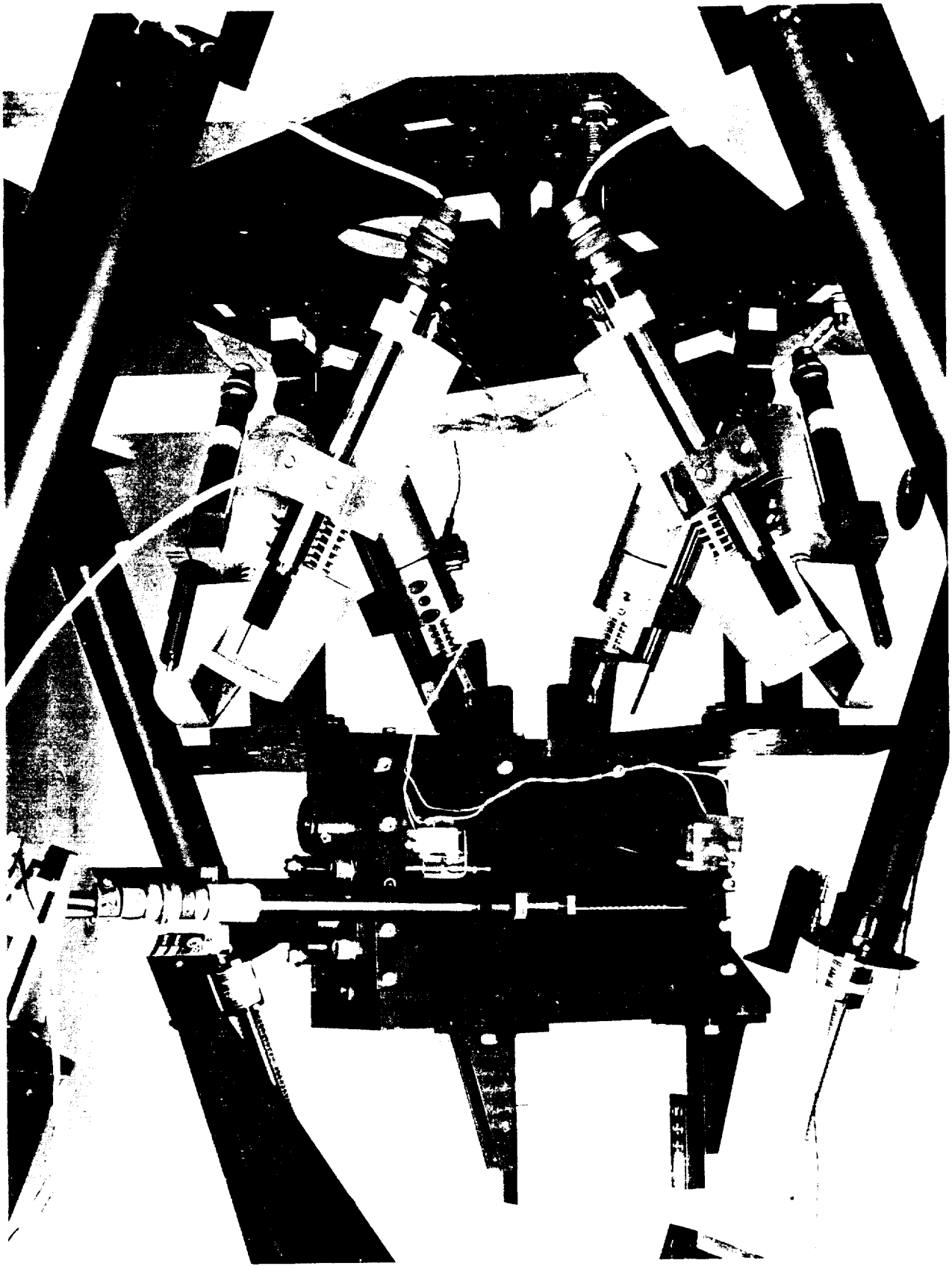

Figure 2: The force/torque sensor

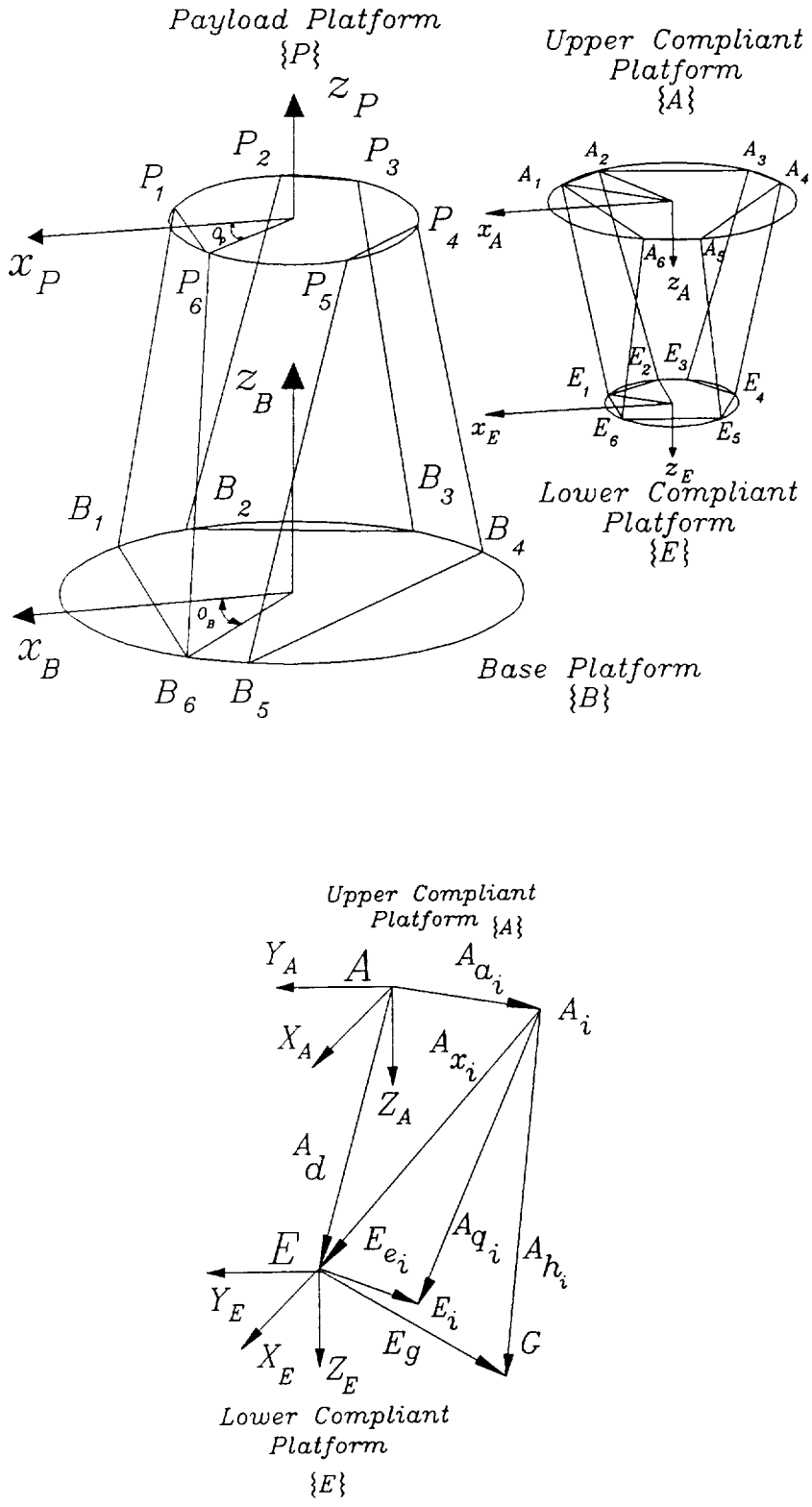

Figure 3: Coordinate frame assignment and vector diagram

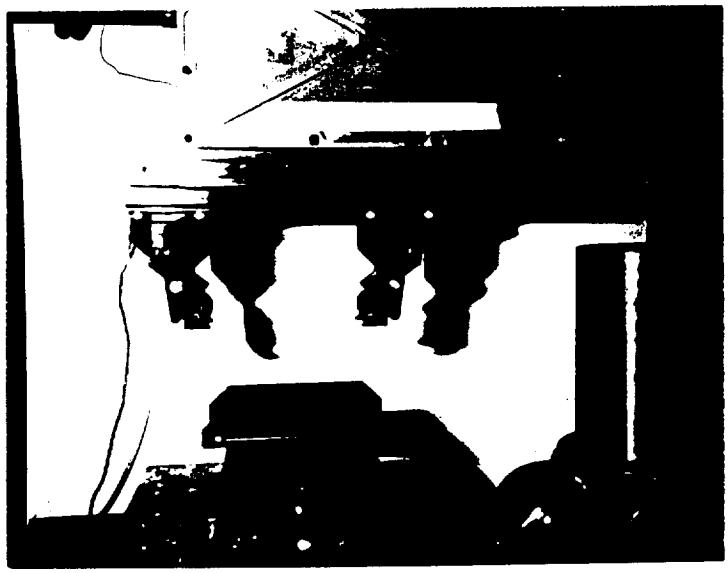

Figure 4: The test setup

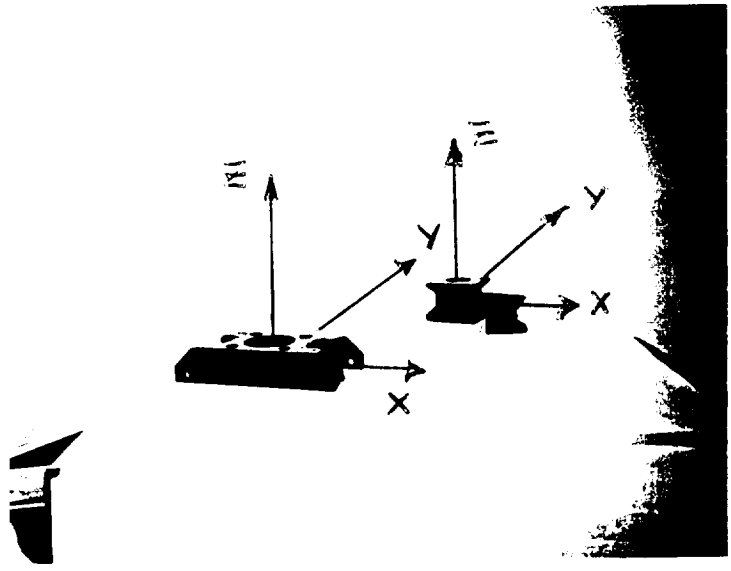

Figure 5: Misalignment coordinate frames for 'H' handle and 'Micro' square interfaces

H-Interface
Force Time History
Rotational Misalignment

Force (in lb) along the X-axis
for 0.0 degrees misalignment about the Z-axis

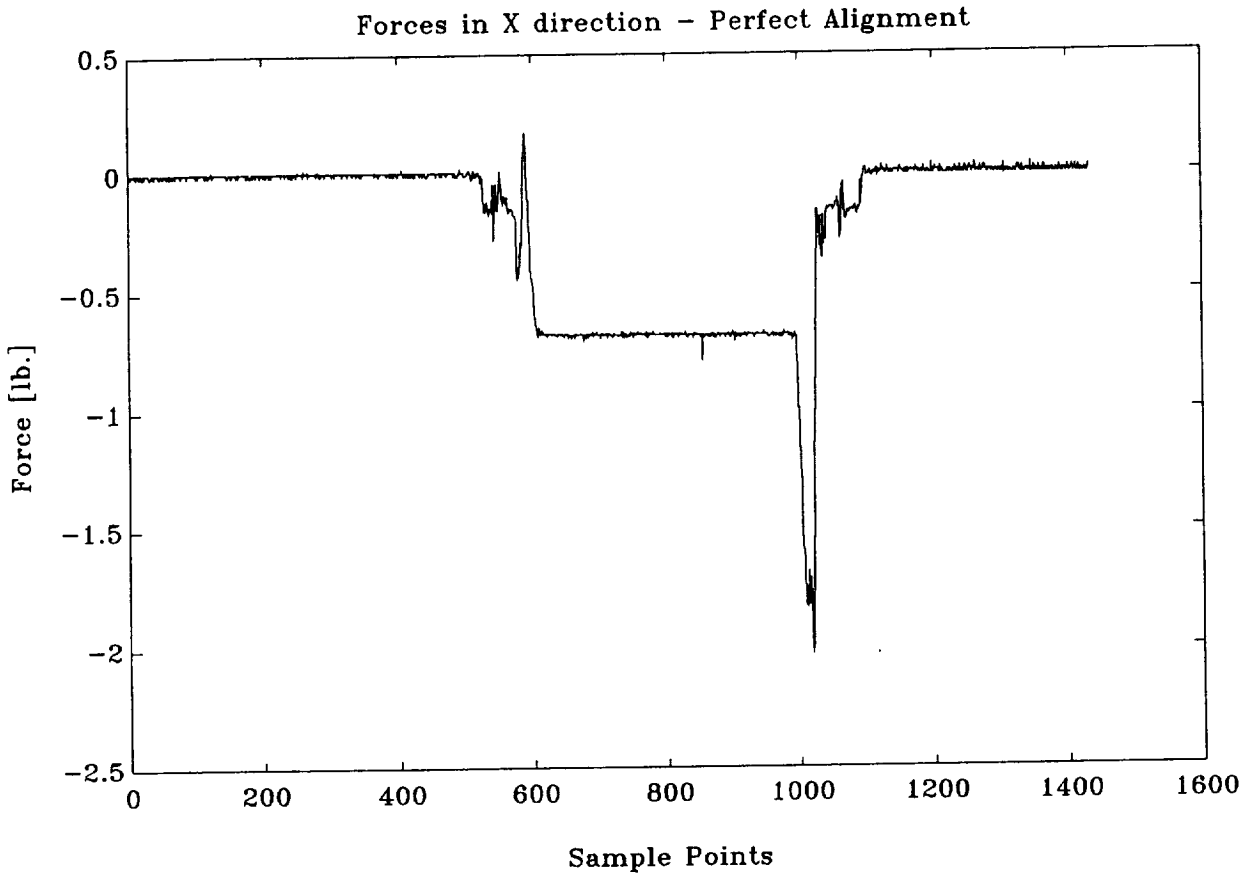

Figure 6

H-Interface
Force Time History
Rotational Misalignment

Force (in lb) along the X-axis
for 1.0 degrees misalignment about the Z-axis

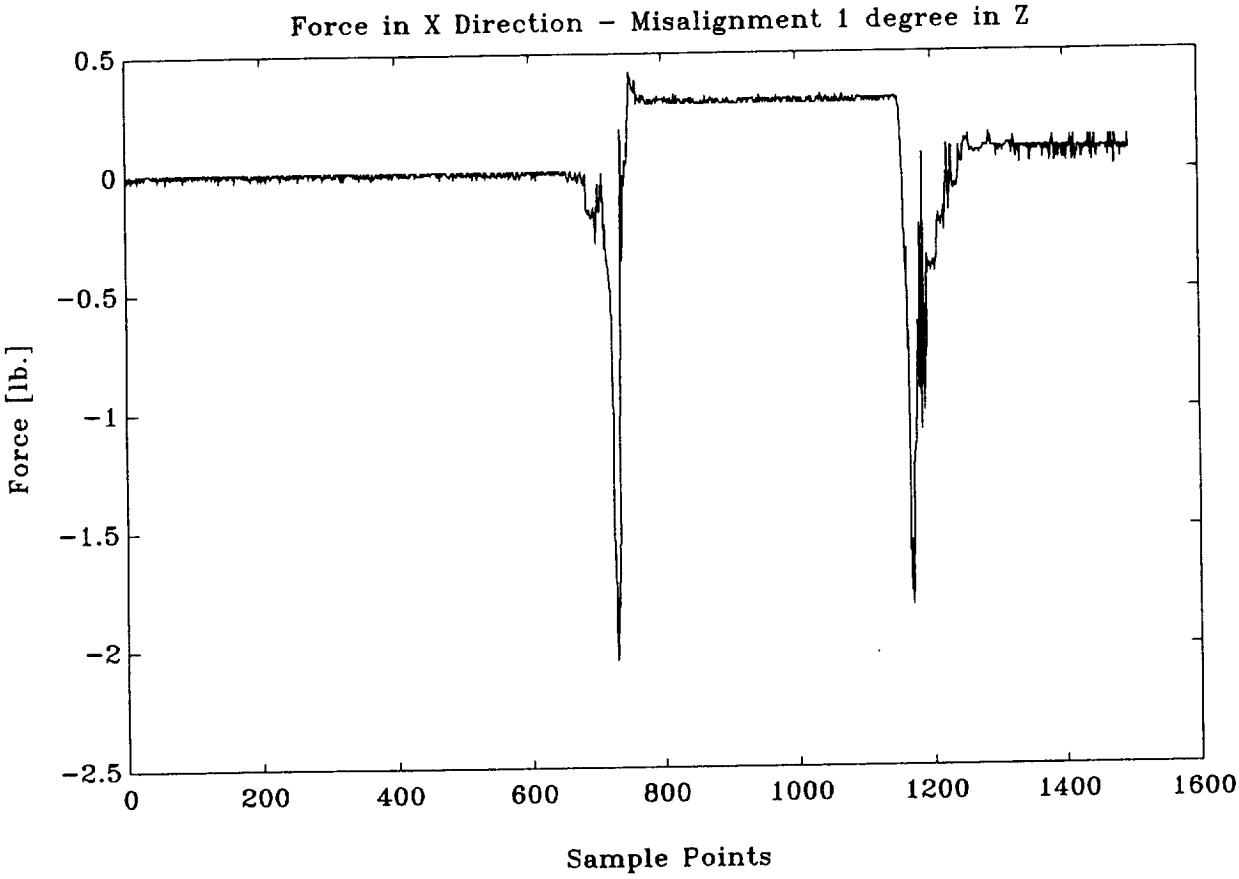

Figure 7

H-Interface
Force Time History
Rotational Misalignment

Force (in lb) along the X-axis
for 2.0 degrees misalignment about the Z-axis

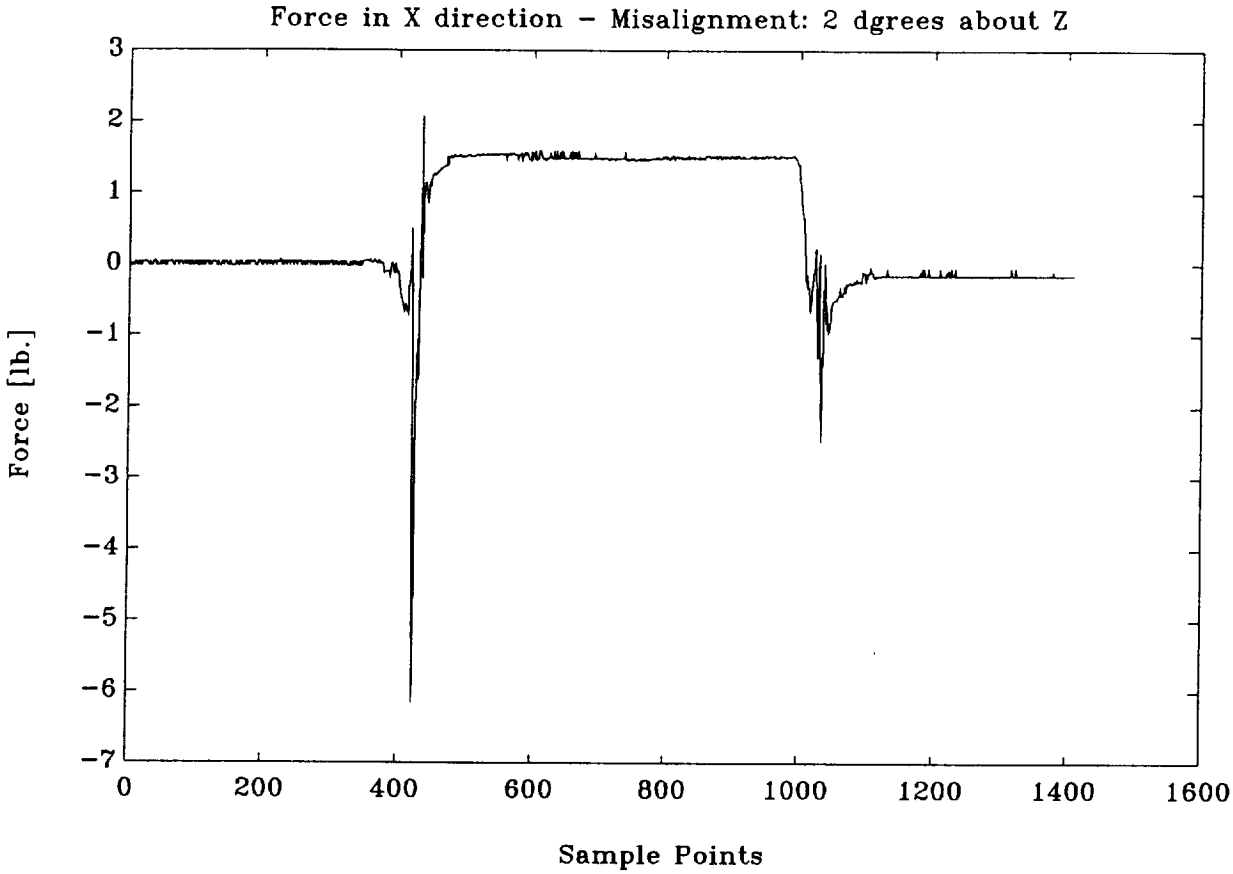

Figure 8

H-Interface
Force Time History
Rotational Misalignment

Force (in lb) along the X-axis
for 3.0 degrees misalignment about the Z-axis

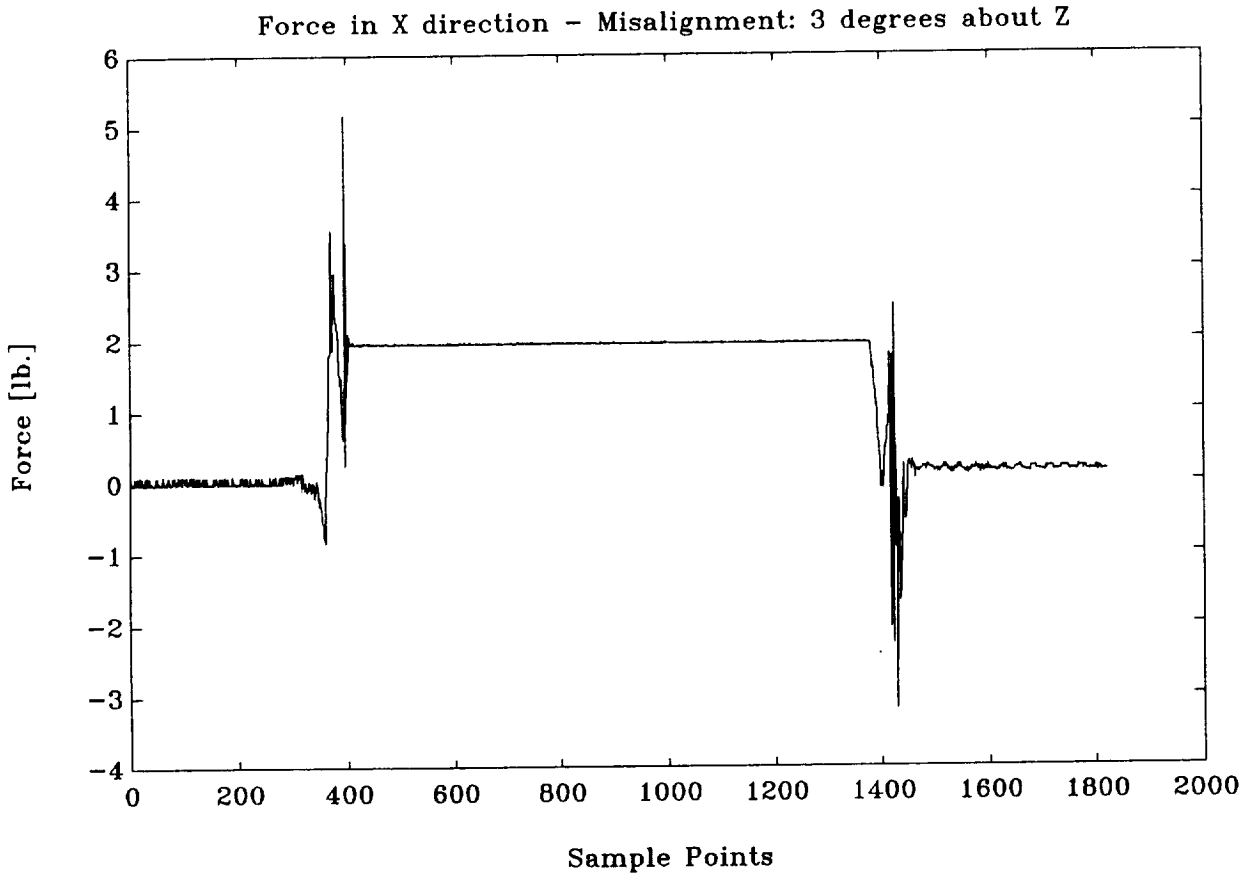

Figure 9

H-Interface
Force Time History
Rotational Misalignment

Force (in lb) along the Y-axis
for 0.0 degrees misalignment about the Z-axis

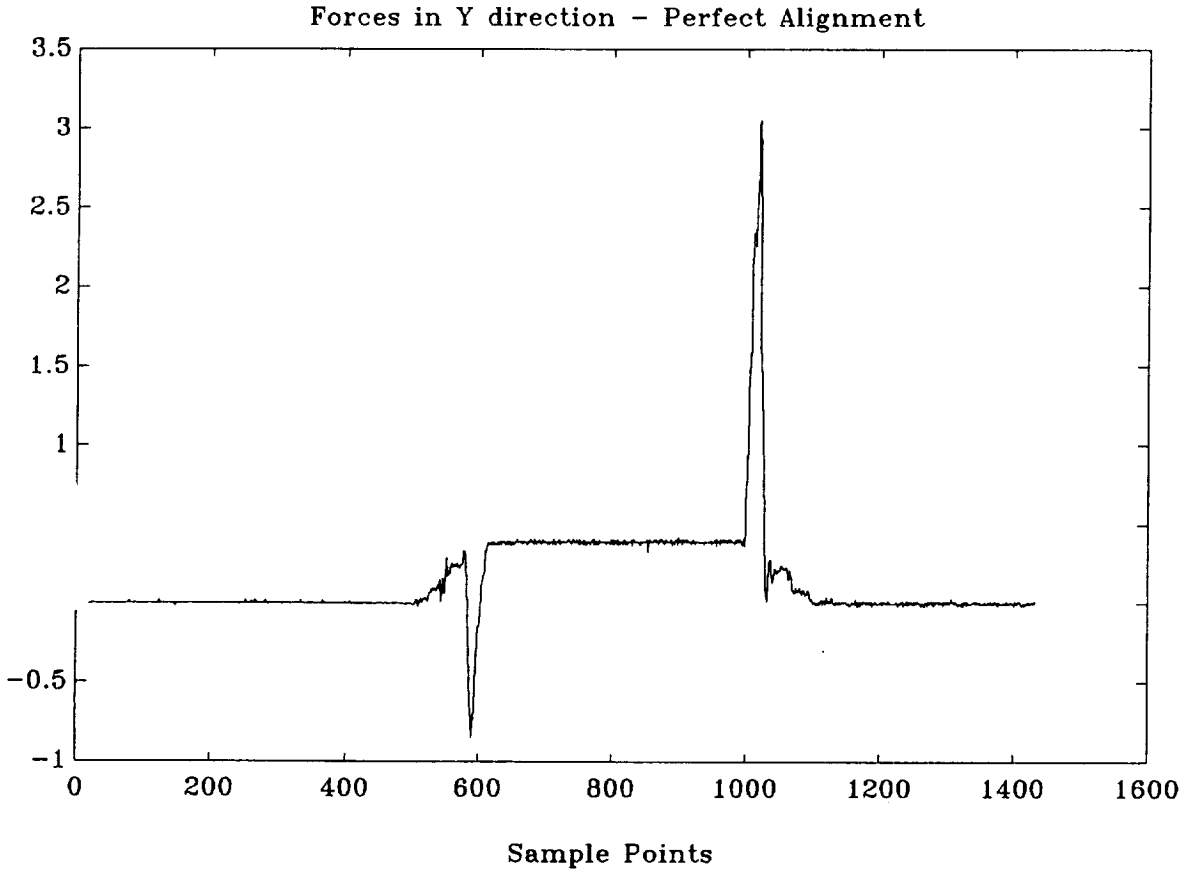

Figure 10

H-Interface
Force Time History
Rotational Misalignment

Force (in lb) along the Y-axis
for 1.0 degrees misalignment about the Z-axis

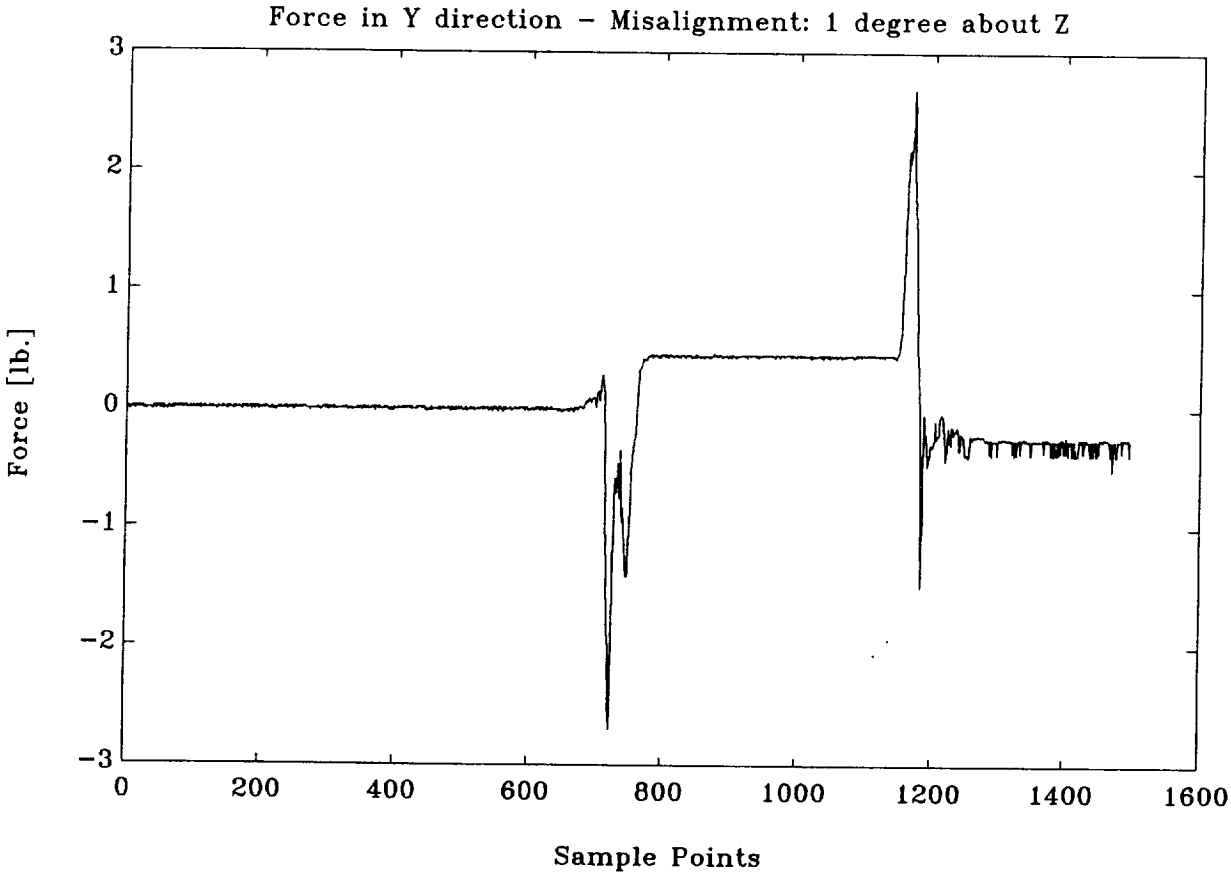

Figure 11

H-Interface
Force Time History
Rotational Misalignment

Force (in lb) along the Y-axis
for 2.0 degrees misalignment about the Z-axis

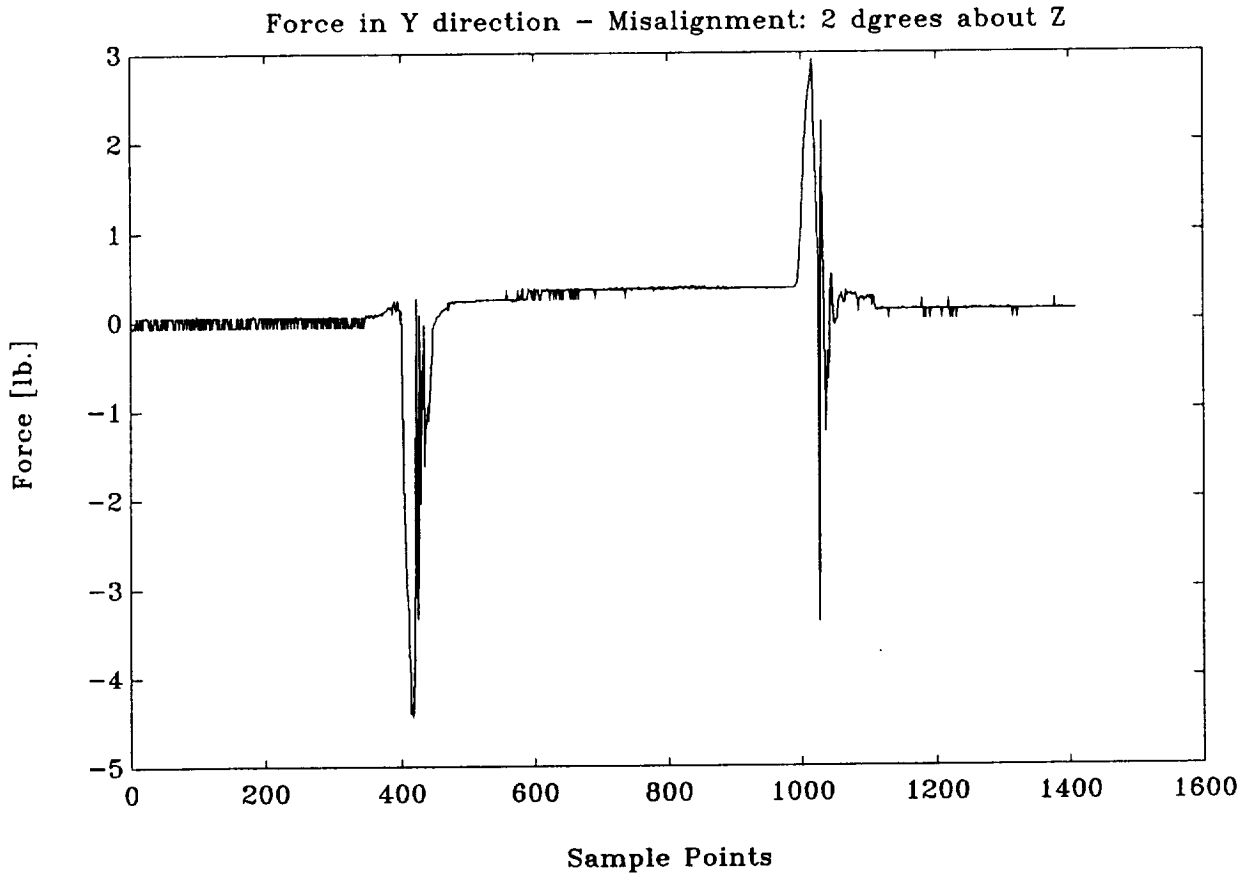

Figure 12

H-Interface
Force Time History
Rotational Misalignment

Force (in lb) along the Y-axis
for 3.0 degrees misalignment about the Z-axis

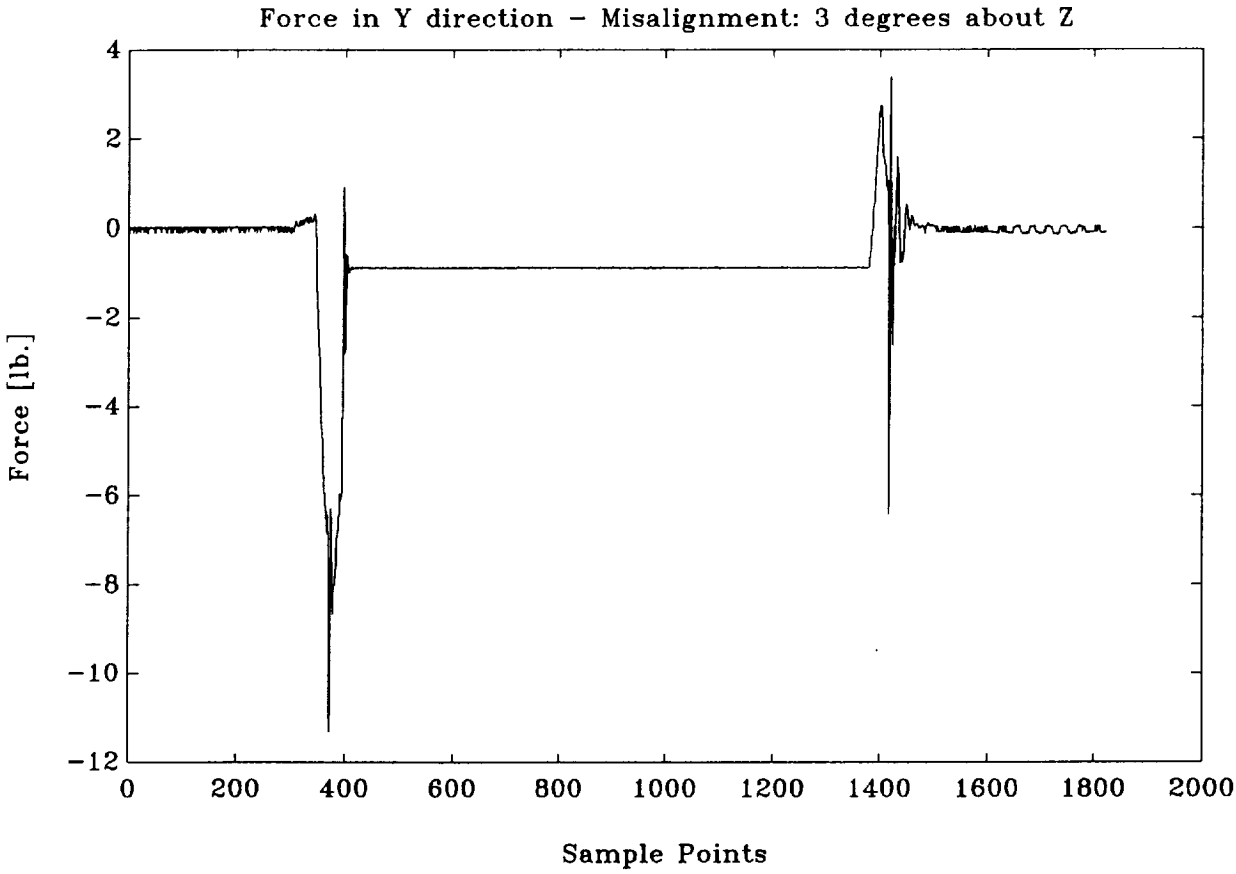

Figure 13

H-Interface
Force Time History
Rotational Misalignment

Force (in lb) along the Z-axis
for 0.0 degrees misalignment about the Z-axis

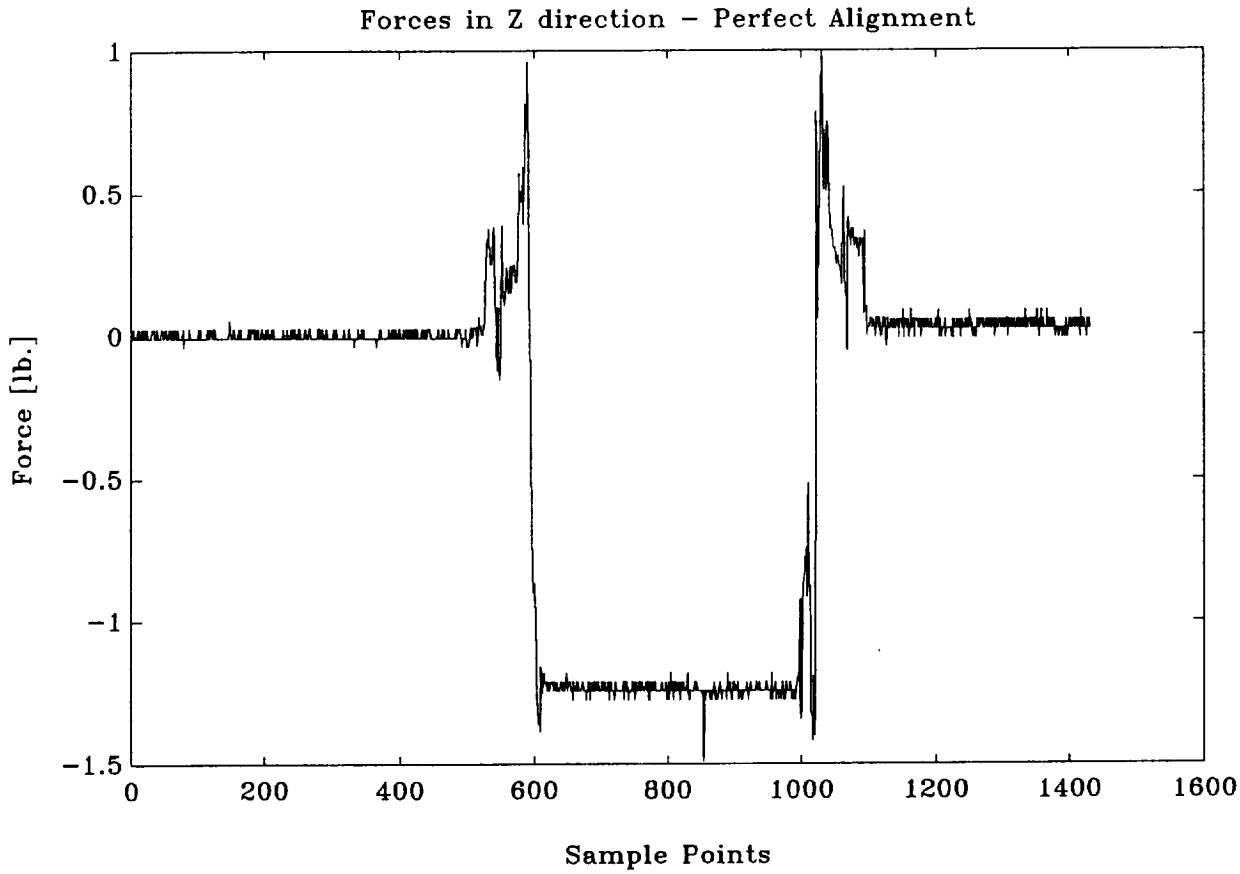

Figure 14

H-Interface
Force Time History
Rotational Misalignment

Force (in lb) along the Z-axis
for 1.0 degrees misalignment about the Z-axis

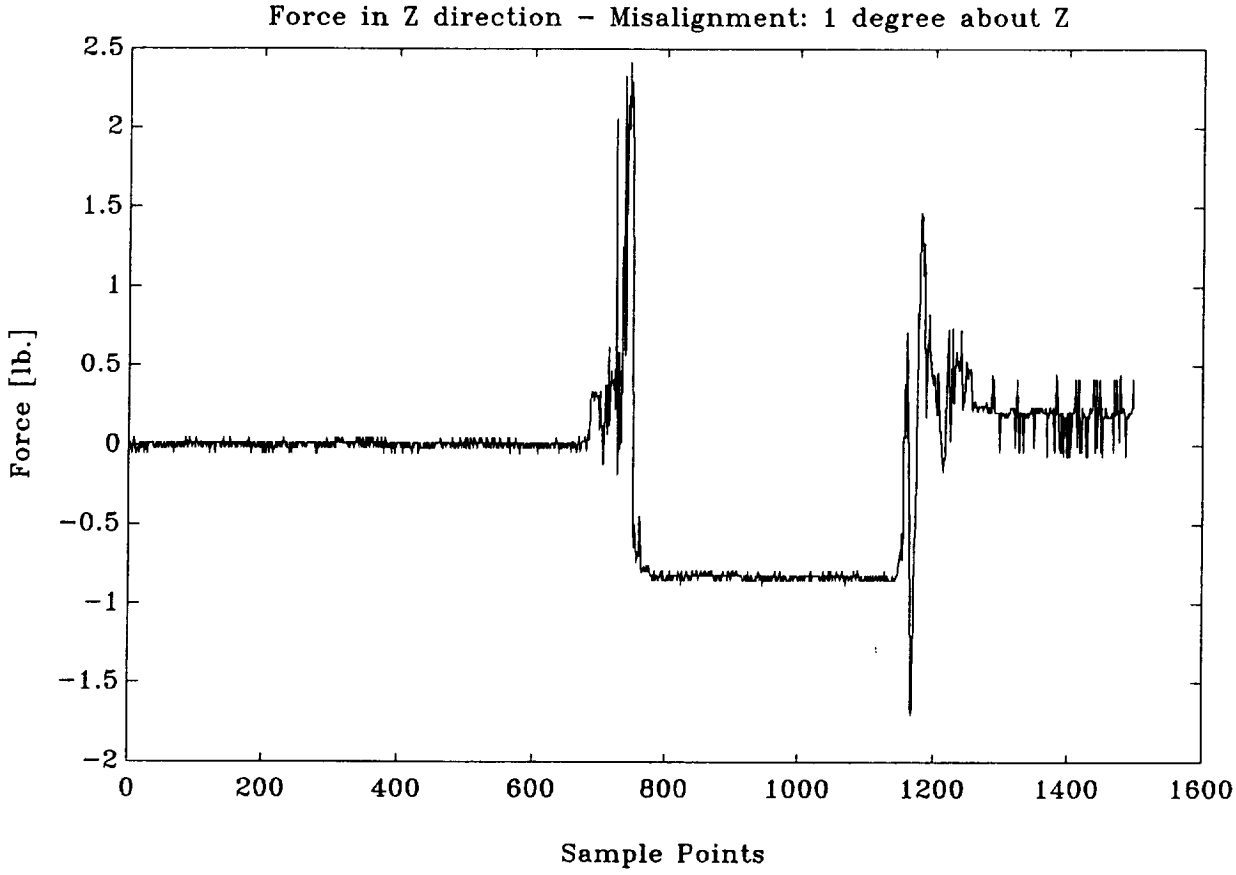

Figure 15

H-Interface
Force Time History
Rotational Misalignment

Force (in lb) along the Z-axis
for 2.0 degrees misalignment about the Z-axis

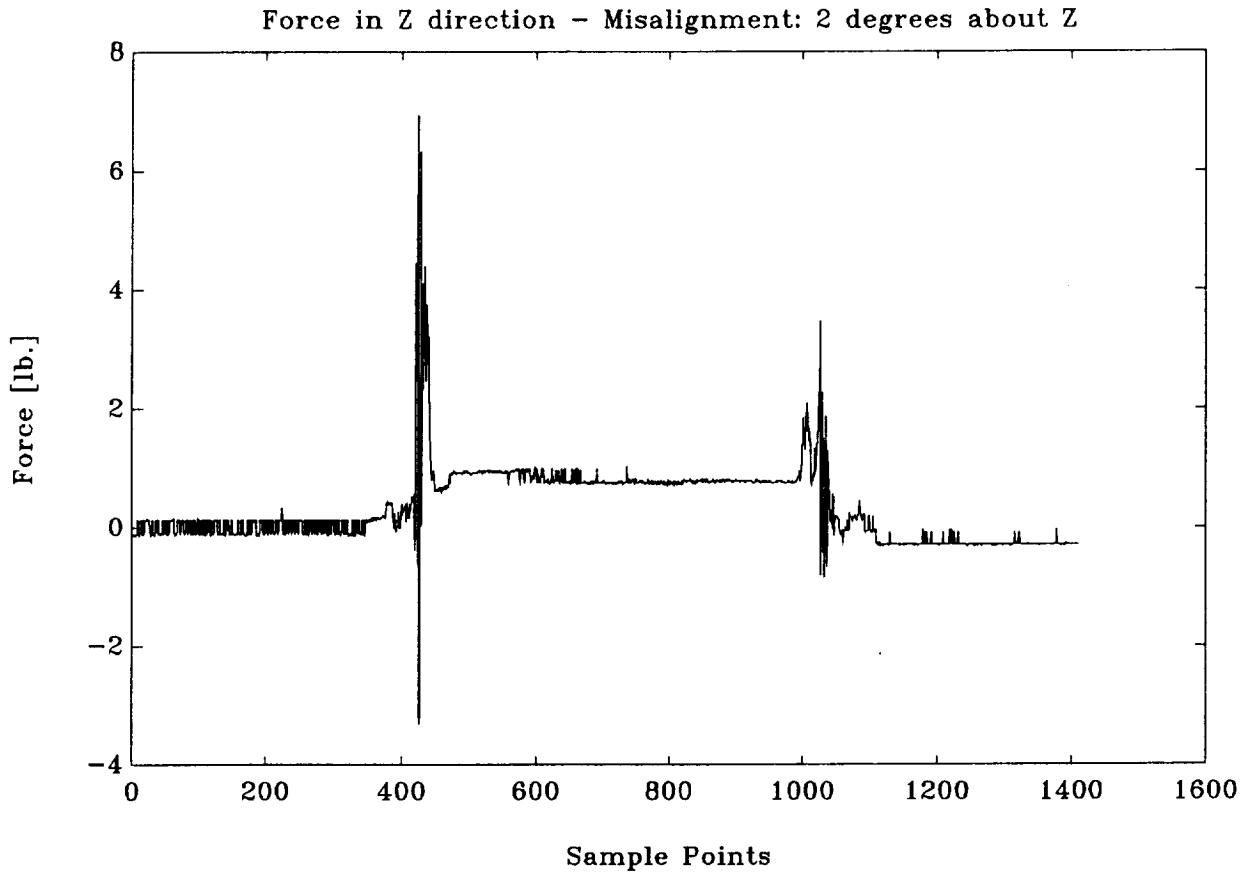

Figure 16

H-Interface
Force Time History
Rotational Misalignment

Force (in lb) along the Z-axis
for 3.0 degrees misalignment about the Z-axis

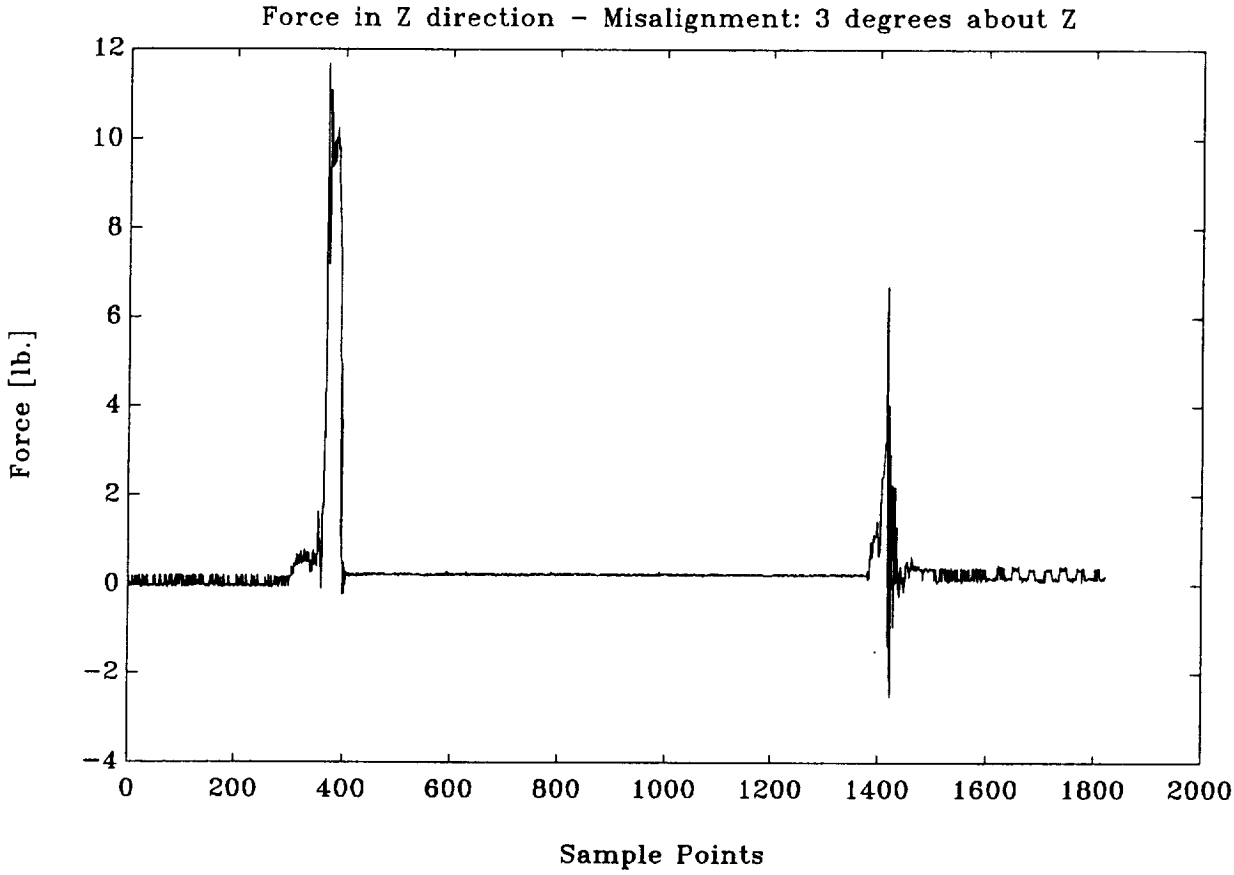

Figure 17

H-Interface
Force Time History
Translational Misalignment

Force (in lb) along the X-axis
for -0.1 inch misalignment along the Y-axis

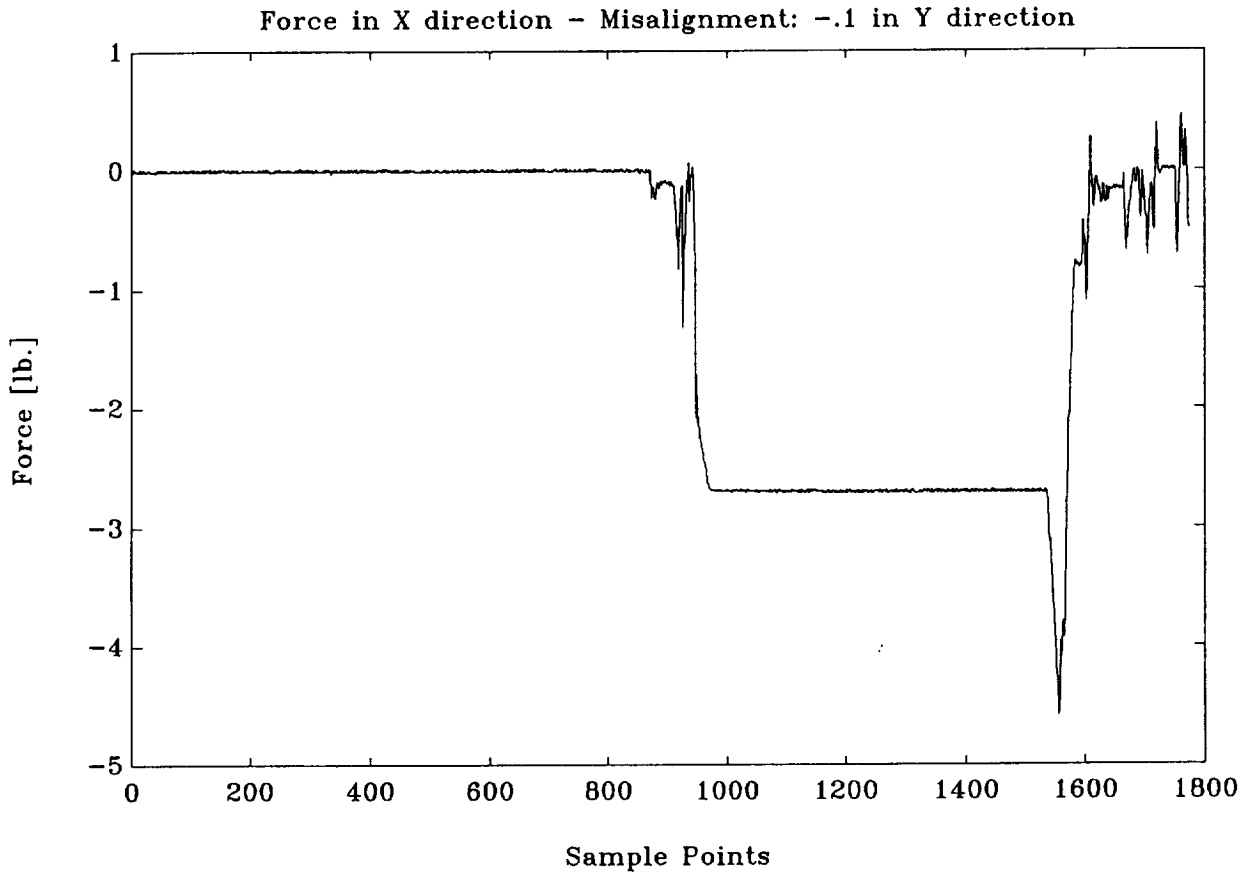

Figure 18

H-Interface
Force Time History
Translational Misalignment

Force (in lb) along the X-axis
for -0.2 inch misalignment along the Y-axis

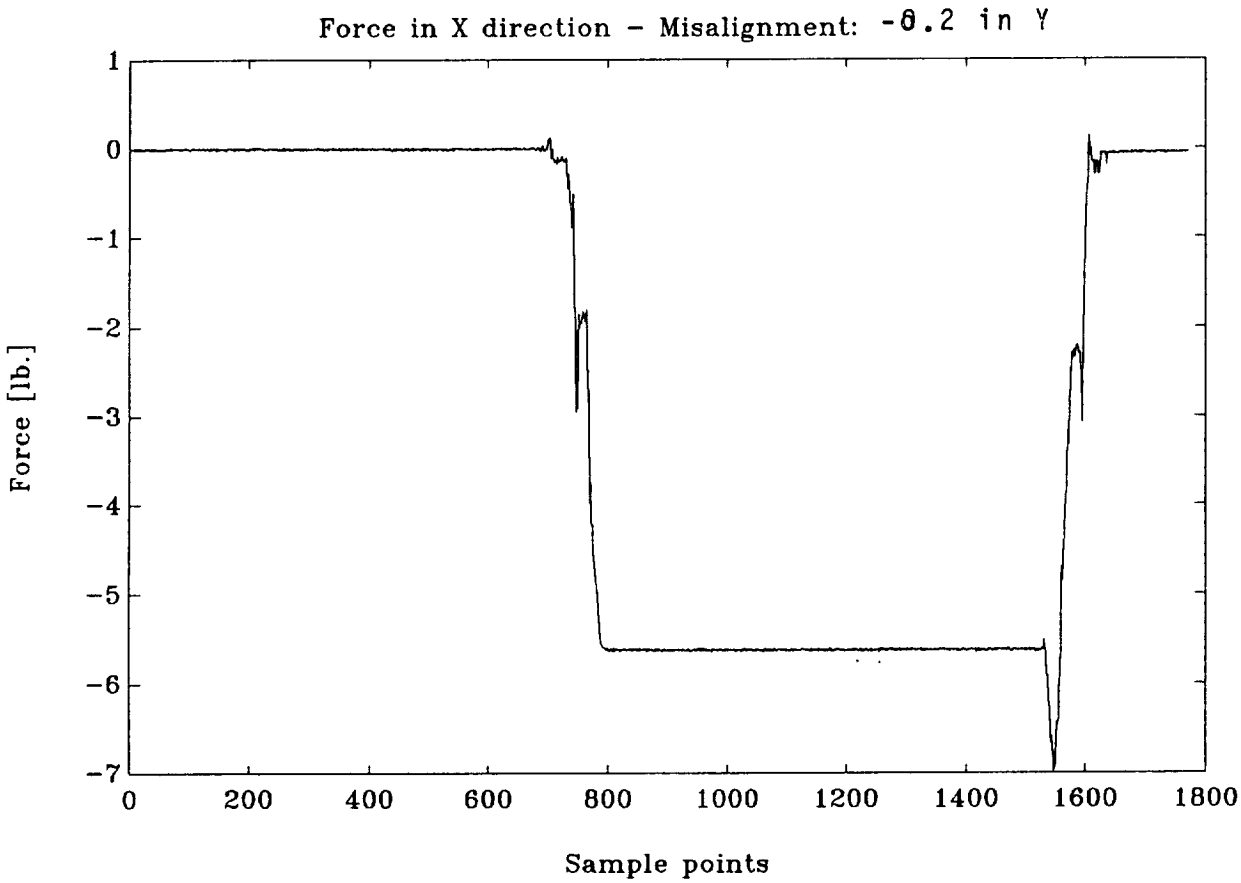

Figure 19

H-Interface
Force Time History
Translational Misalignment

Force (in lb) along the X-axis
for -0.3 inch misalignment along the Y-axis

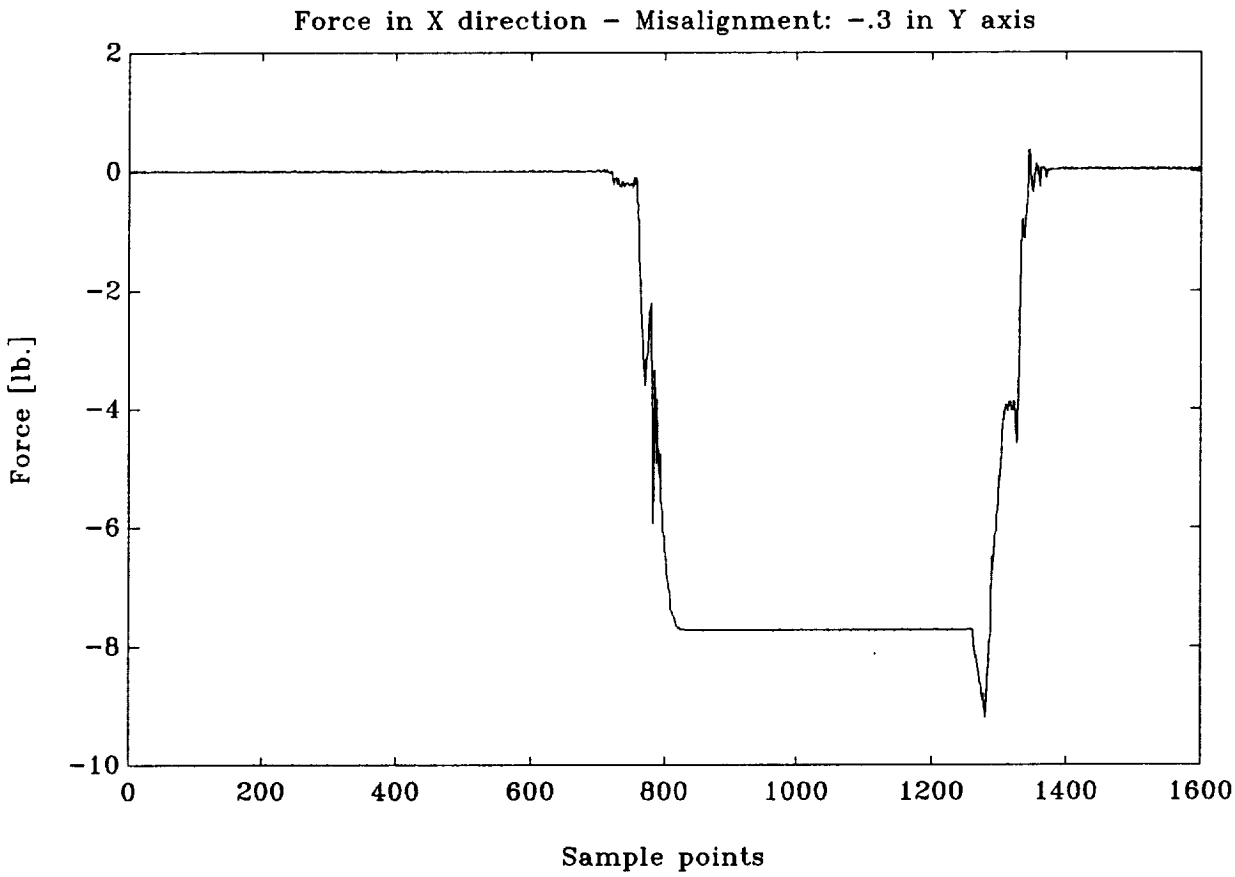

Figure 20

H-Interface
Force Time History
Translational Misalignment

Force (in lb) along the X-axis
for -0.4 inch misalignment along the Y-axis

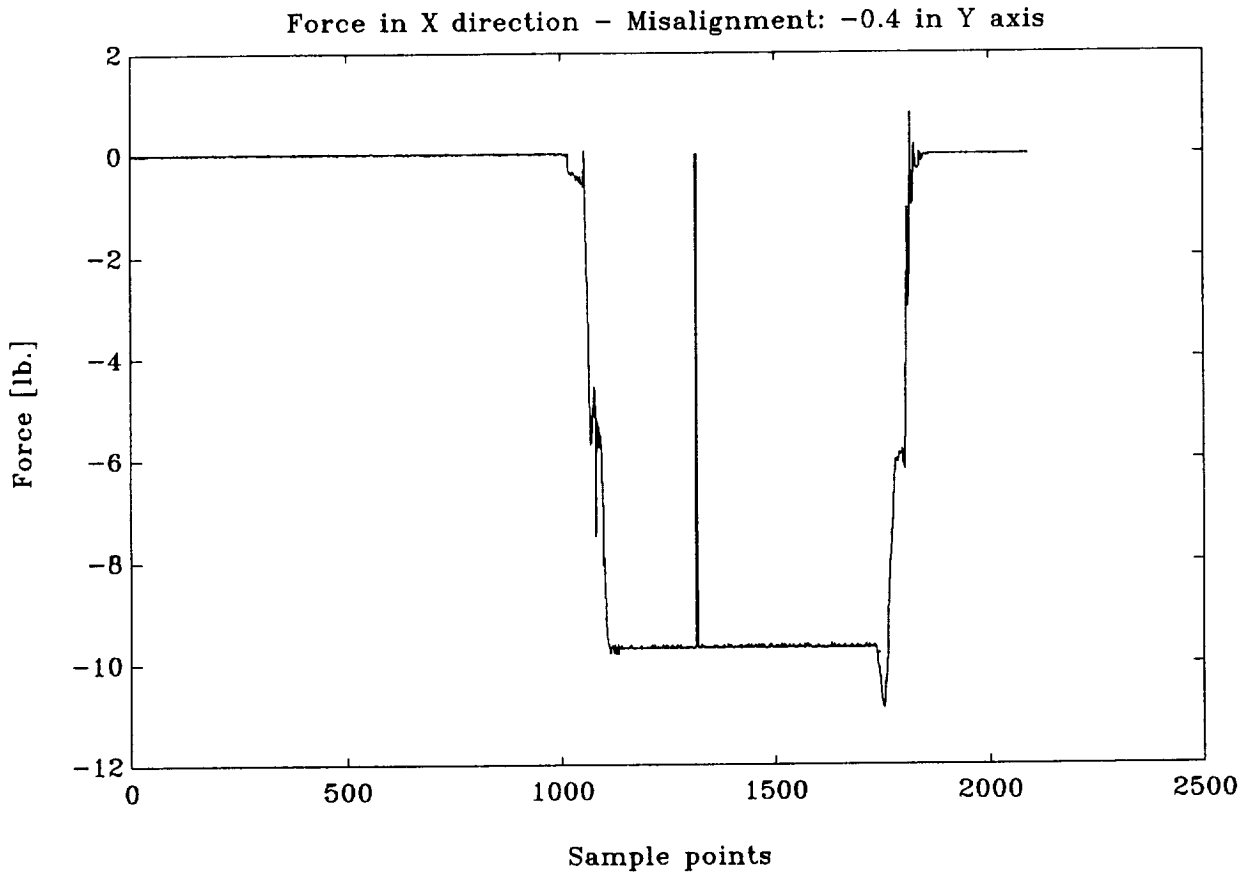

Figure 21

H-Interface
Force Time History
Translational Misalignment

Force (in lb) along the Y-axis
for -0.1 inch misalignment along the Y-axis

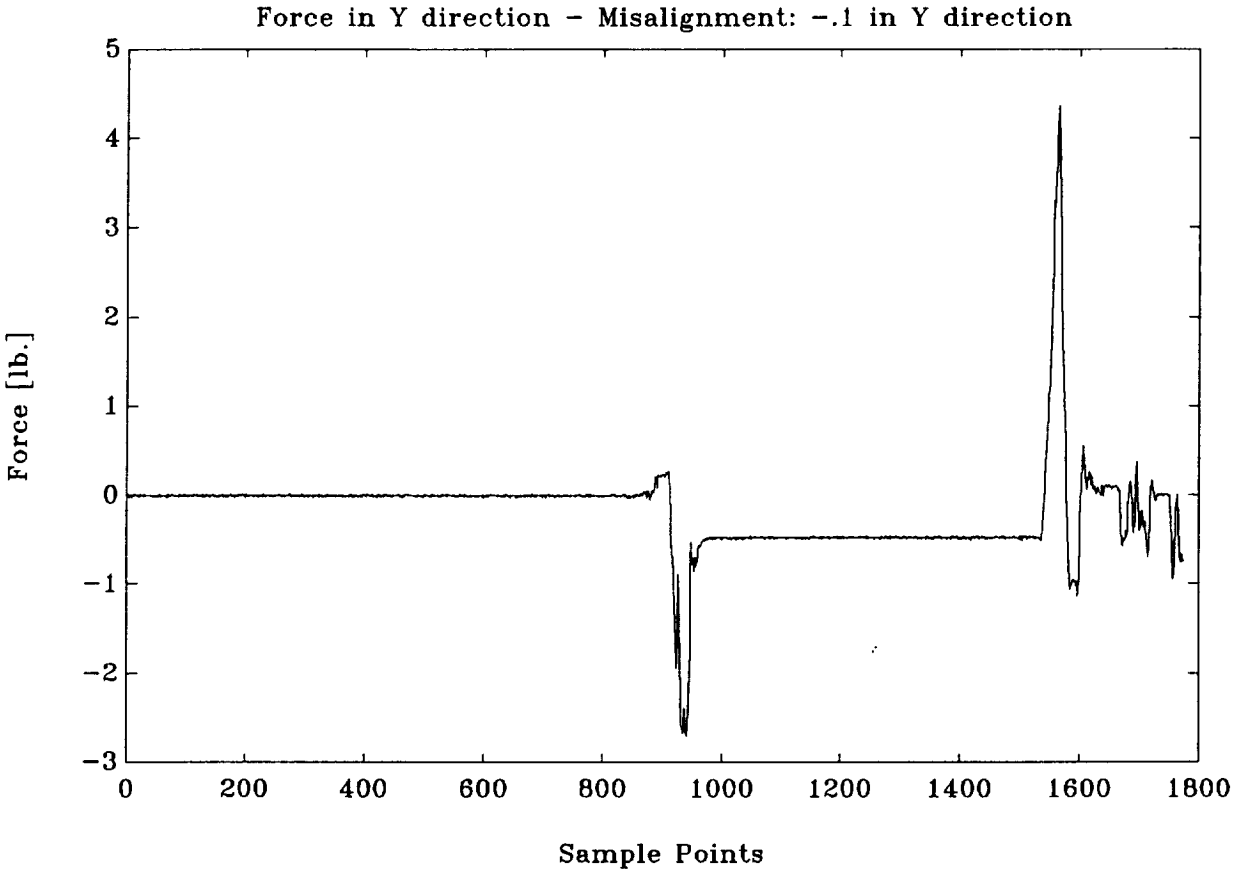

Figure 22

H-Interface
Force Time History
Translational Misalignment

Force (in lb) along the Y-axis
for -0.2 inch misalignment along the Y-axis

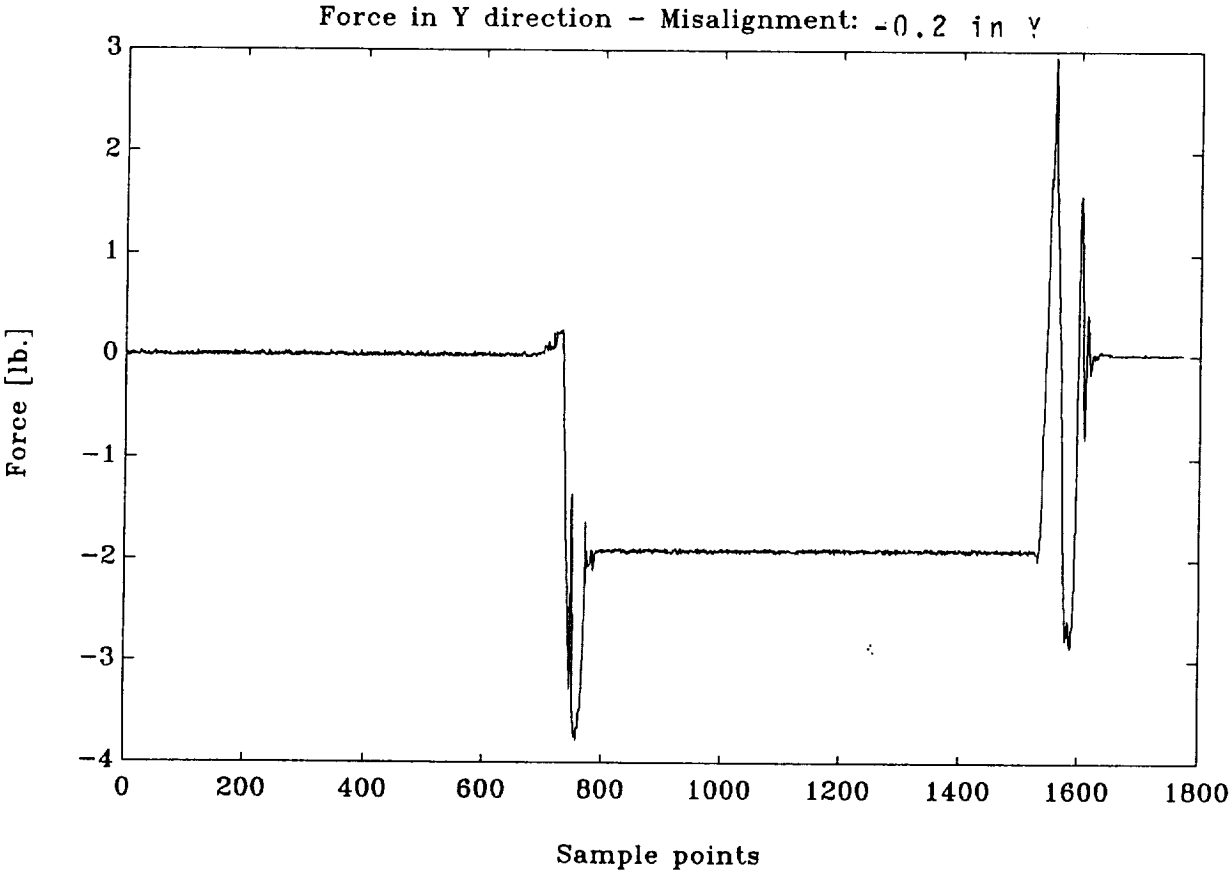

Figure 23

H-Interface
Force Time History
Translational Misalignment

Force (in lb) along the Y-axis
for -0.3 inch misalignment along the Y-axis

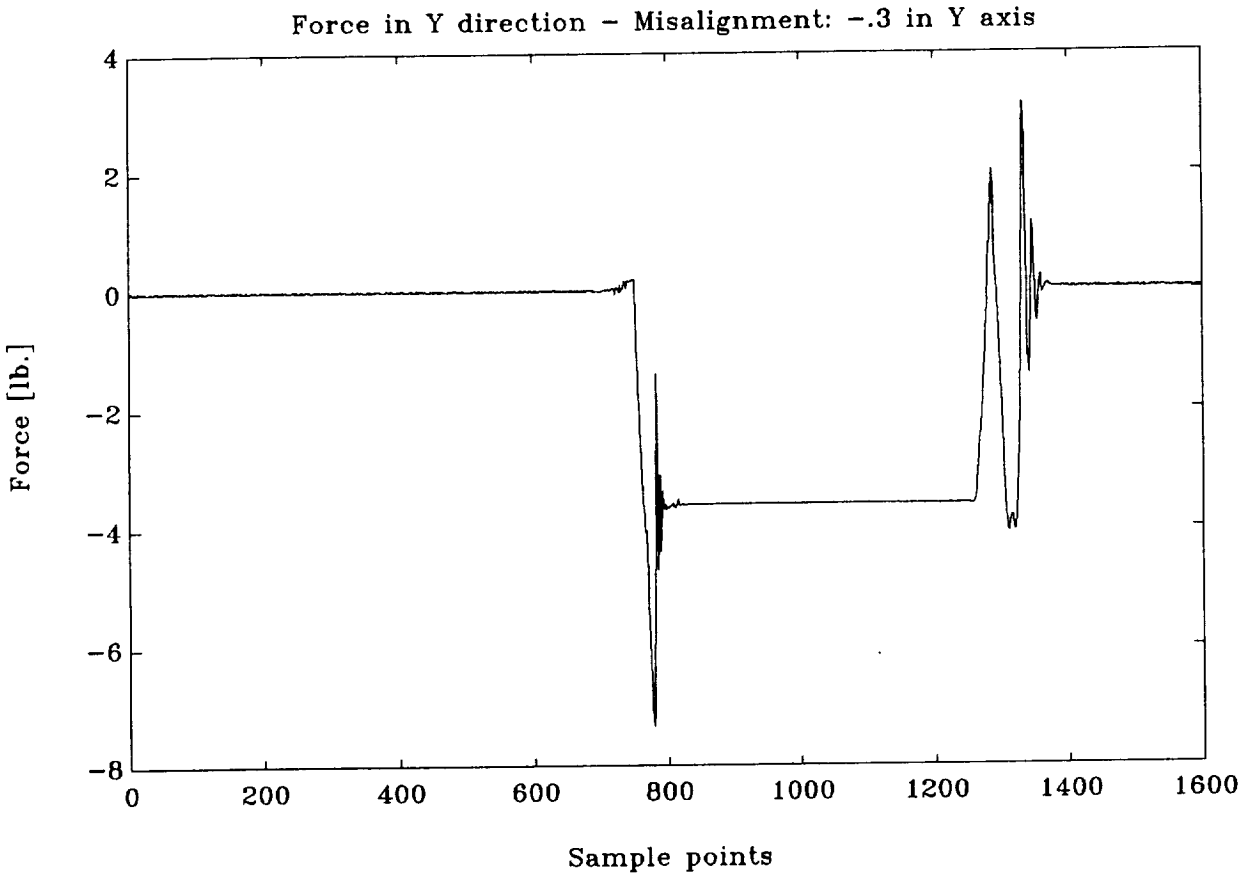

Figure 24

H-Interface
Force Time History
Translational Misalignment

Force (in lb) along the Y-axis
for -0.4 inch misalignment along the Y-axis

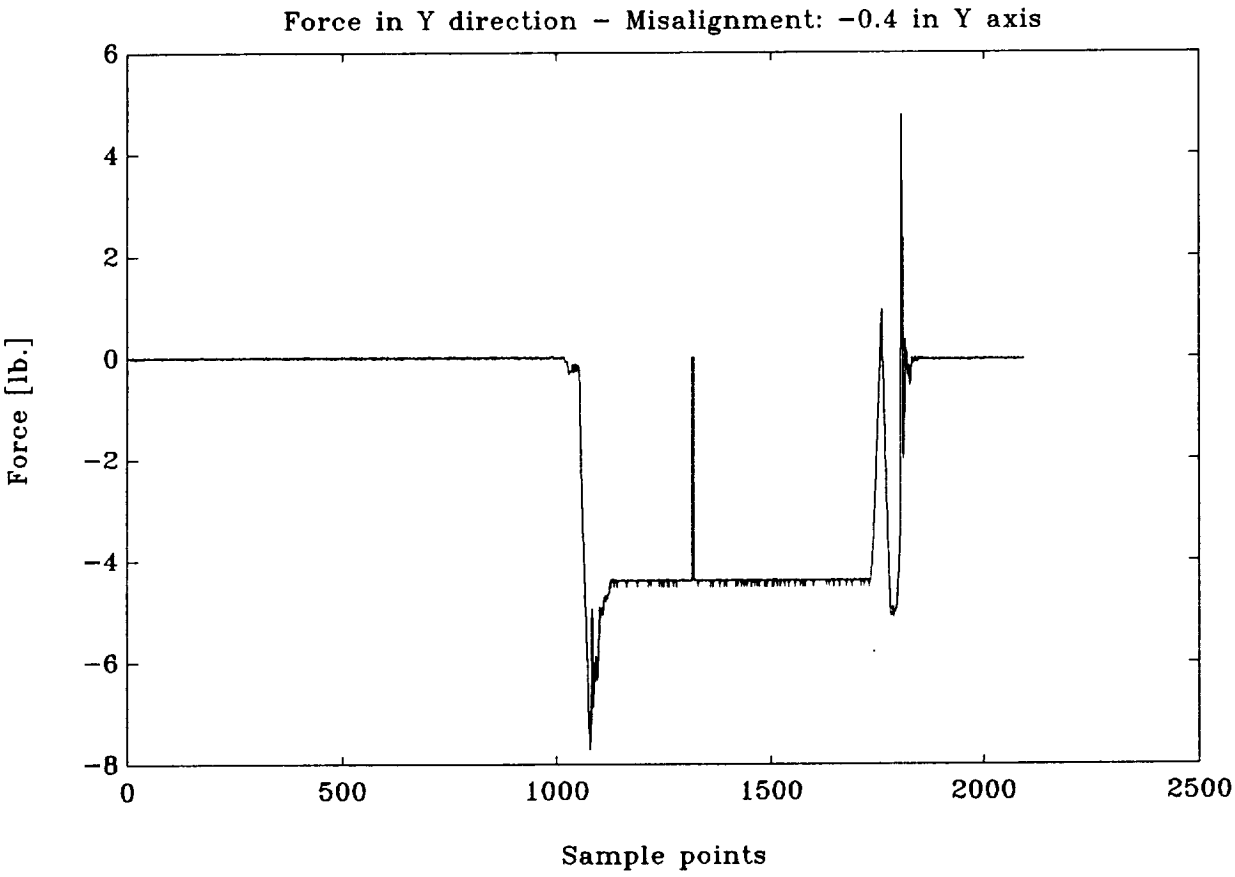

Figure 25

H-Interface
Force Time History
Translational Misalignment

Force (in lb) along the Z-axis
for -0.1 inch misalignment along the Y-axis

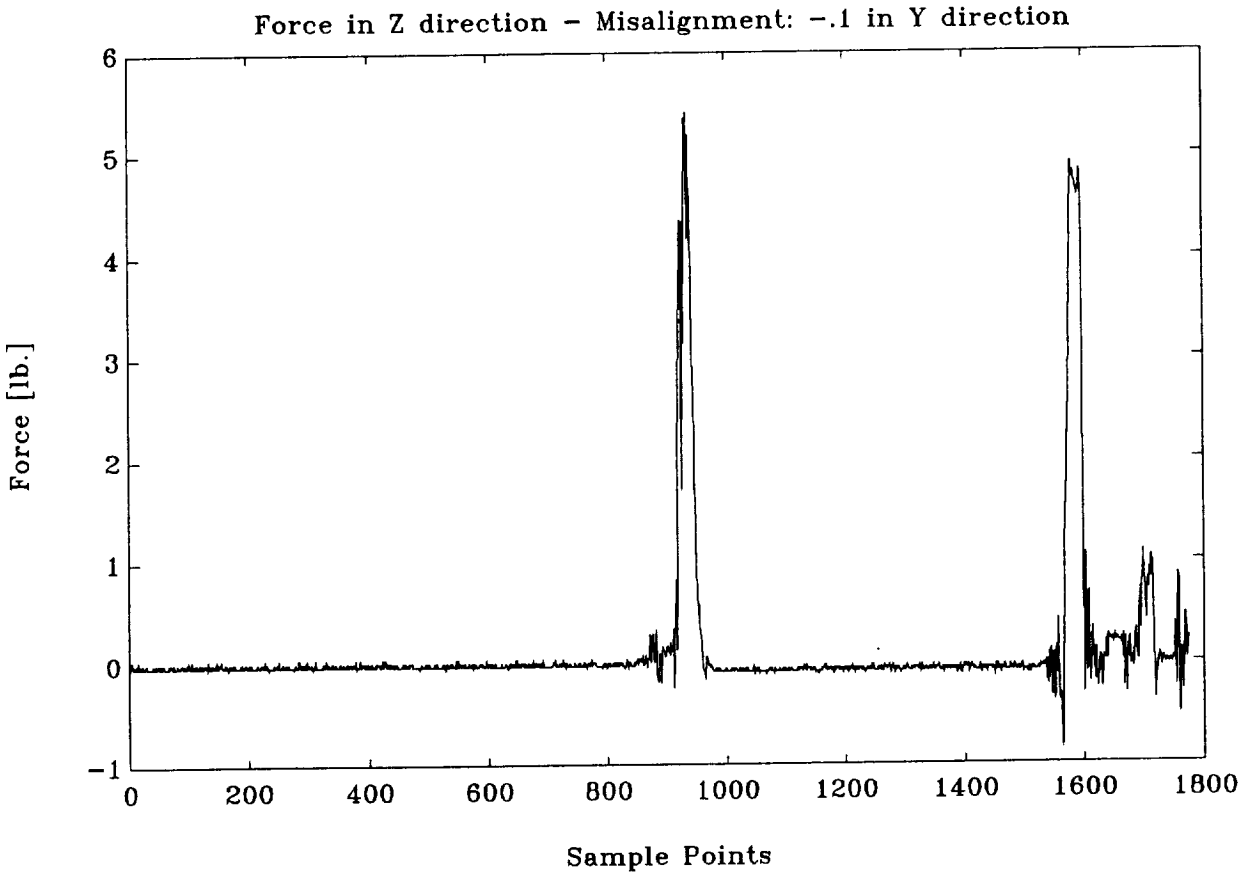

Figure 26

H-Interface
Force Time History
Translational Misalignment

Force (in lb) along the Z-axis
for -0.2 inch misalignment along the Y-axis

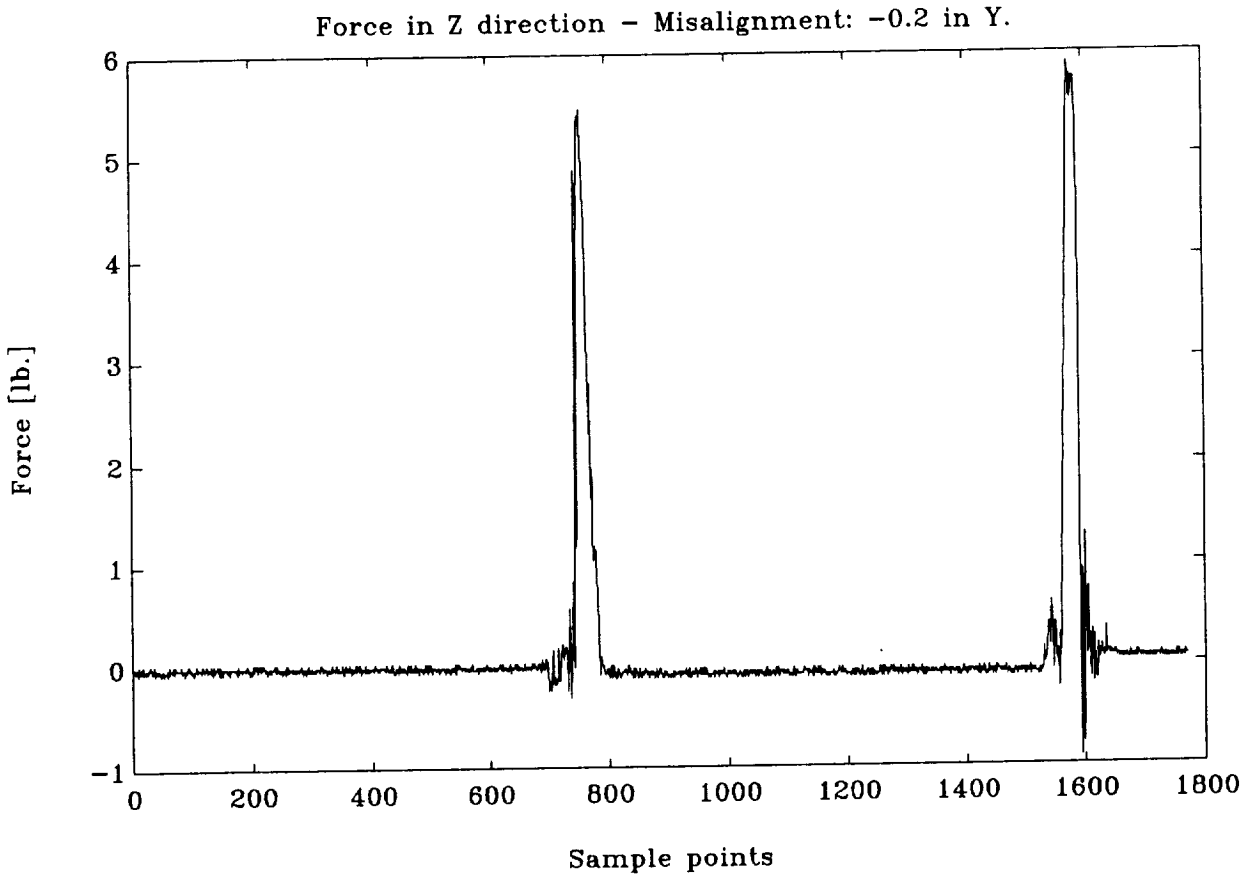

Figure 27

H-Interface
Force Time History
Translational Misalignment

Force (in lb) along the Z-axis
for -0.3 inch misalignment along the Y-axis

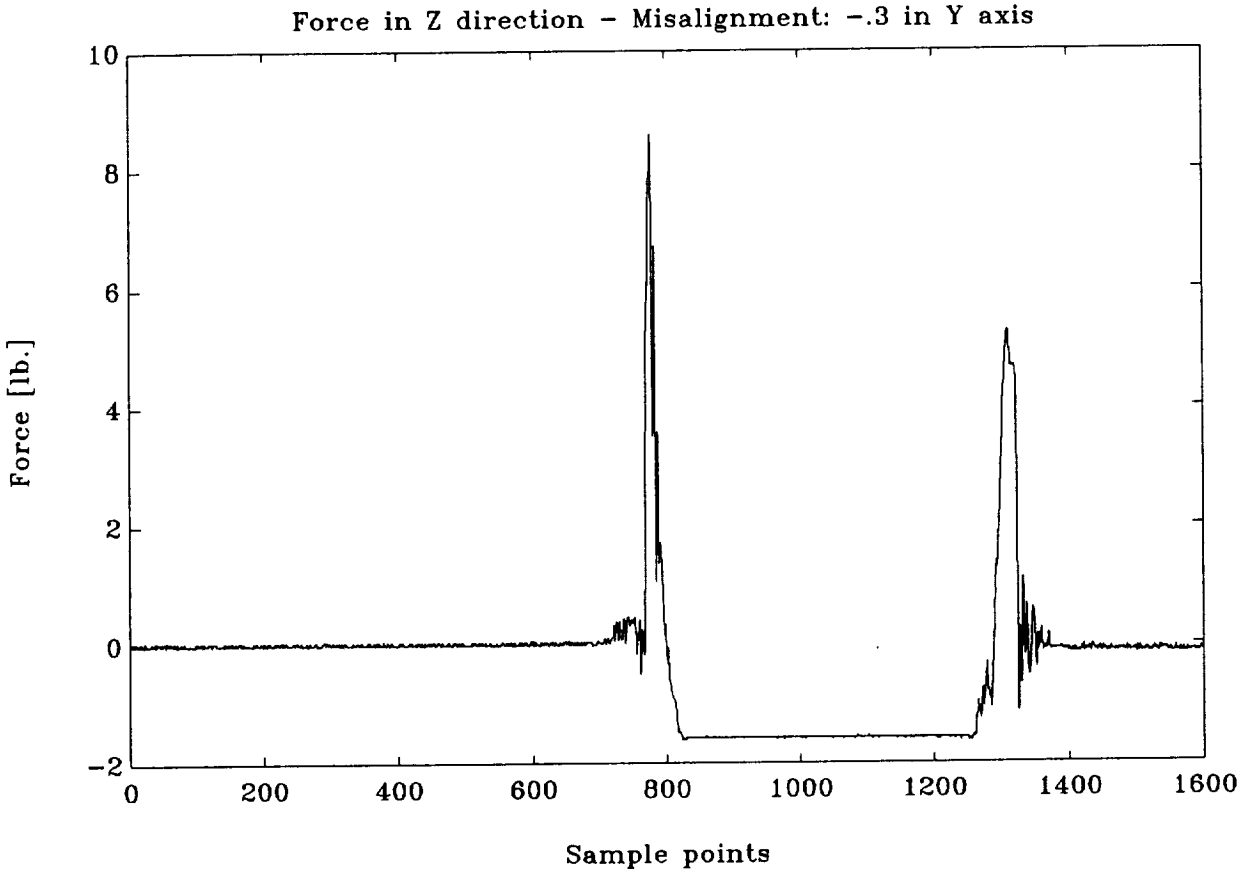

Figure 28

H-Interface
Force Time History
Translational Misalignment

Force (in lb) along the Z-axis
for -0.4 inch misalignment along the Y-axis

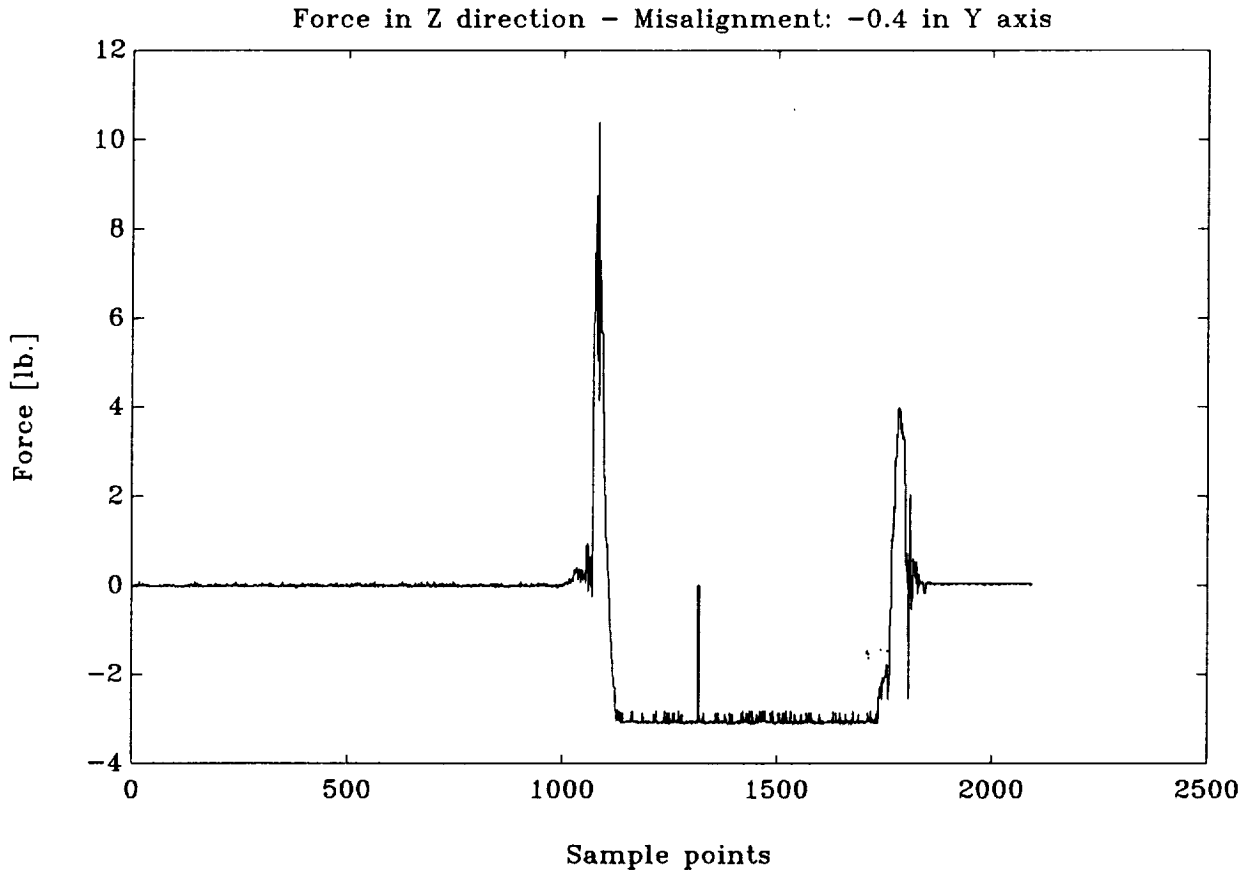

Figure 29

H-Interface
Force Time History
Translational Misalignment

Force (in lb) along the X-axis
for 0.0 inches misalignment along the Z-axis

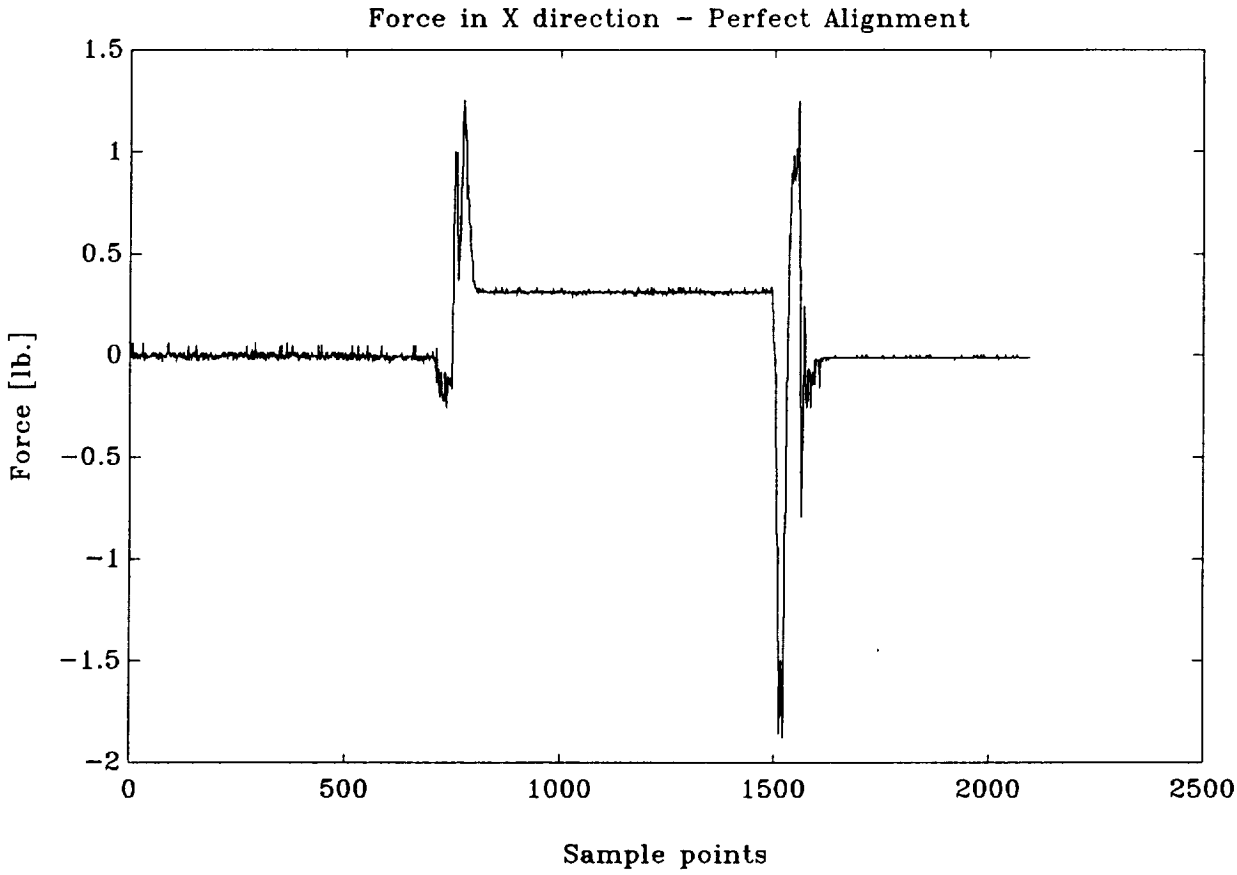

Figure 30

H-Interface
Force Time History
Translational Misalignment

Force (in lb) along the X-axis
for 0.1 inches misalignment along the Z-axis

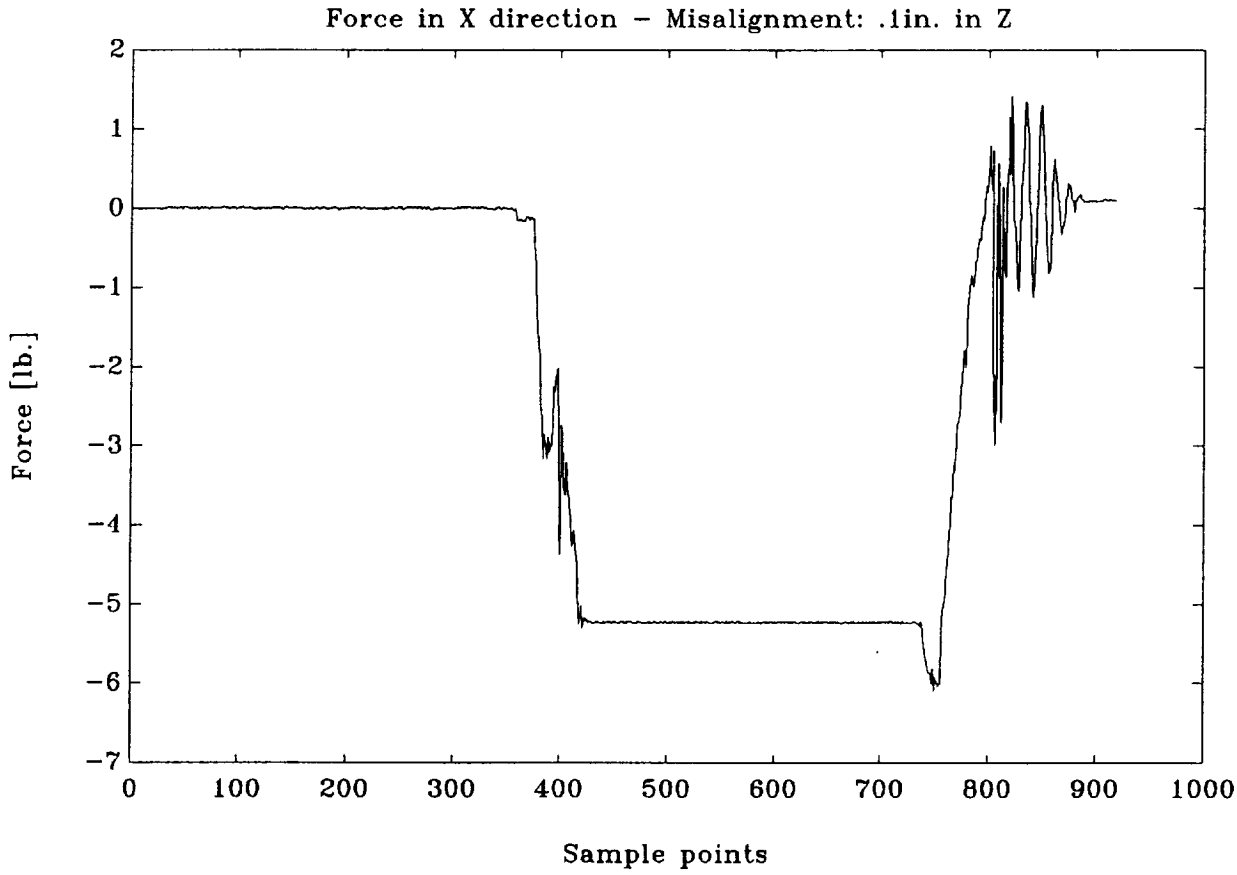

Figure 31

H-Interface
Force Time History
Translational Misalignment

Force (in lb) along the X-axis
for 0.15 inches misalignment along the Z-axis

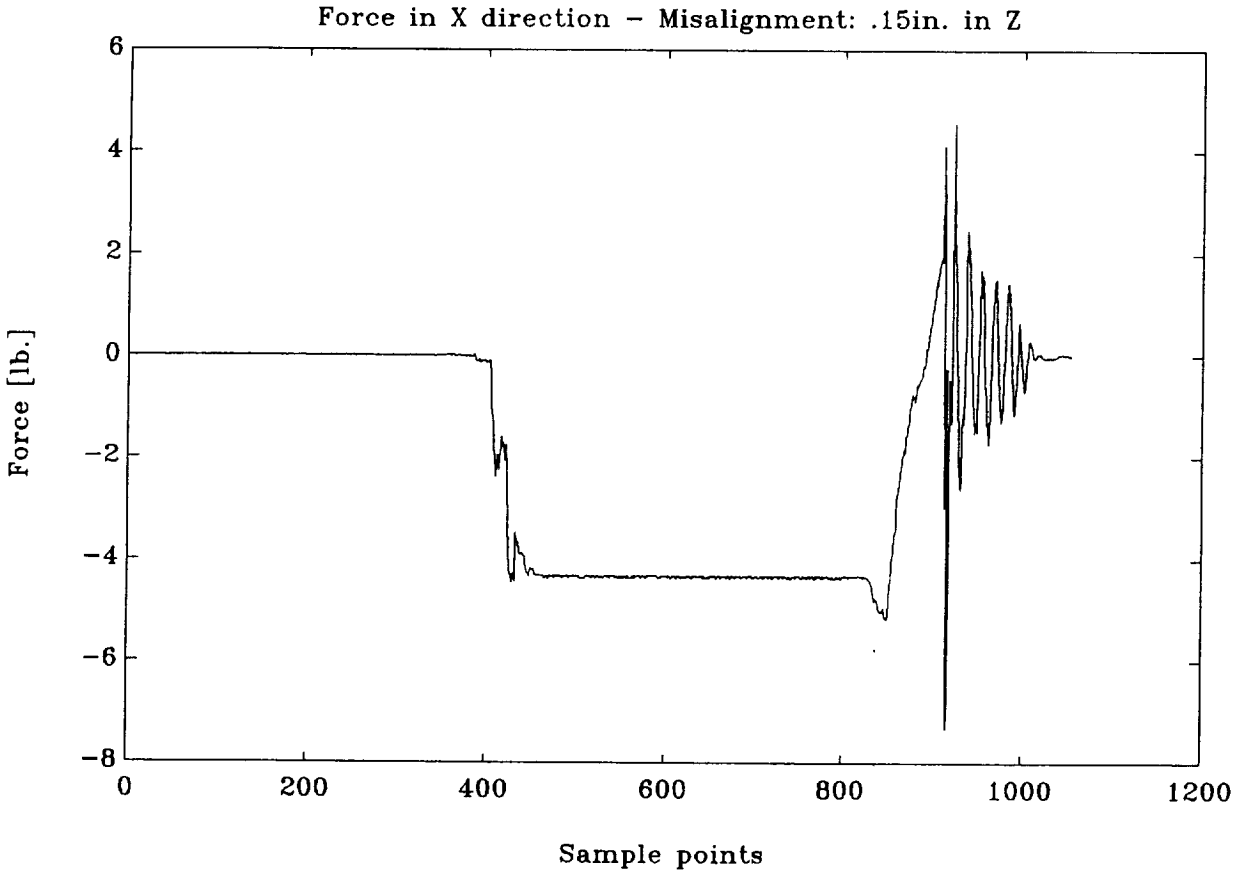

Figure 32

H-Interface
Force Time History
Translational Misalignment

Force (in lb) along the X-axis
for 0.20 inches misalignment along the Z-axis

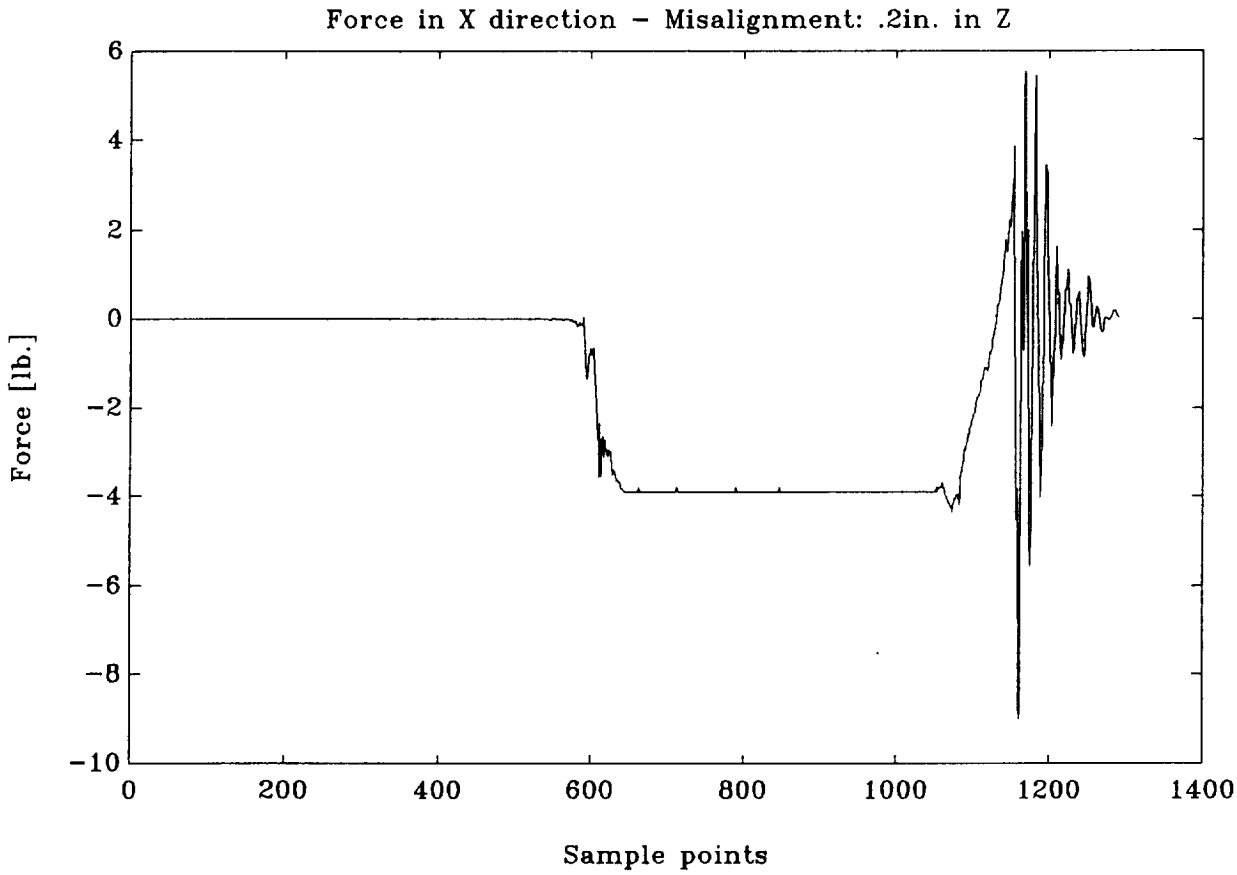

Figure 33

H-Interface
Force Time History
Translational Misalignment

Force (in lb) along the X-axis
for 0.30 inches misalignment along the Z-axis

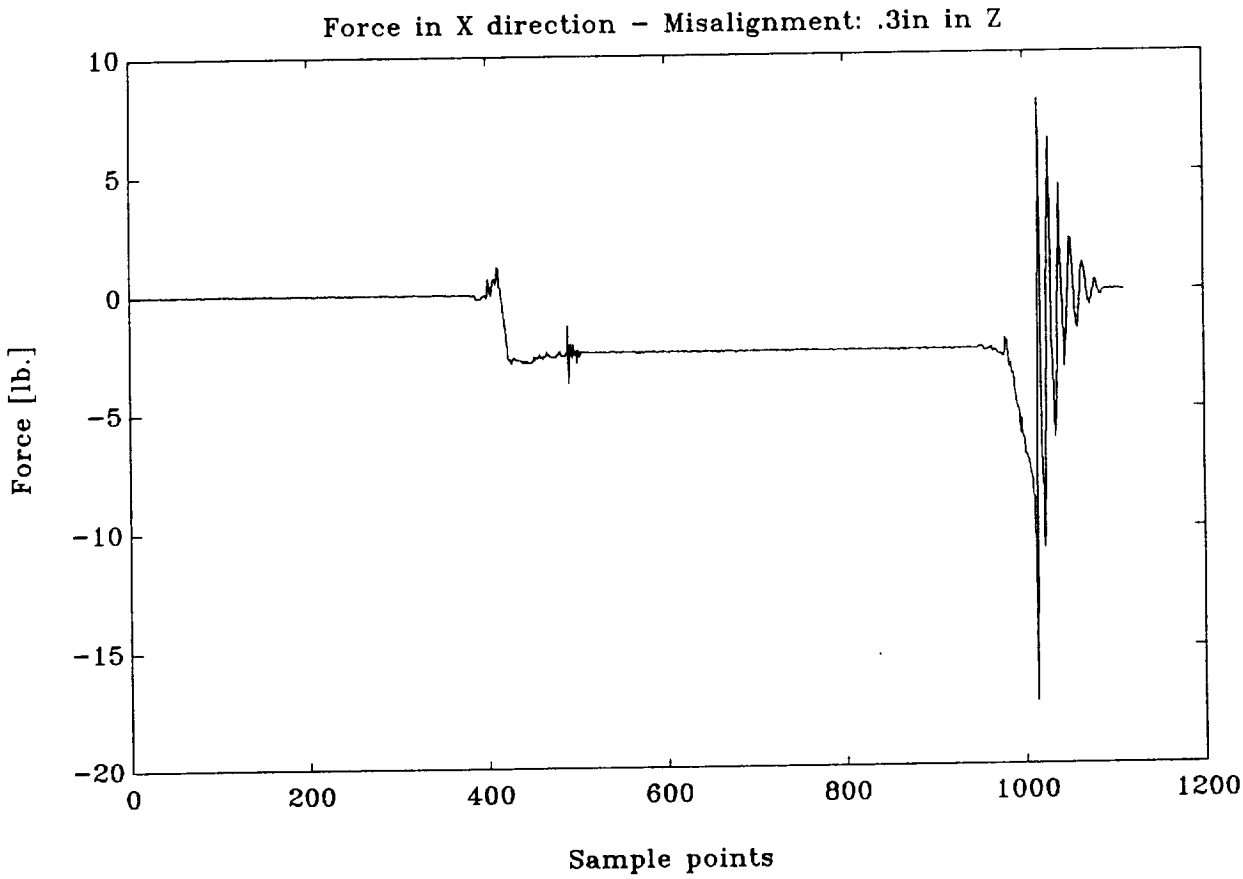

Figure 34

H-Interface
Force Time History
Translational Misalignment

Force (in lb) along the Y-axis
for 0.00 inches misalignment along the Z-axis

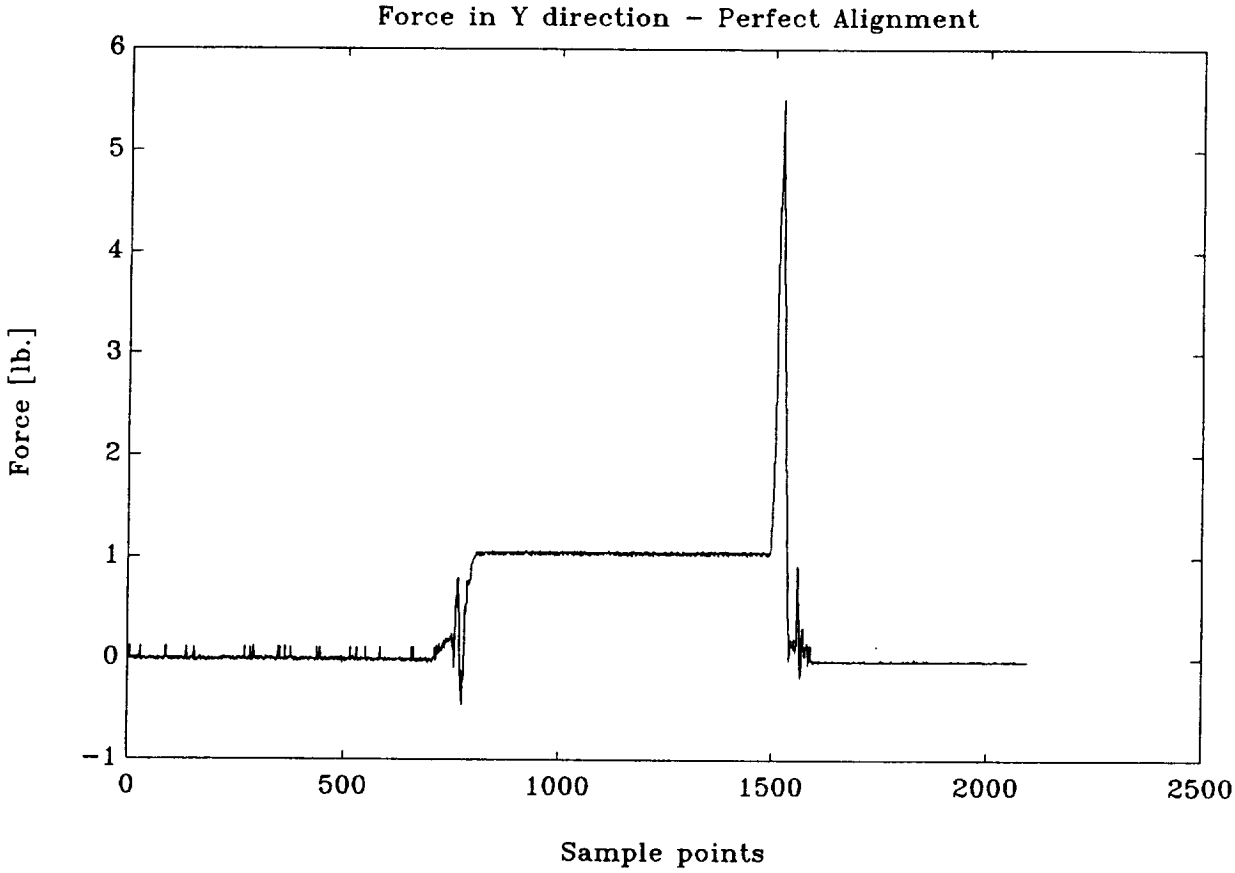

Figure 35

H-Interface
Force Time History
Translational Misalignment

Force (in lb) along the Y-axis
for 0.10 inches misalignment along the Z-axis

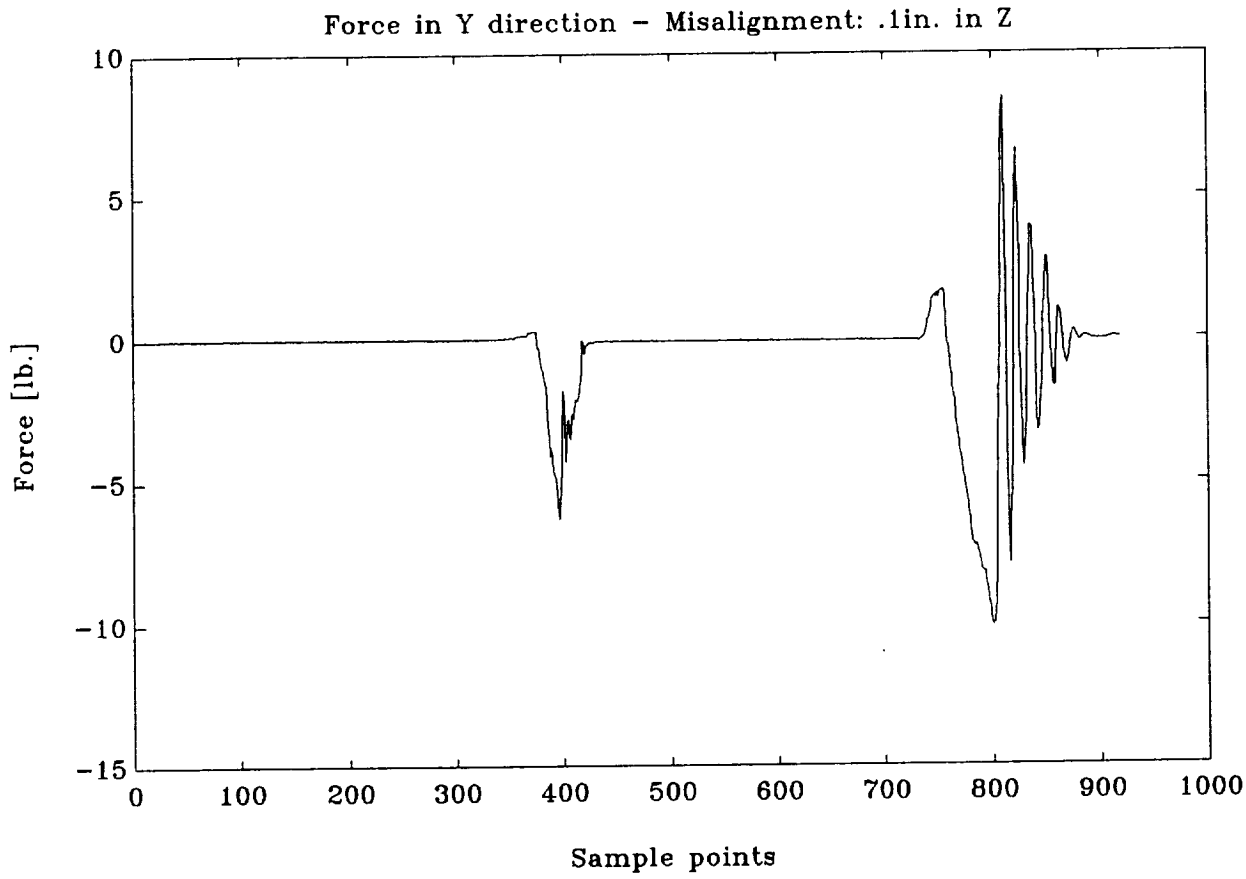

Figure 36

H-Interface
Force Time History
Translational Misalignment

Force (in lb) along the Y-axis
for 0.15 inches misalignment along the Z-axis

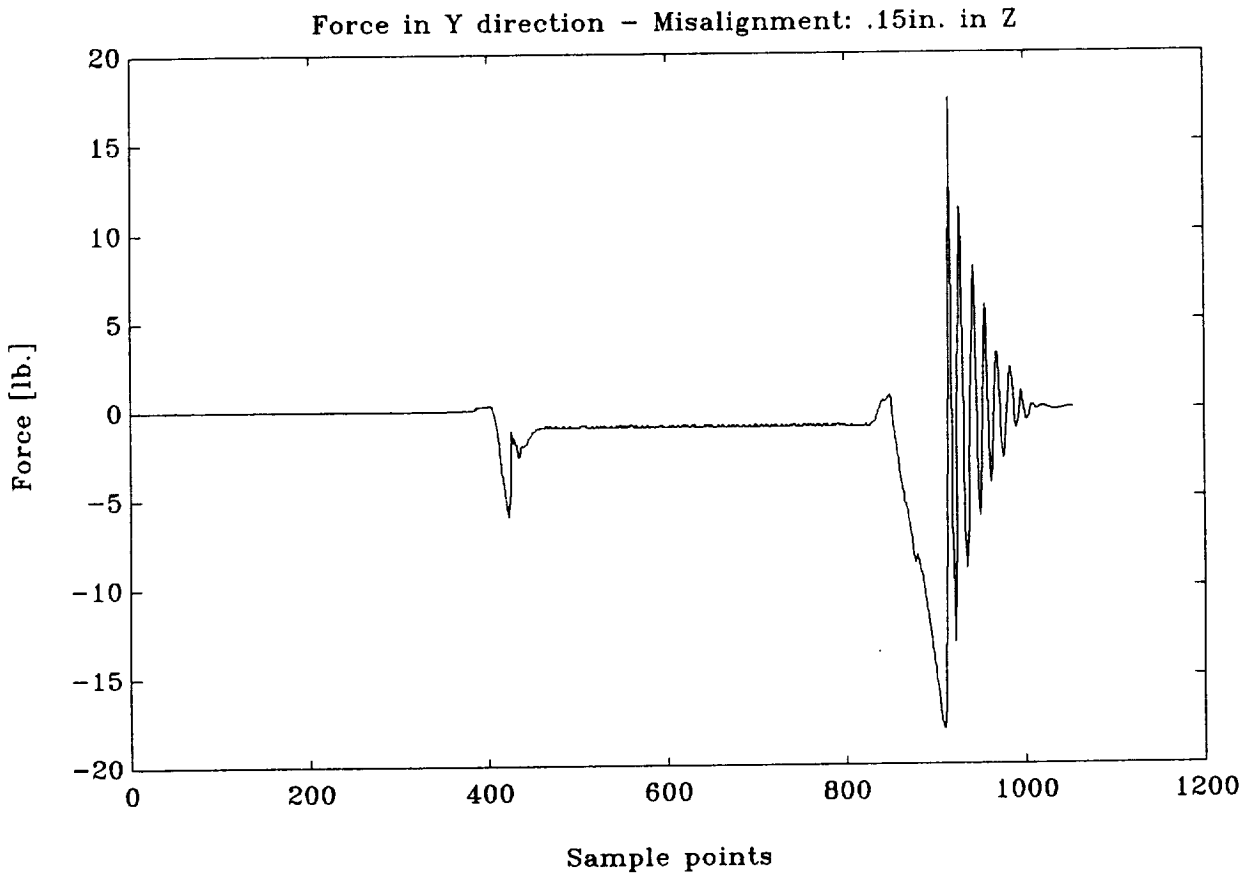

Figure 37

H-Interface
Force Time History
Translational Misalignment

Force (in lb) along the Y-axis
for 0.20 inches misalignment along the Z-axis

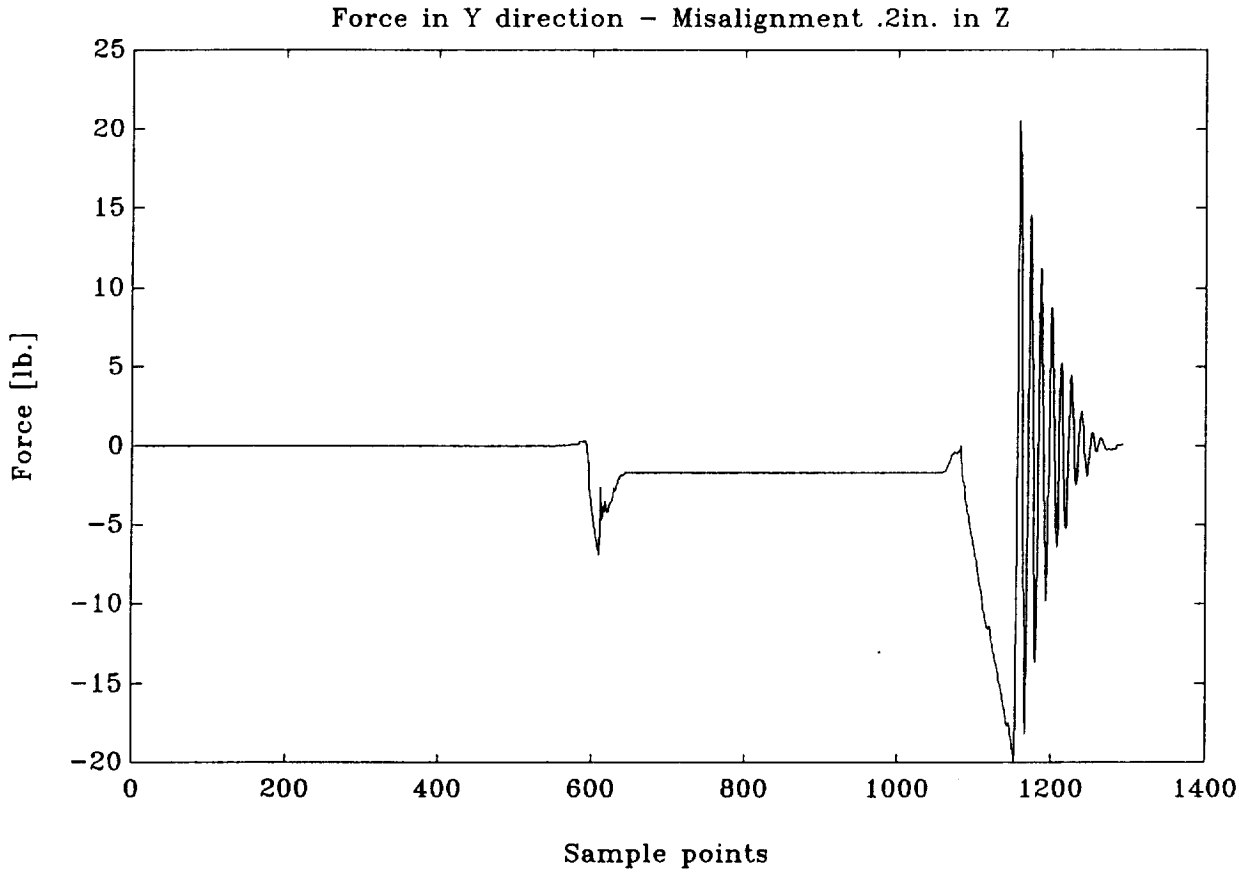

Figure 38

H-Interface
Force Time History
Translational Misalignment

Force (in lb) along the Y-axis
for 0.30 inches misalignment along the Z-axis

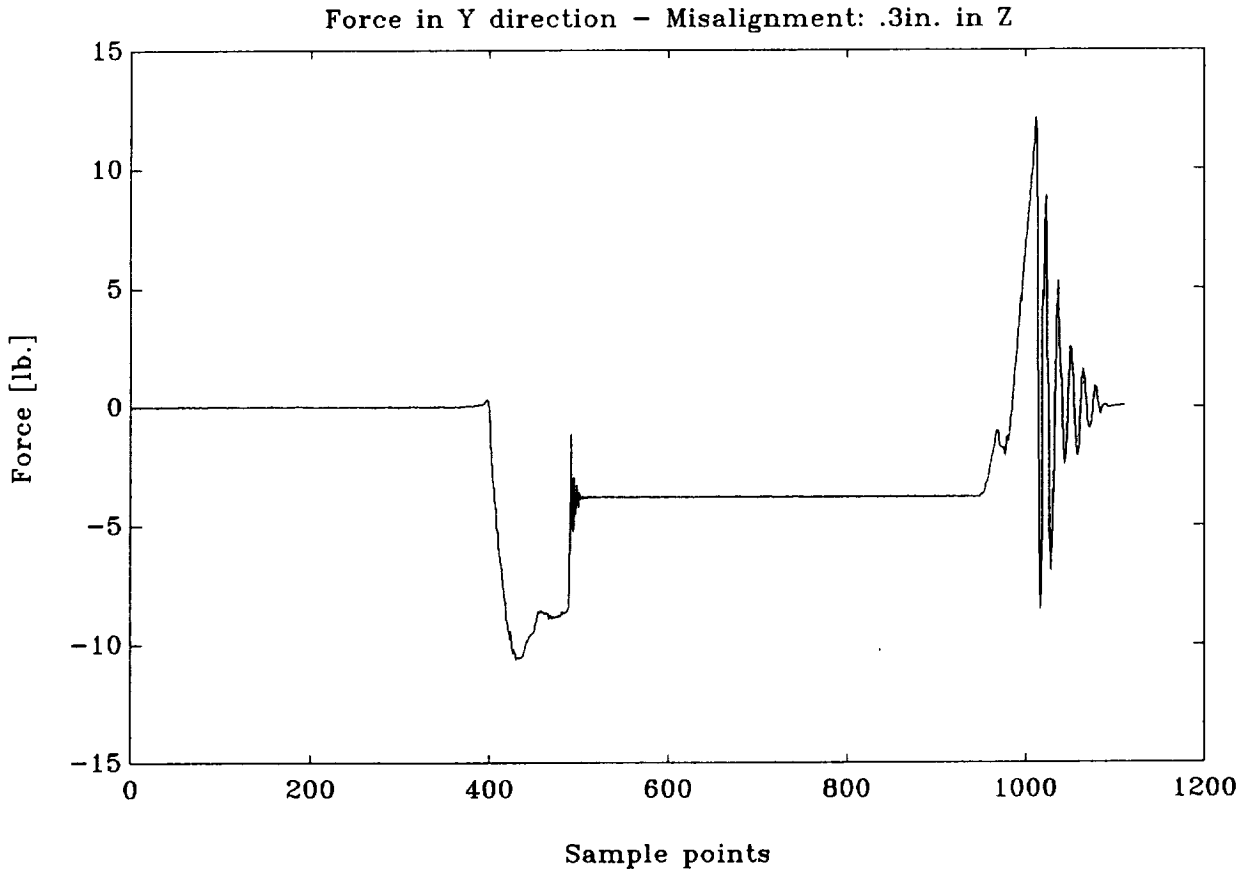

Figure 39

H-Interface
Force Time History
Translational Misalignment

Force (in lb) along the Z-axis
for 0.00 inches misalignment along the Z-axis

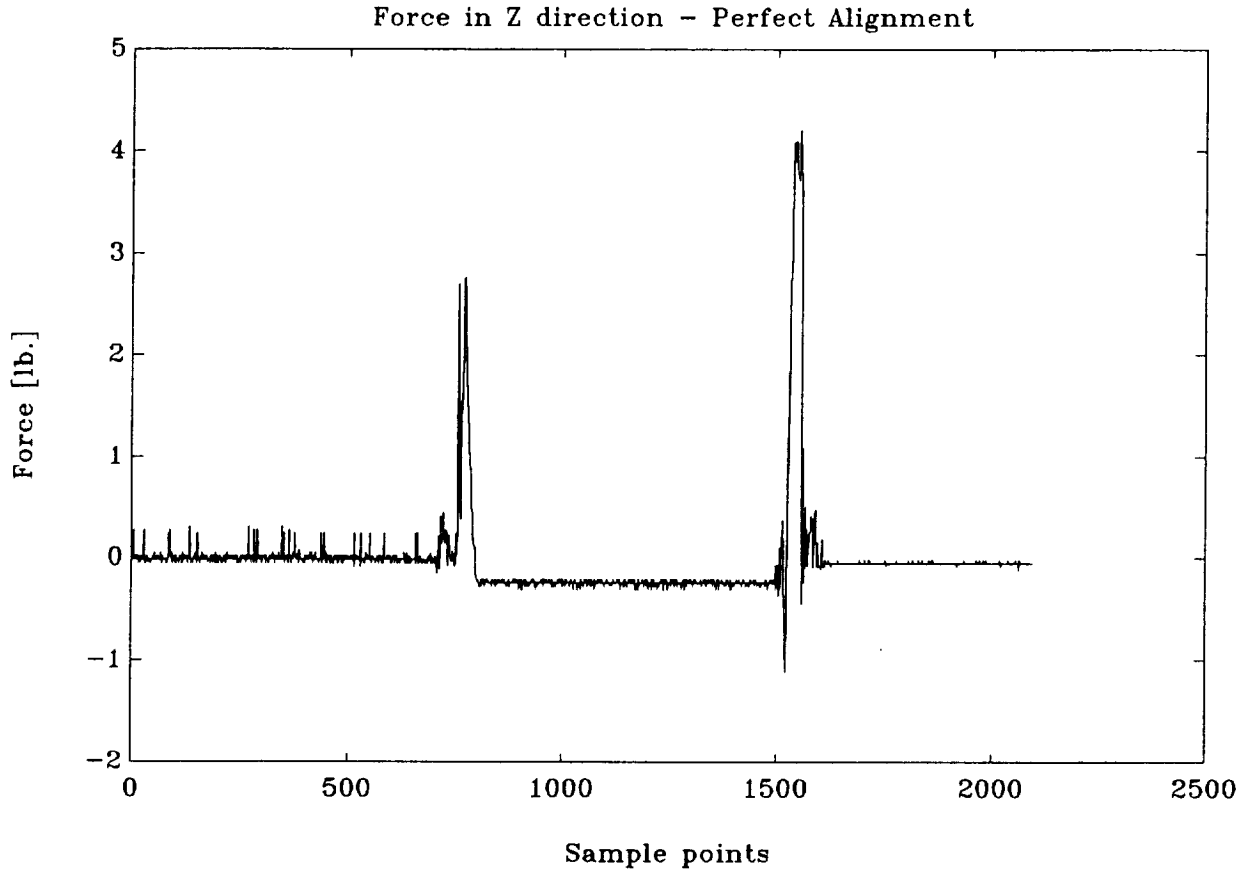

Figure 40

H-Interface
Force Time History
Translational Misalignment

Force (in lb) along the Z-axis
for 0.10 inches misalignment along the Z-axis

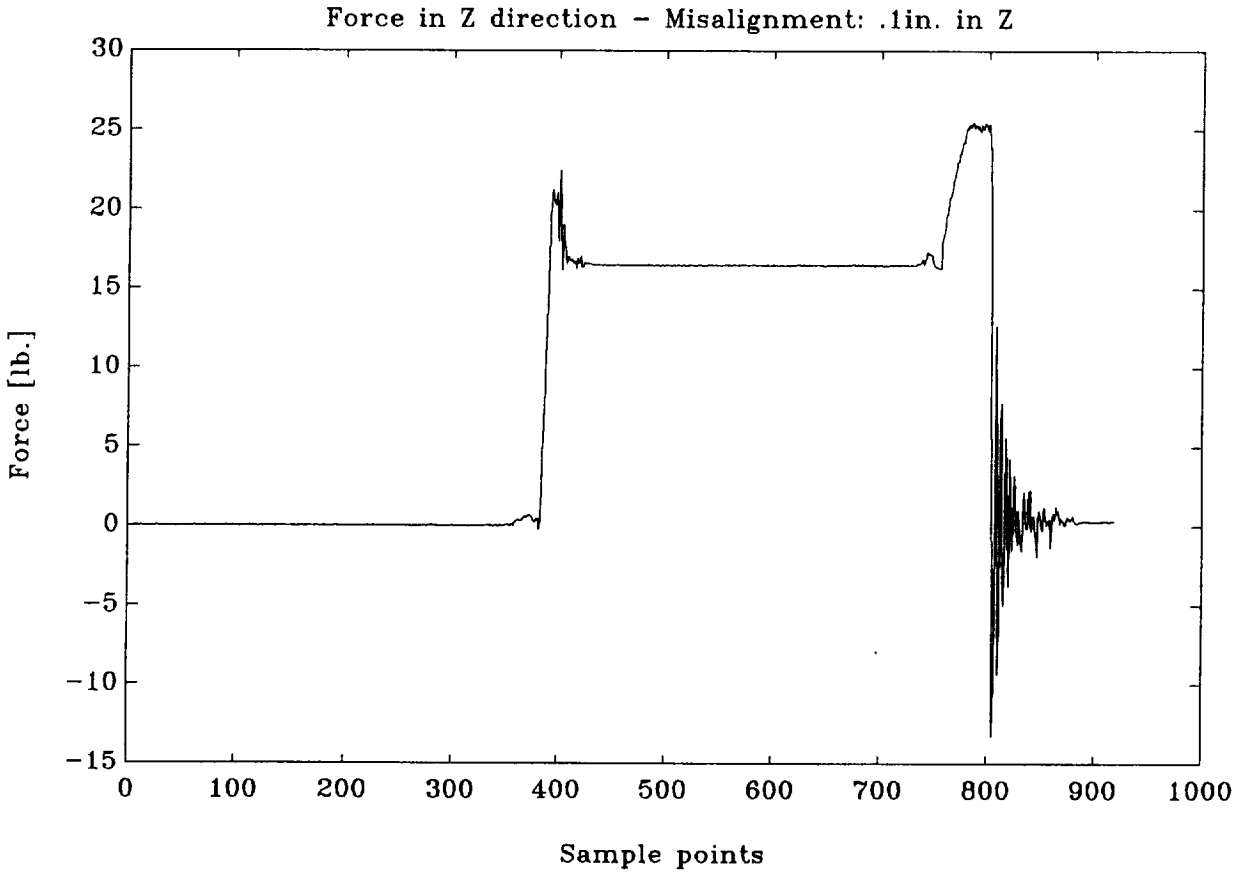

Figure 41

H-Interface
Force Time History
Translational Misalignment

Force (in lb) along the Z-axis
for 0.15 inches misalignment along the Z-axis

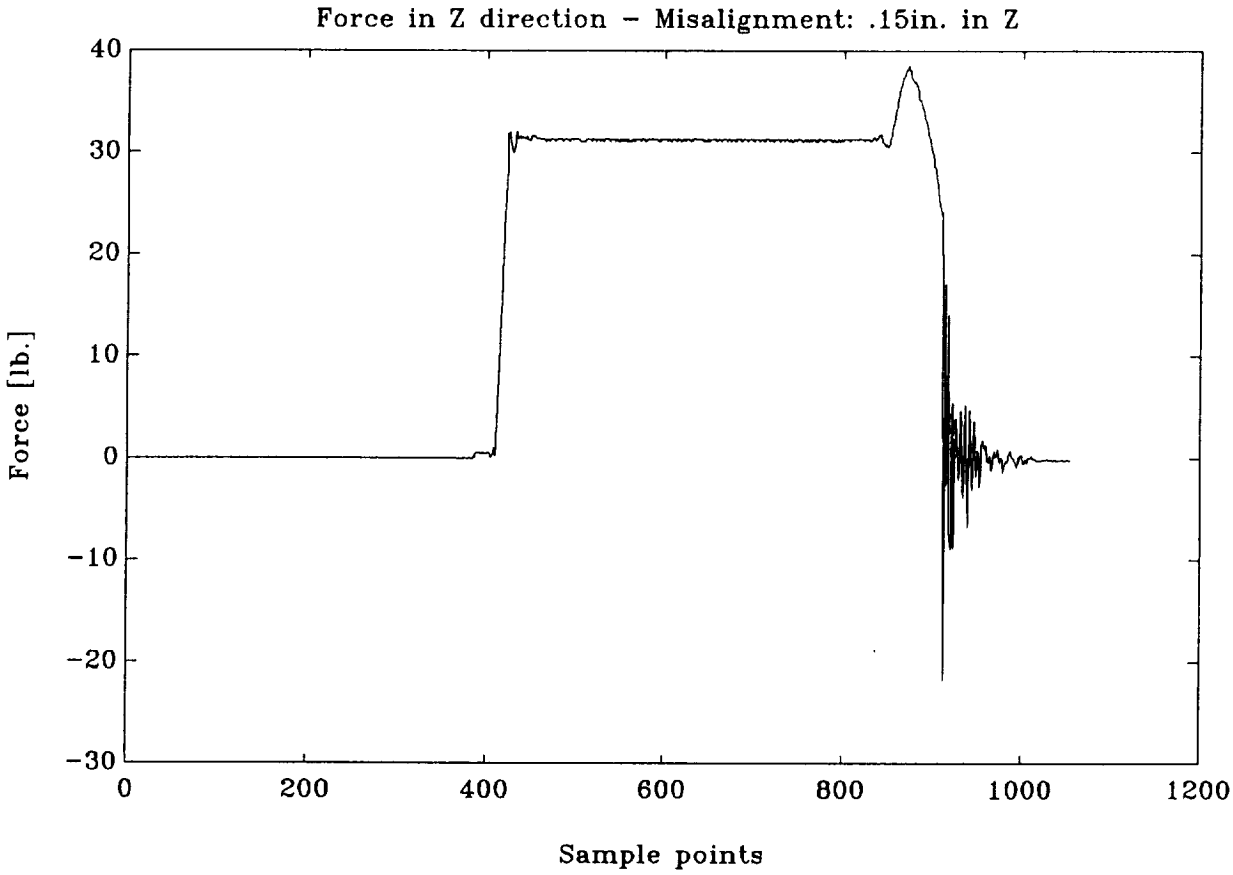

Figure 42

H-Interface
Force Time History
Translational Misalignment

Force (in lb) along the Z-axis
for 0.20 inches misalignment along the Z-axis

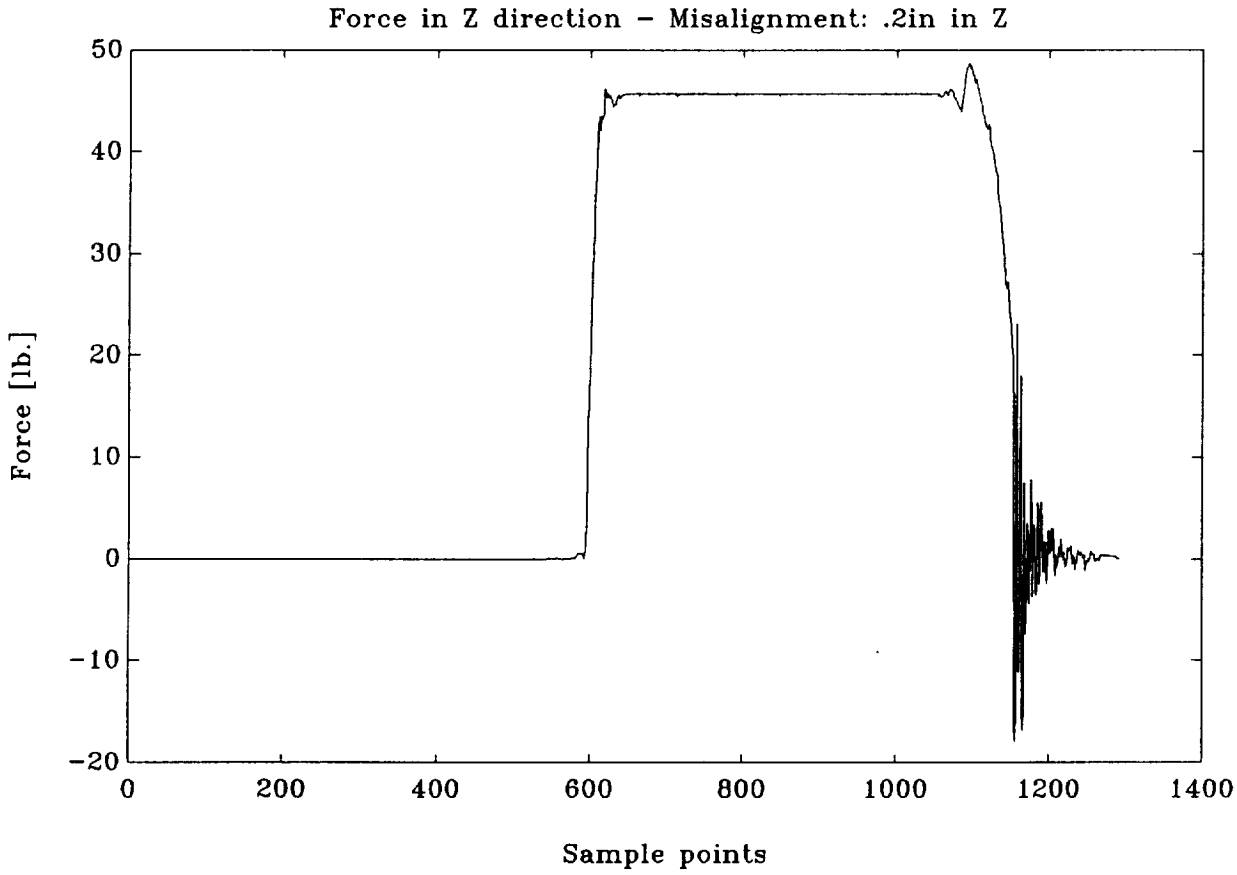

Figure 43

H-Interface
Force Time History
Translational Misalignment

Force (in lb) along the Z-axis
for 0.30 inches misalignment along the Z-axis

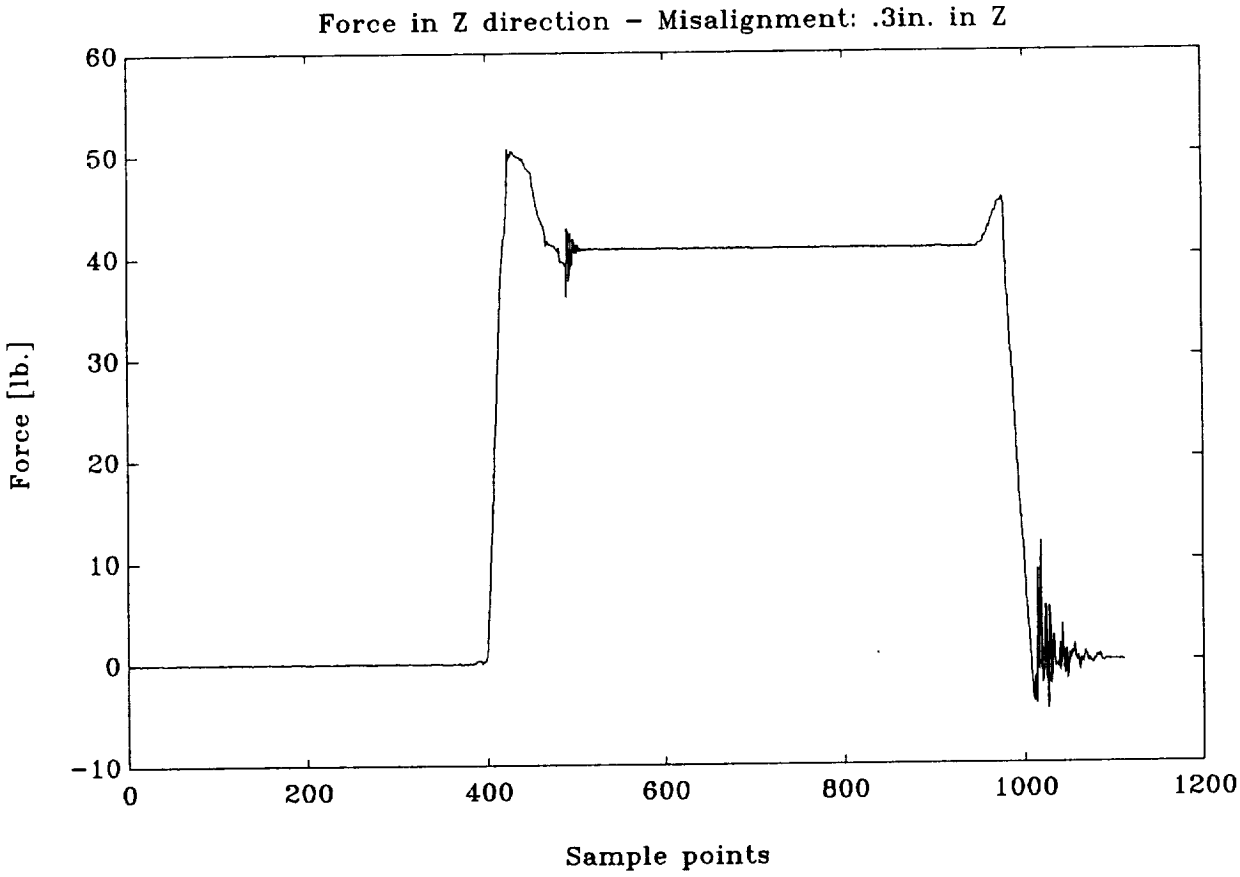

Figure 44

H-Interface
Rotational Misalignment

Maximum mating force (in lb) along the X-axis
versus misalignment degrees about the X-axis

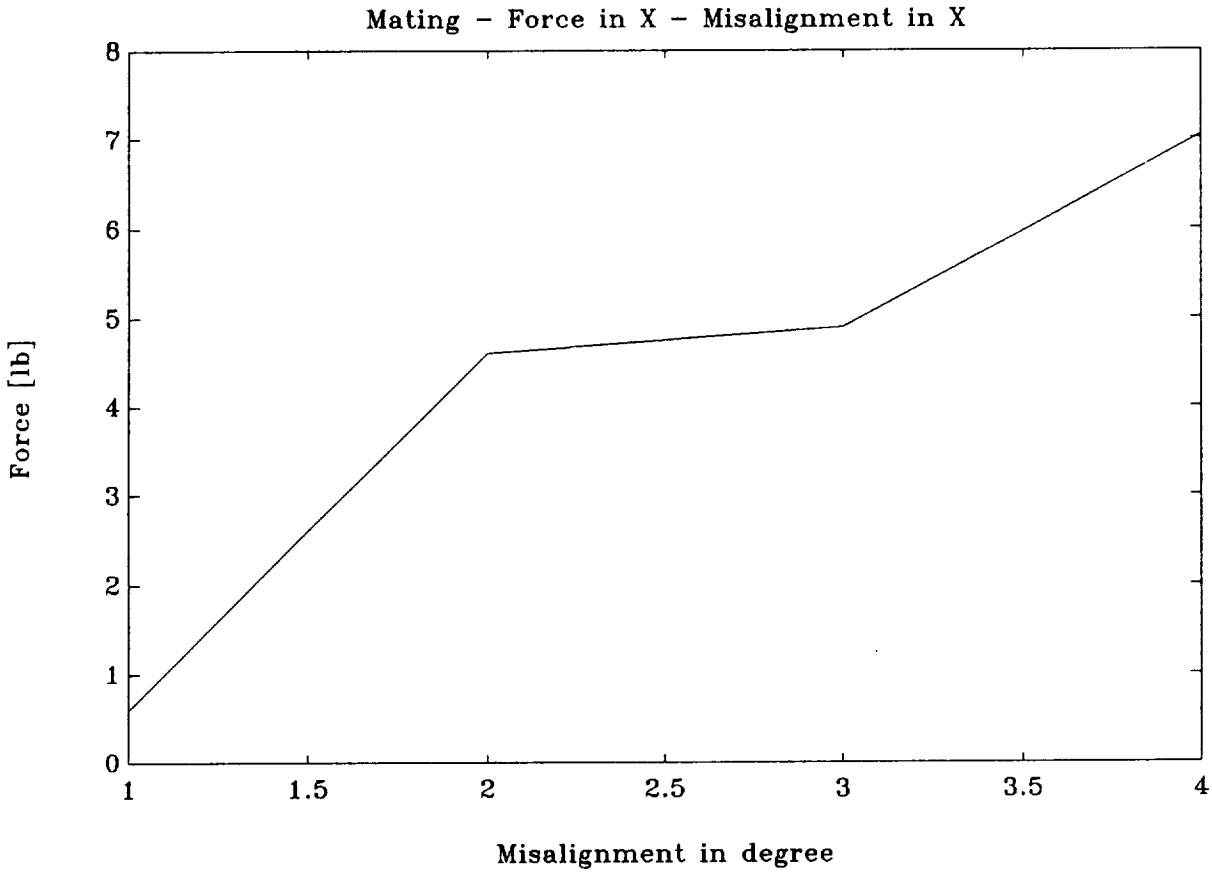

Figure 45

H-Interface
Rotational Misalignment

Maximum mating force (in lb) along the Y-axis
versus misalignment degrees about the X-axis

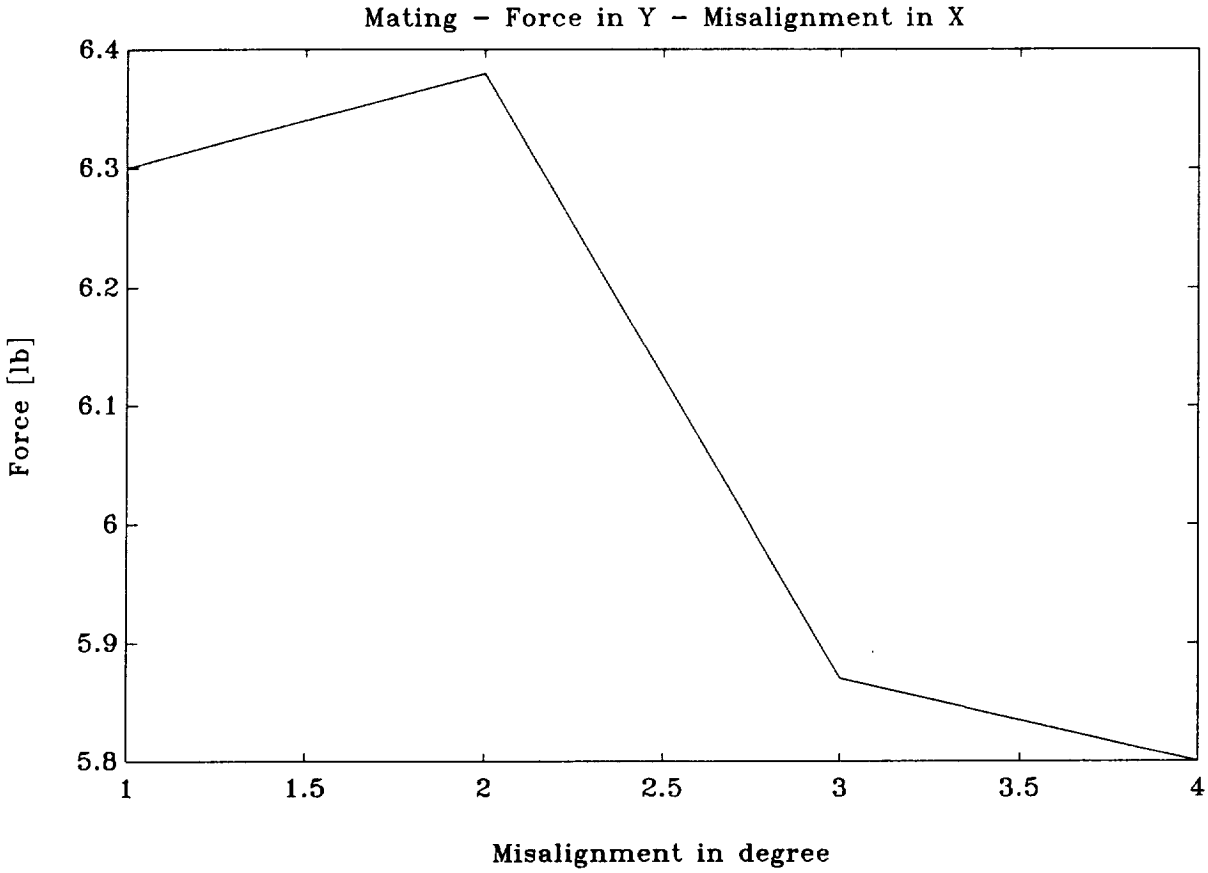

Figure 46

H-Interface
Rotational Misalignment

Maximum mating force (in lb) along the Z-axis
versus misalignment degrees about the X-axis

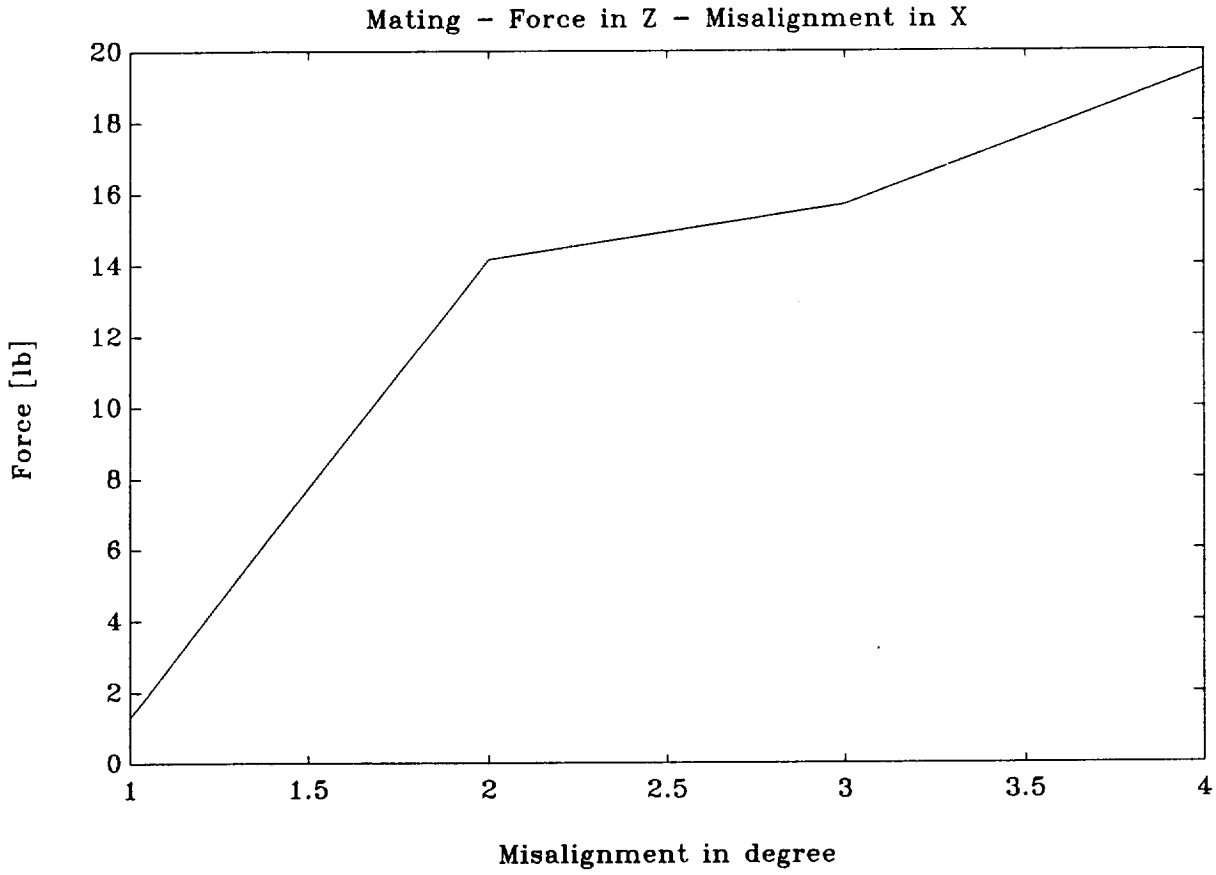

Figure 47

H-Interface
Rotational Misalignment

Maximum demating force (in lb) along the X-axis
versus misalignment degrees about the X-axis

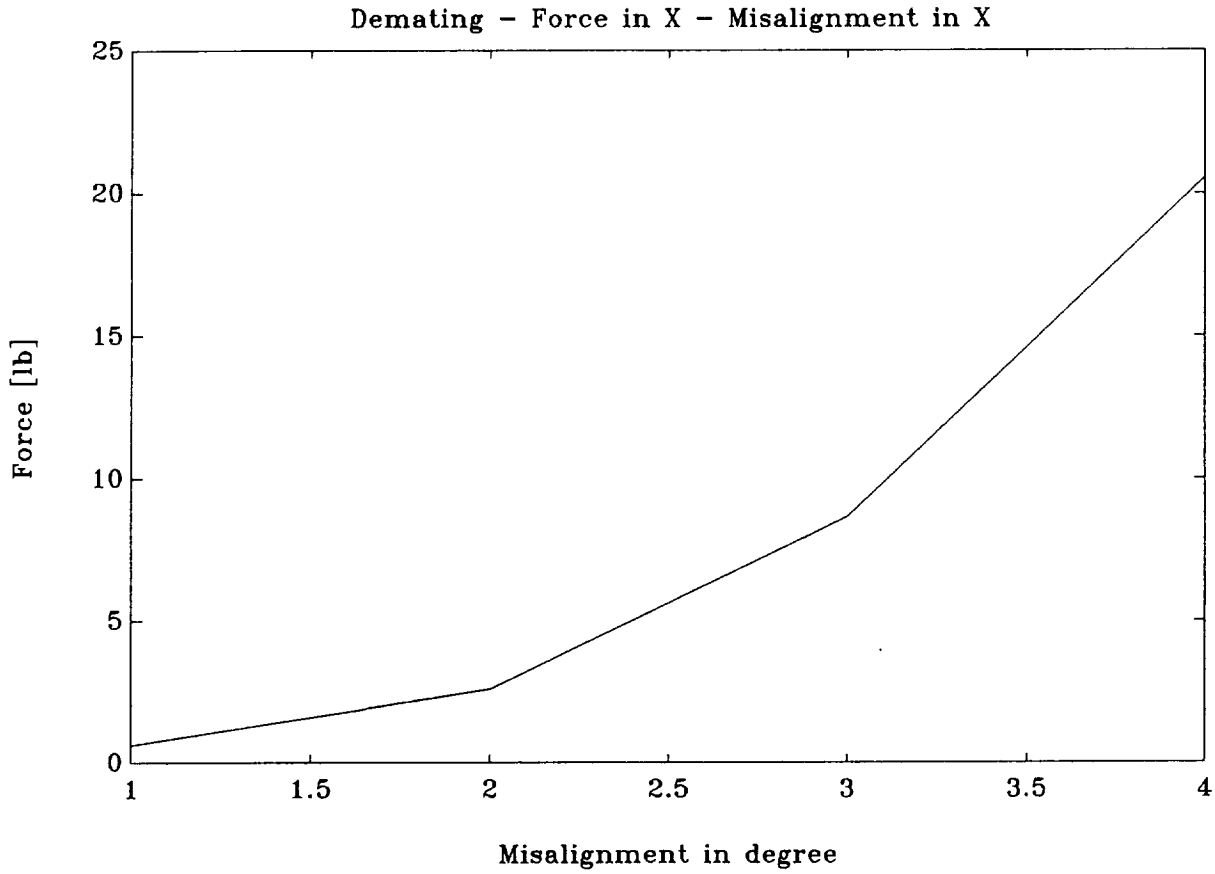

Figure 48

H-Interface
Rotational Misalignment

Maximum demating force (in lb) along the Y-axis
versus misalignment degrees about the X-axis

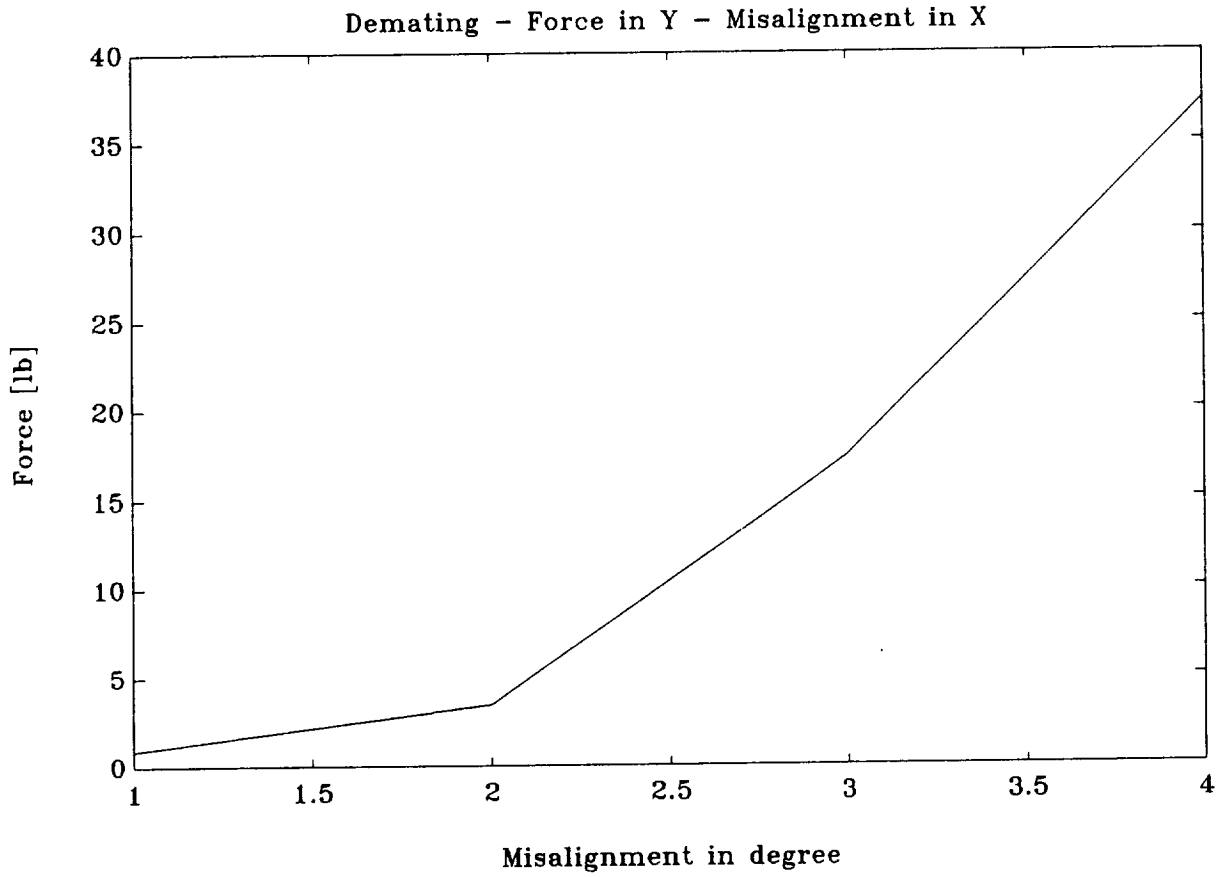

Figure 49

H-Interface
Rotational Misalignment

Maximum demating force (in lb) along the Z-axis
versus misalignment degrees about the X-axis

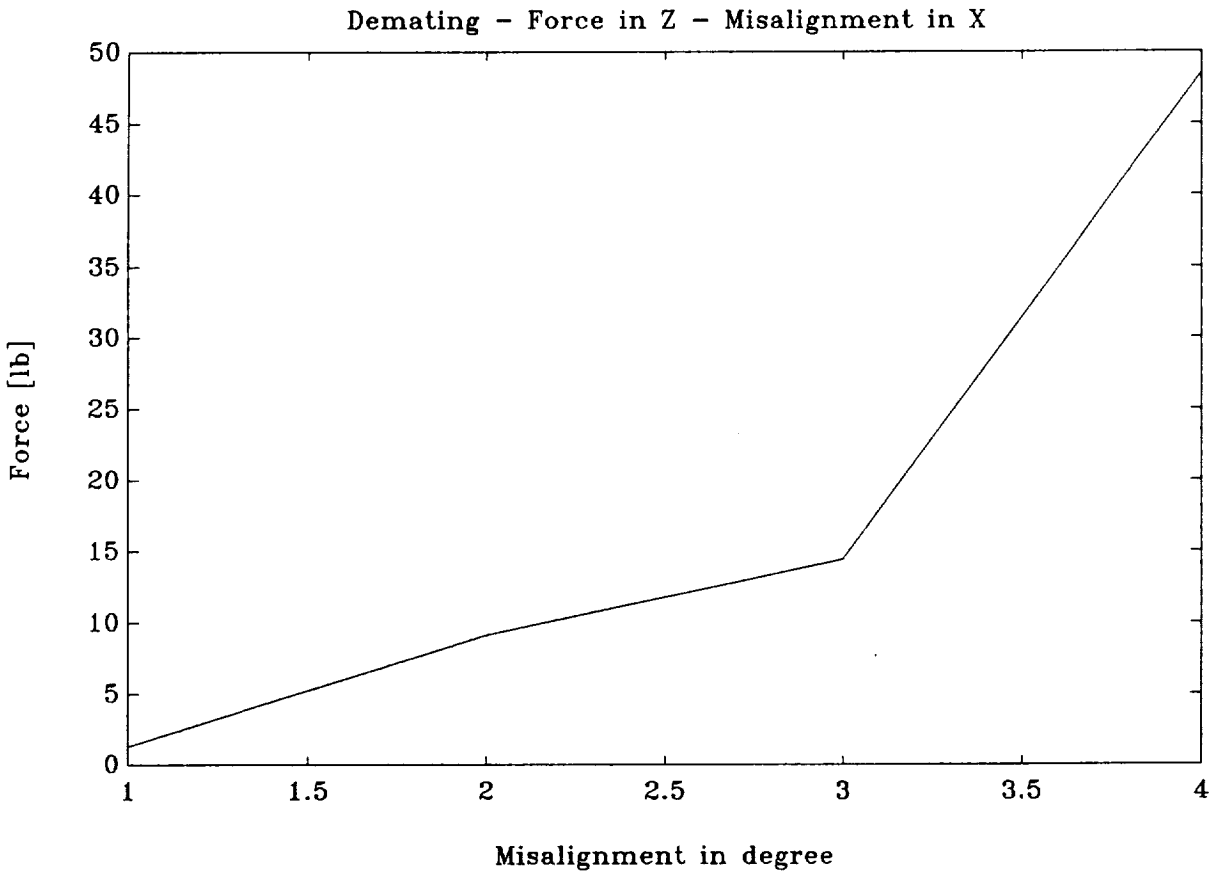

Figure 50

H-Interface
Rotational Misalignment

Maximum mating force (in lb) along the X-axis
versus misalignment degrees about the Z-axis

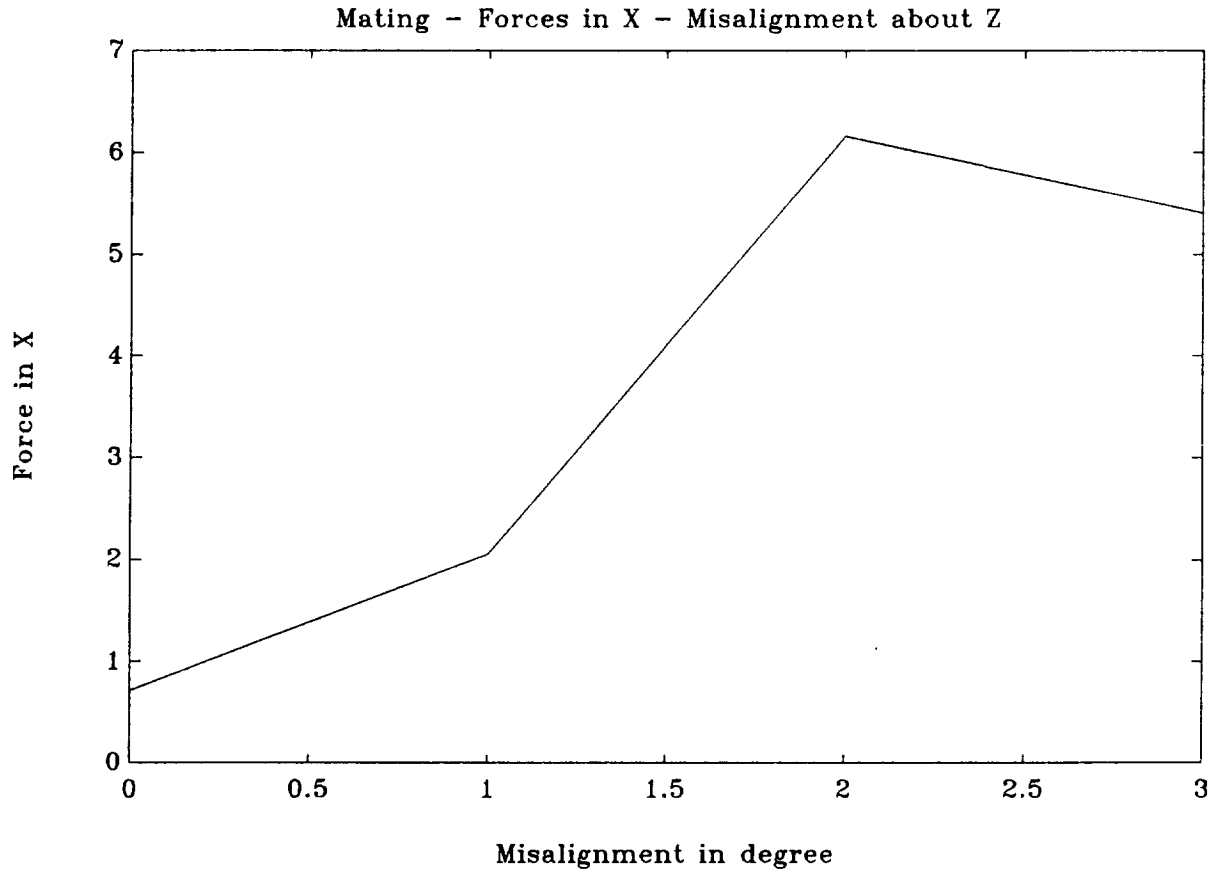

Figure 51

H-Interface
Rotational Misalignment

Maximum mating force (in lb) along the Y-axis
versus misalignment degrees about the Z-axis

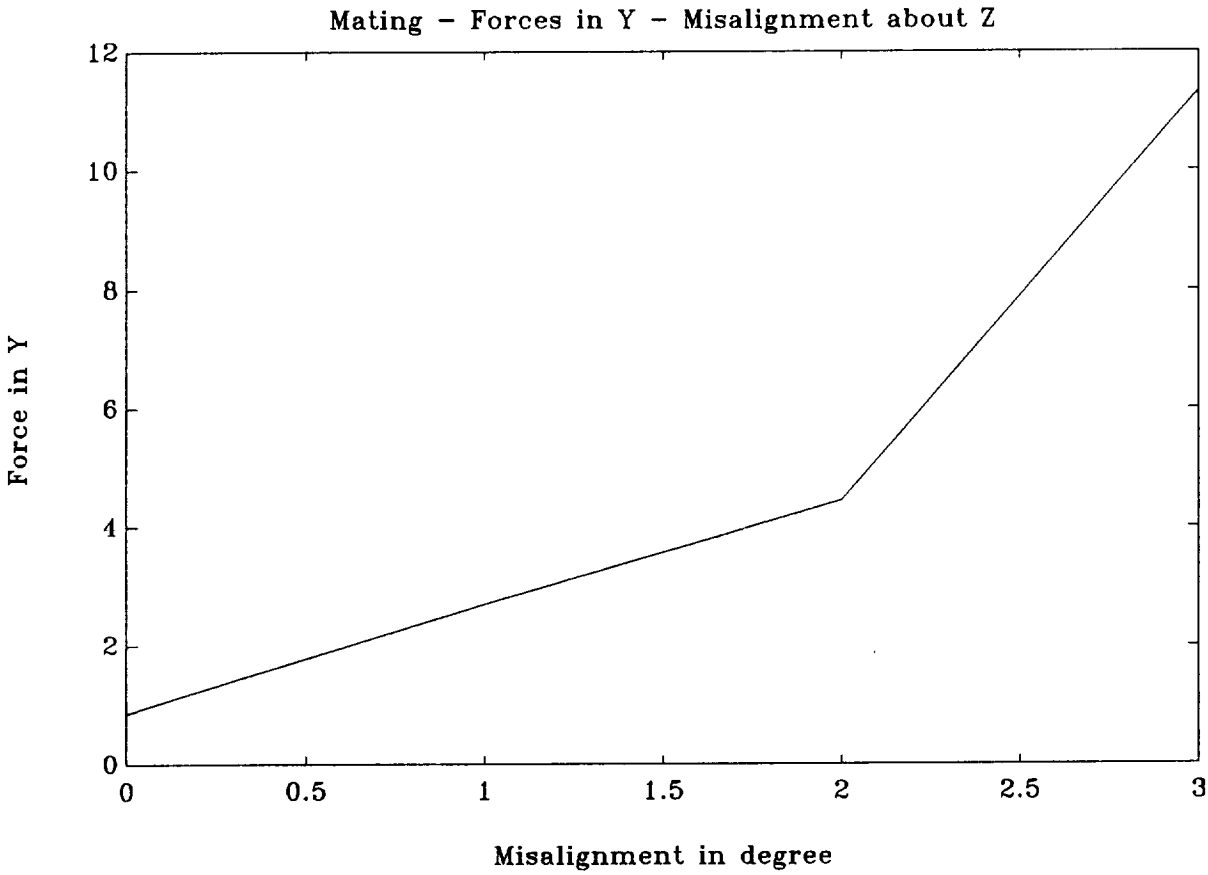

Figure 52

H-Interface
Rotational Misalignment

Maximum mating force (in lb) along the Z-axis
versus misalignment degrees about the Z-axis

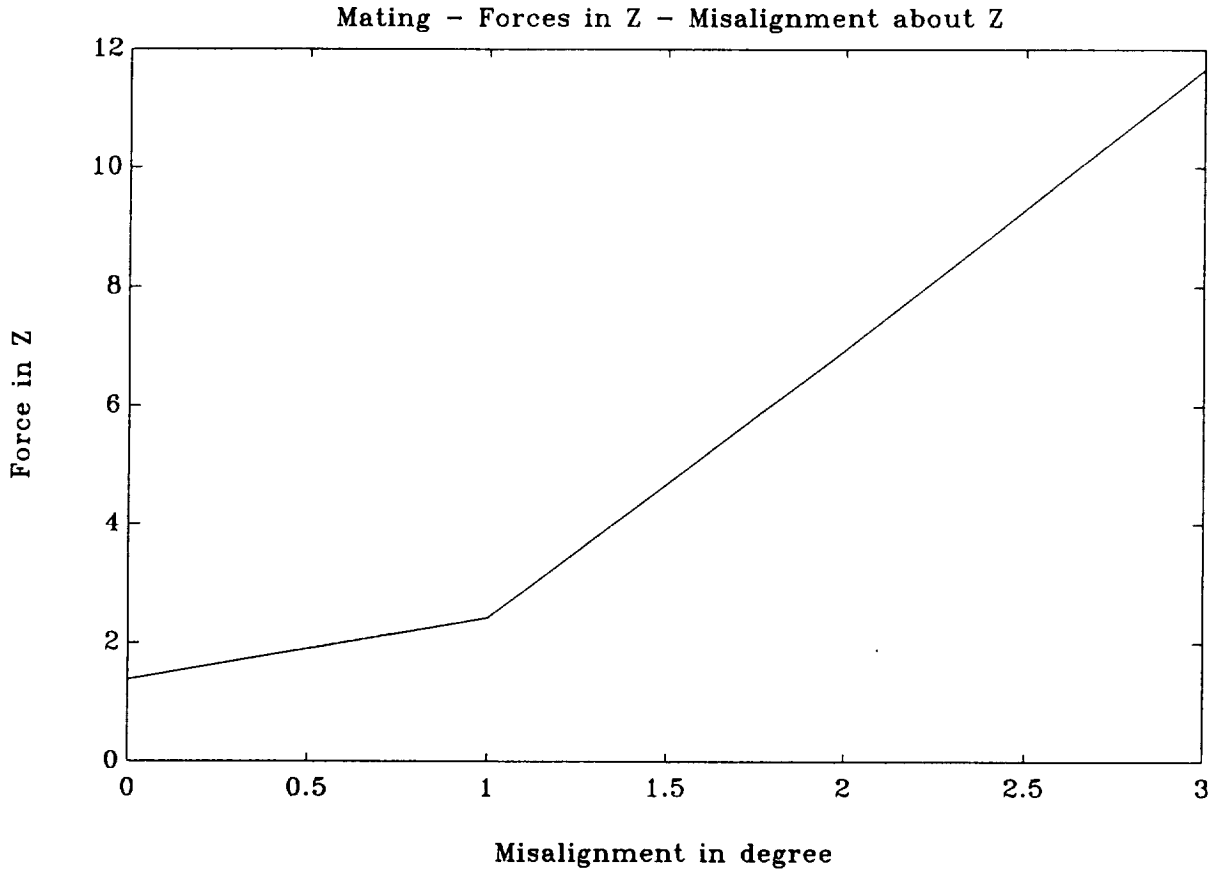

Figure 53

H-Interface
Rotational Misalignment

Maximum demating force (in lb) along the X-axis
versus misalignment degrees about the Z-axis

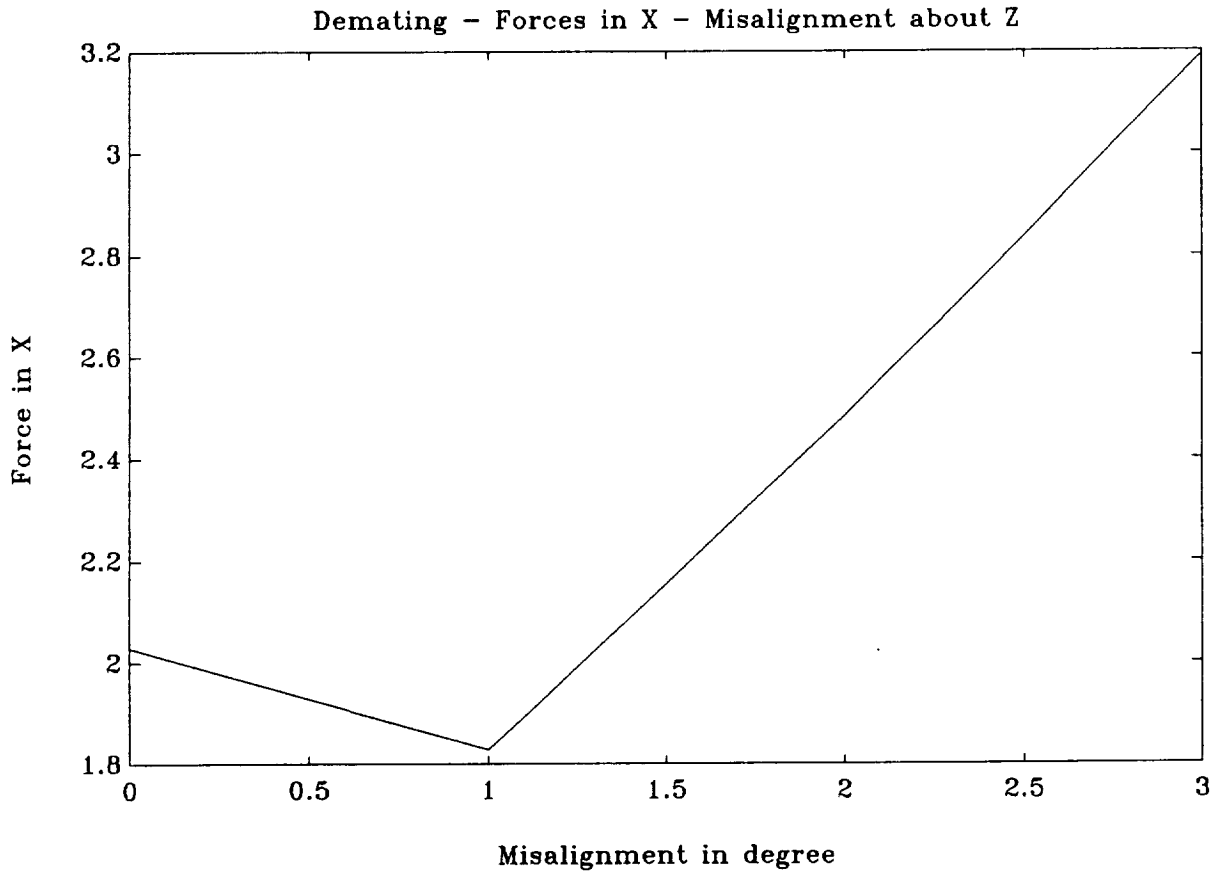

Figure 54

H-Interface
Rotational Misalignment

Maximum demating force (in lb) along the Y-axis
versus misalignment degrees about the Z-axis

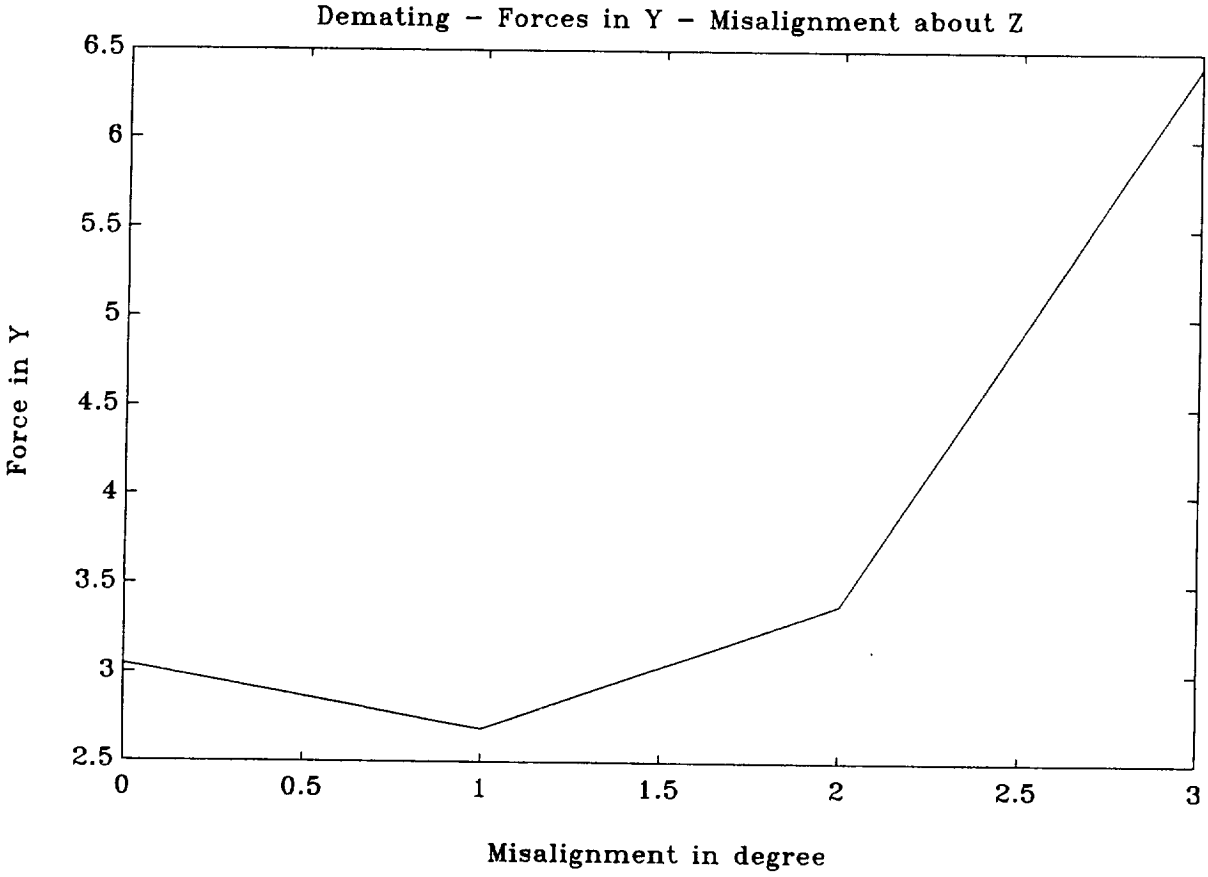

Figure 55

H-Interface
Rotational Misalignment

Maximum demating force (in lb) along the Z-axis
versus misalignment degrees about the Z-axis

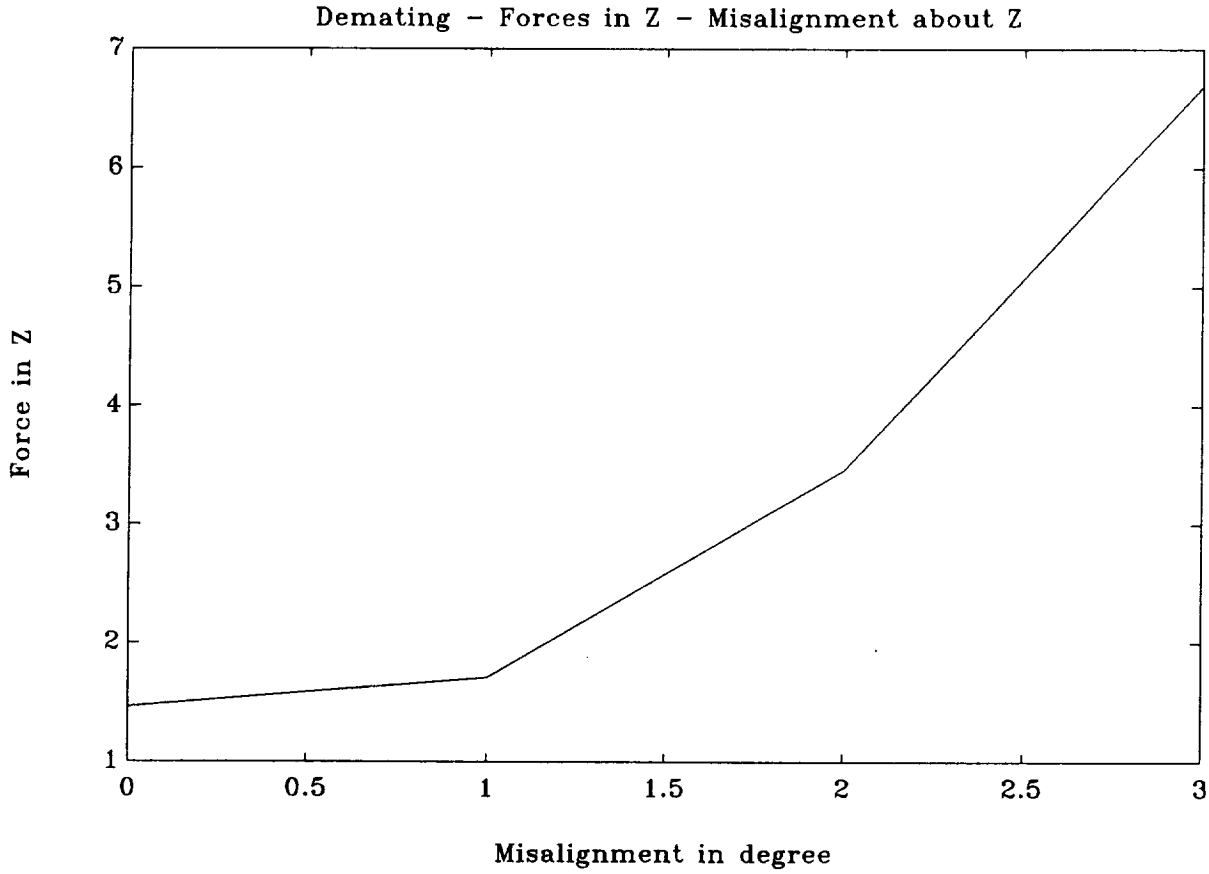

Figure 56

H-Interface
Translational Misalignment

Maximum mating force (in lb) along the X-axis
versus misalignment (in inches) in the Y-axis

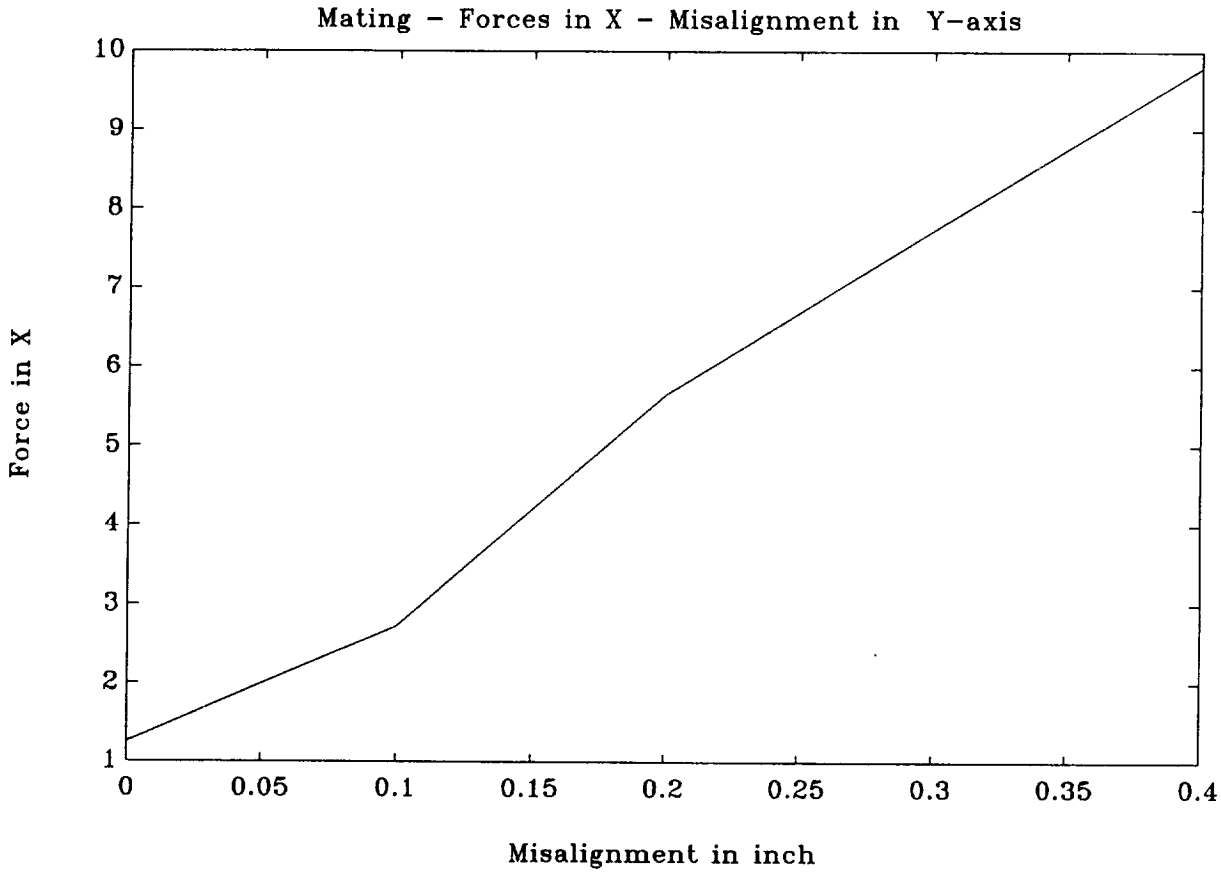

Figure 57

H-Interface
Translational Misalignment

Maximum mating force (in lb) along the Y-axis
versus misalignment (in inches) in the Y-axis

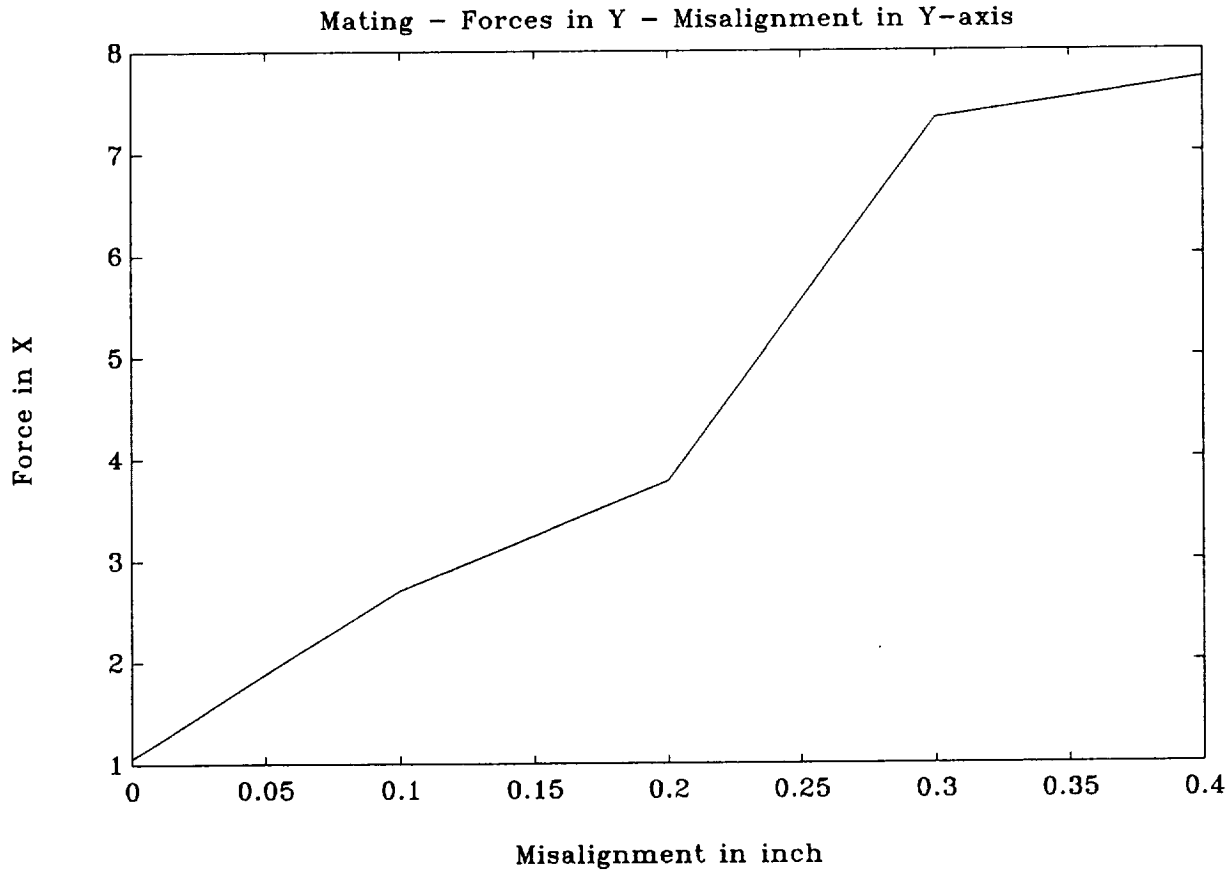

Figure 58

H-Interface
Translational Misalignment

Maximum mating force (in lb) along the Z-axis
versus misalignment (in inches) in the Y-axis

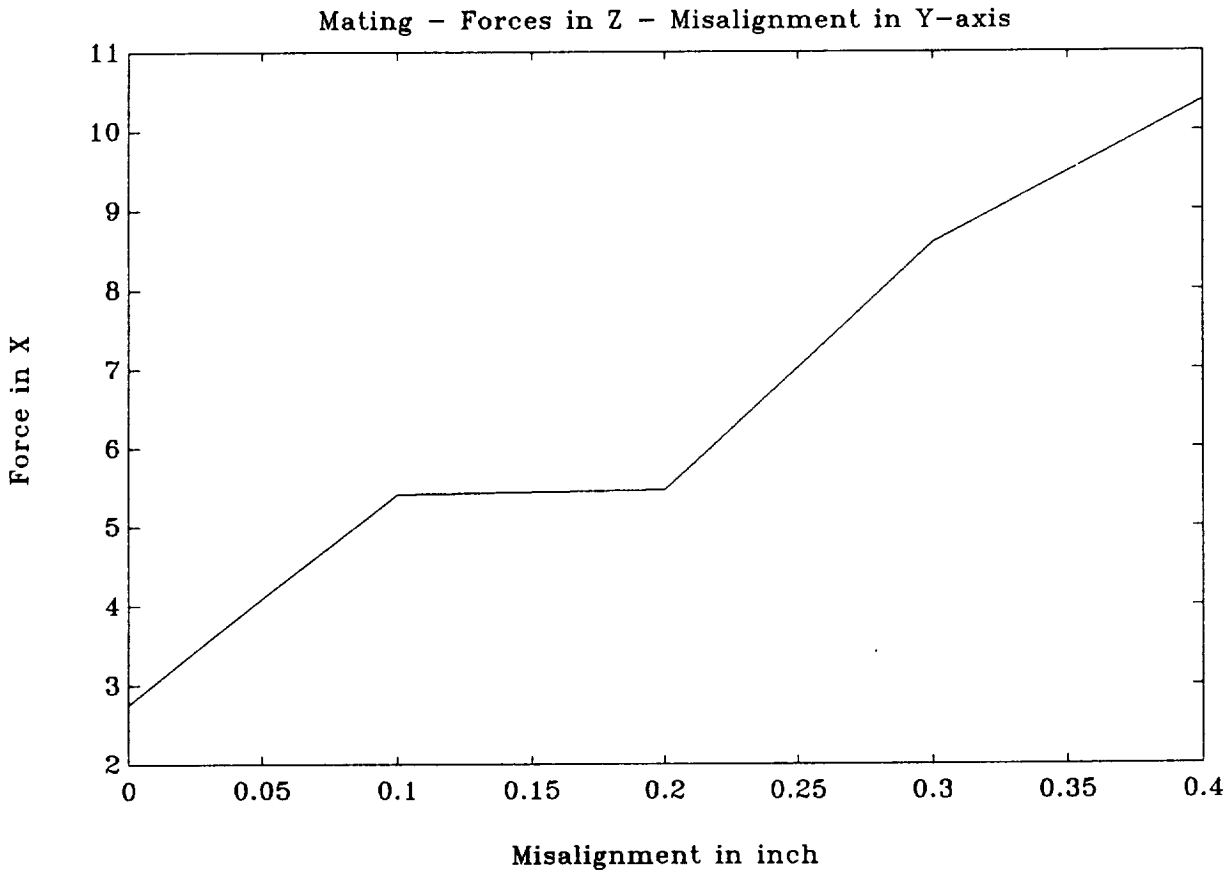

Figure 59

H-Interface
Translational Misalignment

Maximum demating force (in lb) along the X-axis
versus misalignment (in inches) in the Y-axis

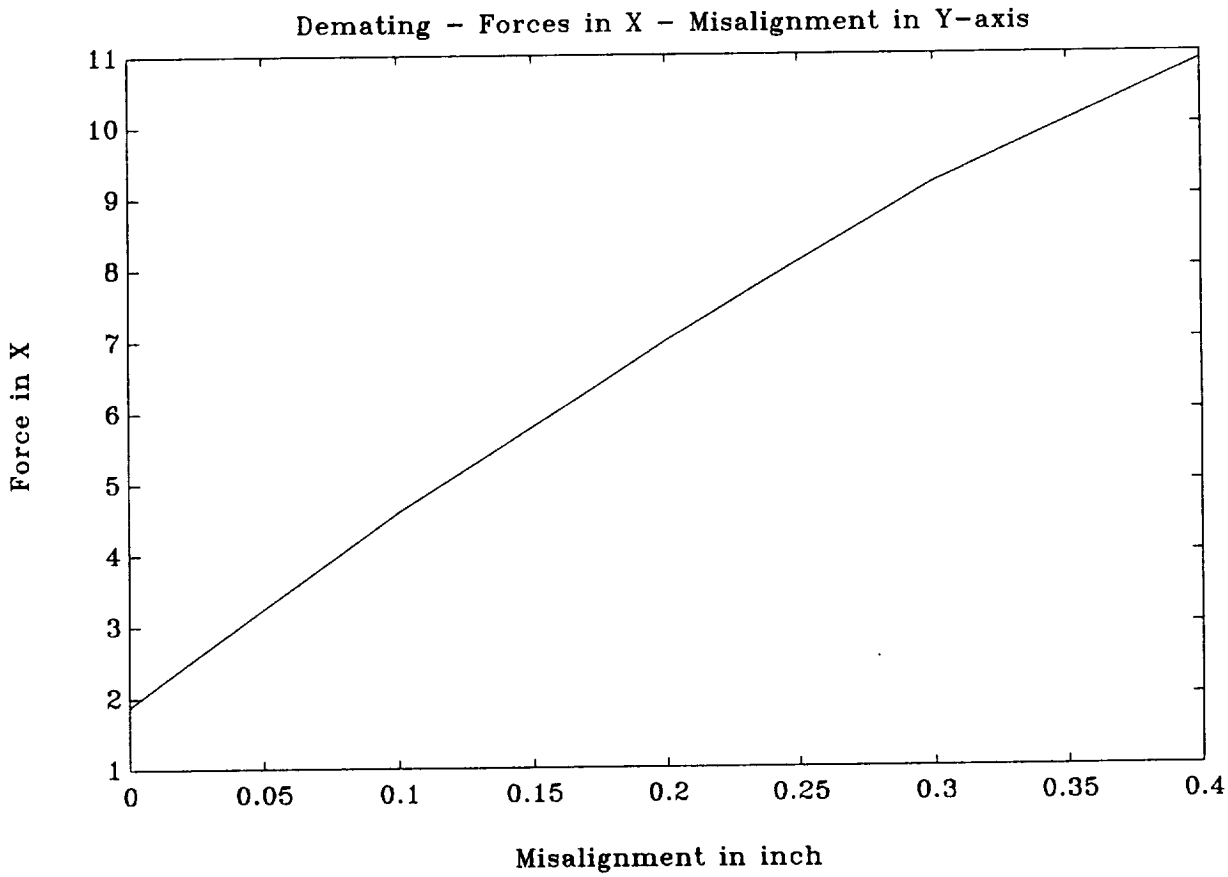

Figure 60

H-Interface
Translational Misalignment

Maximum demating force (in lb) along the Y-axis
versus misalignment (in inches) in the Y-axis

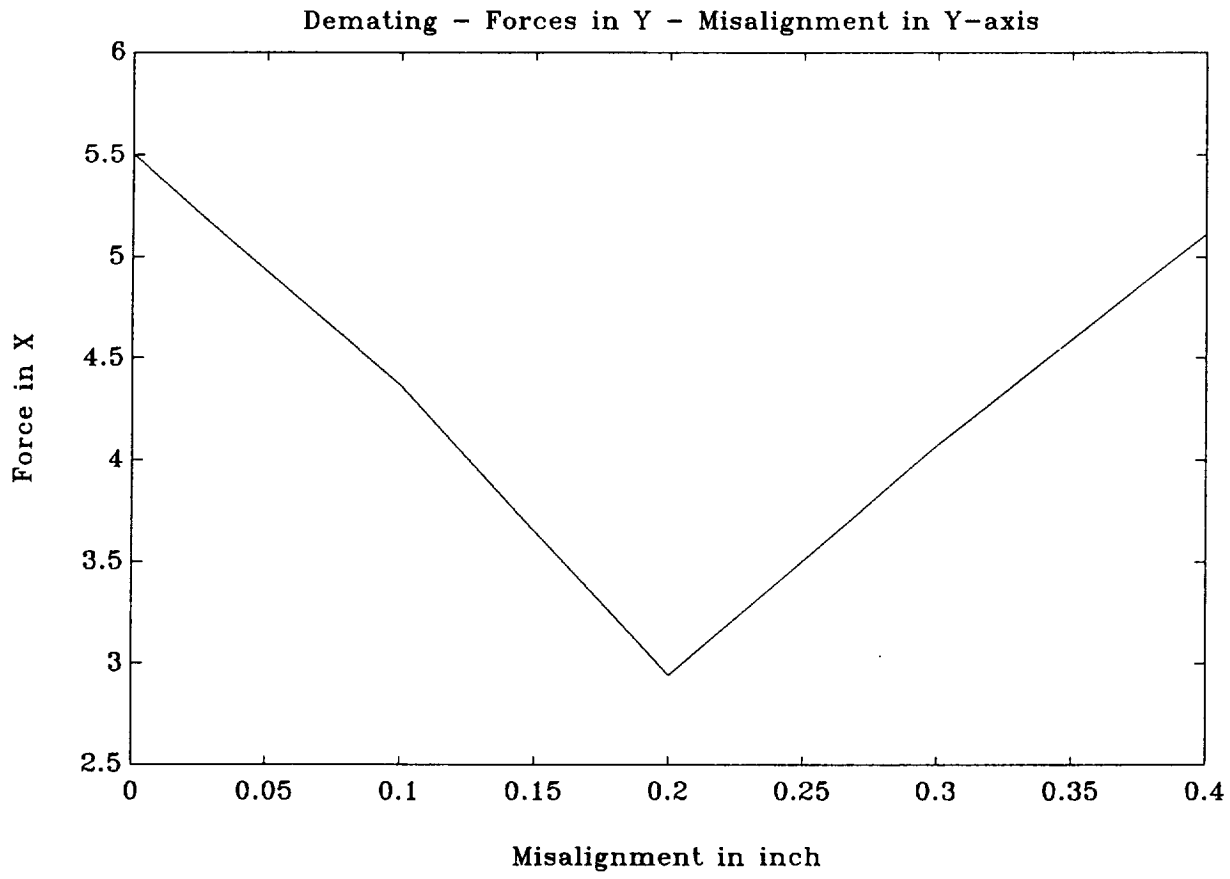

Figure 61

H-Interface
Translational Misalignment

Maximum demating force (in lb) along the Z-axis
versus misalignment (in inches) in the Y-axis

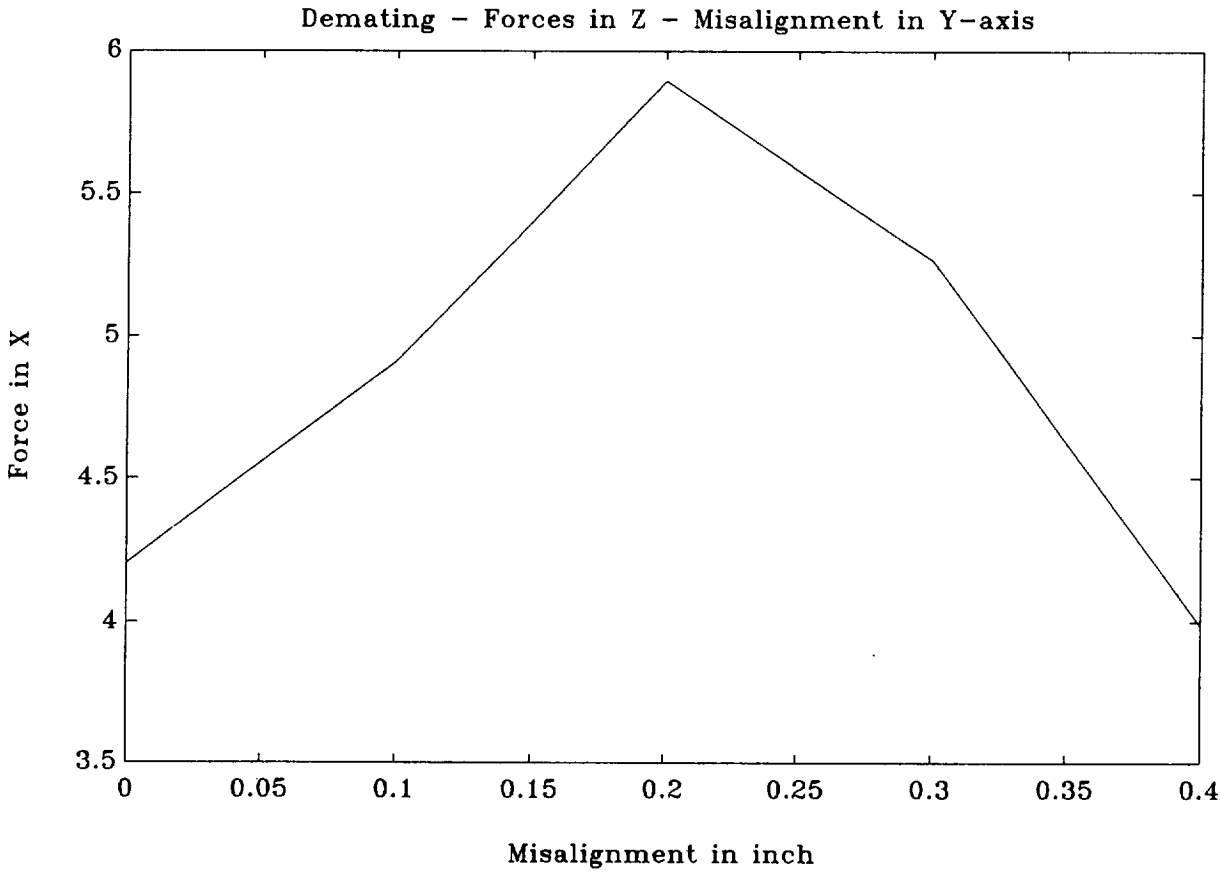

Figure 62

H-Interface
Translational Misalignment

Maximum mating force (in lb) along the X-axis
versus misalignment (in inches) in the Z-axis

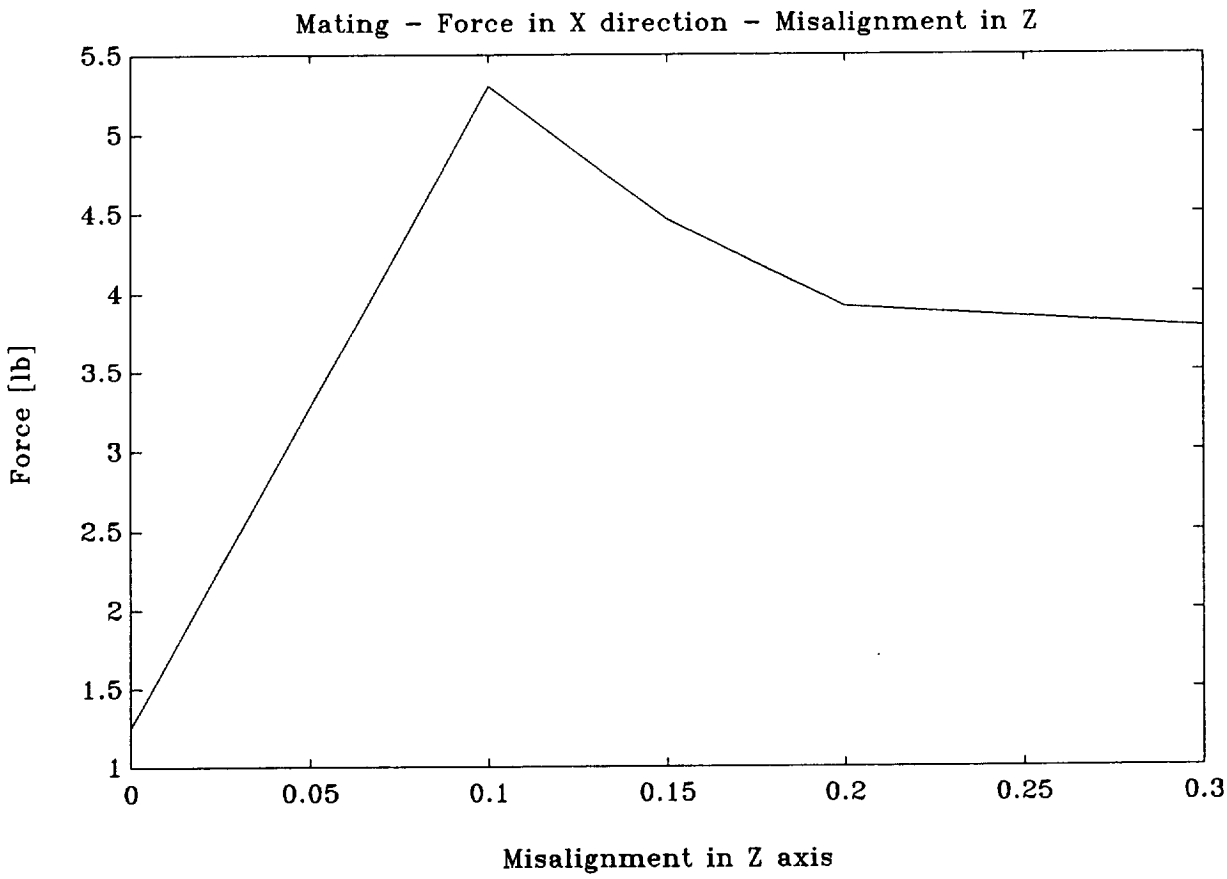

Figure 63

H-Interface
Translational Misalignment

Maximum mating force (in lb) along the Y-axis
versus misalignment (in inches) in the Z-axis

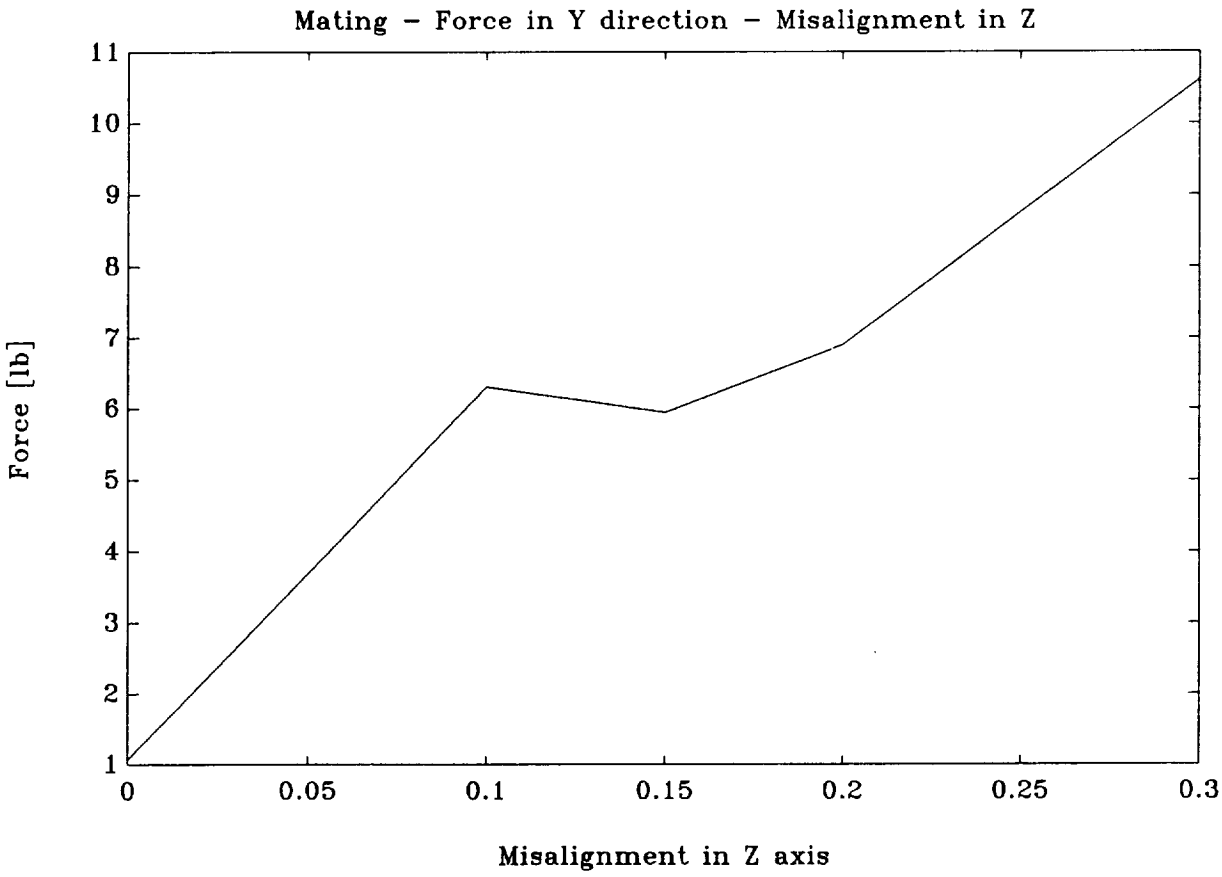

Figure 64

H-Interface
Translational Misalignment

Maximum mating force (in lb) along the Z-axis
versus misalignment (in inches) in the Z-axis

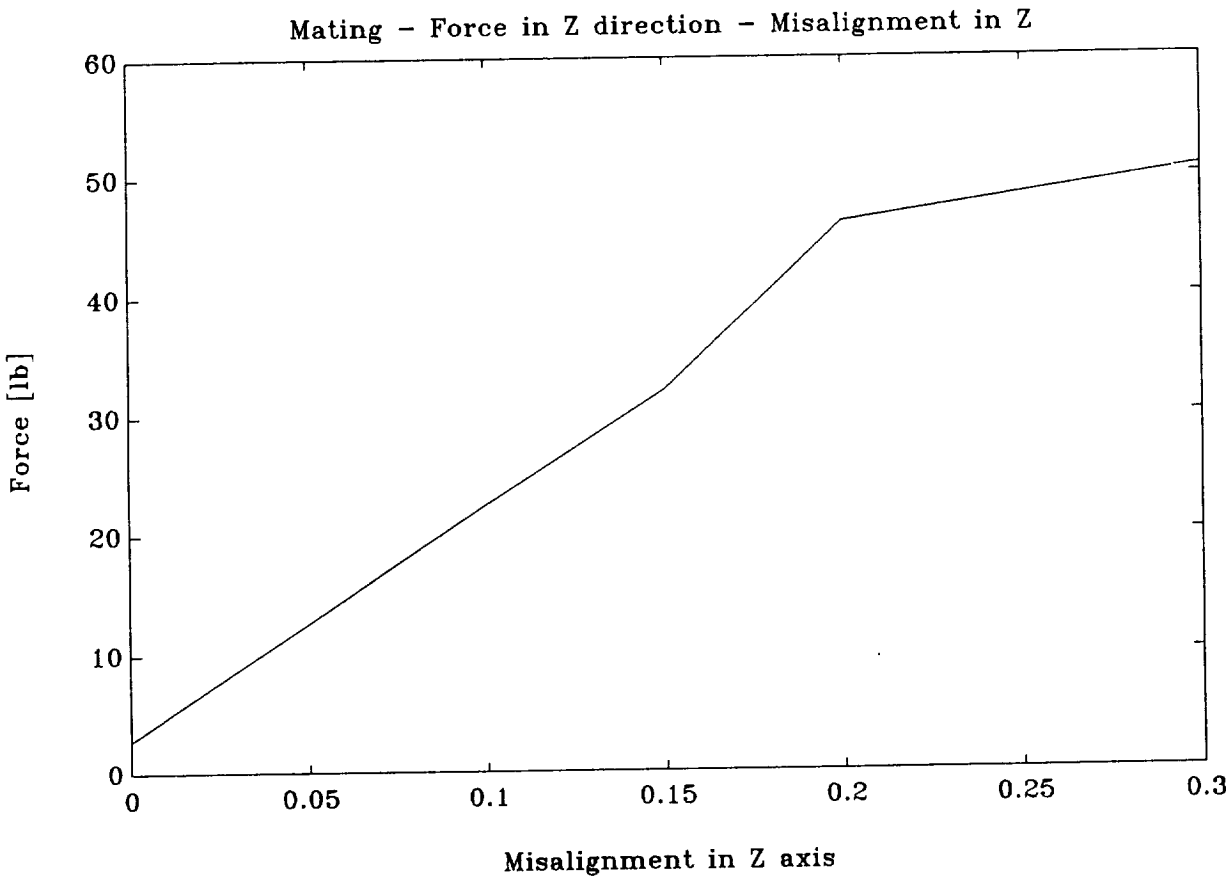

Figure 65

H-Interface
Translational Misalignment

Maximum demating force (in lb) along the X-axis
versus misalignment (in inches) in the Z-axis

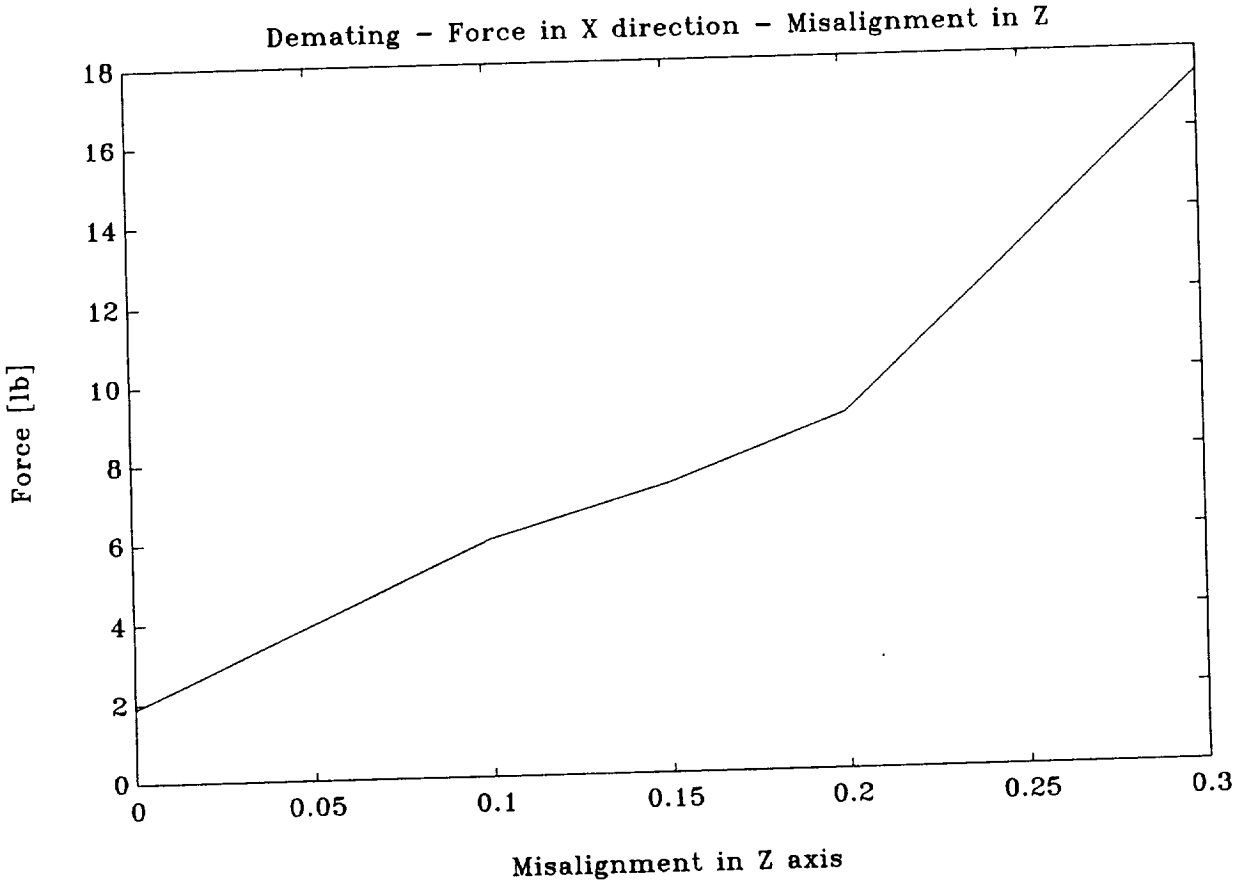

Figure 66

H-Interface
Translational Misalignment

Maximum demating force (in lb) along the Y-axis
versus misalignment (in inches) in the Z-axis

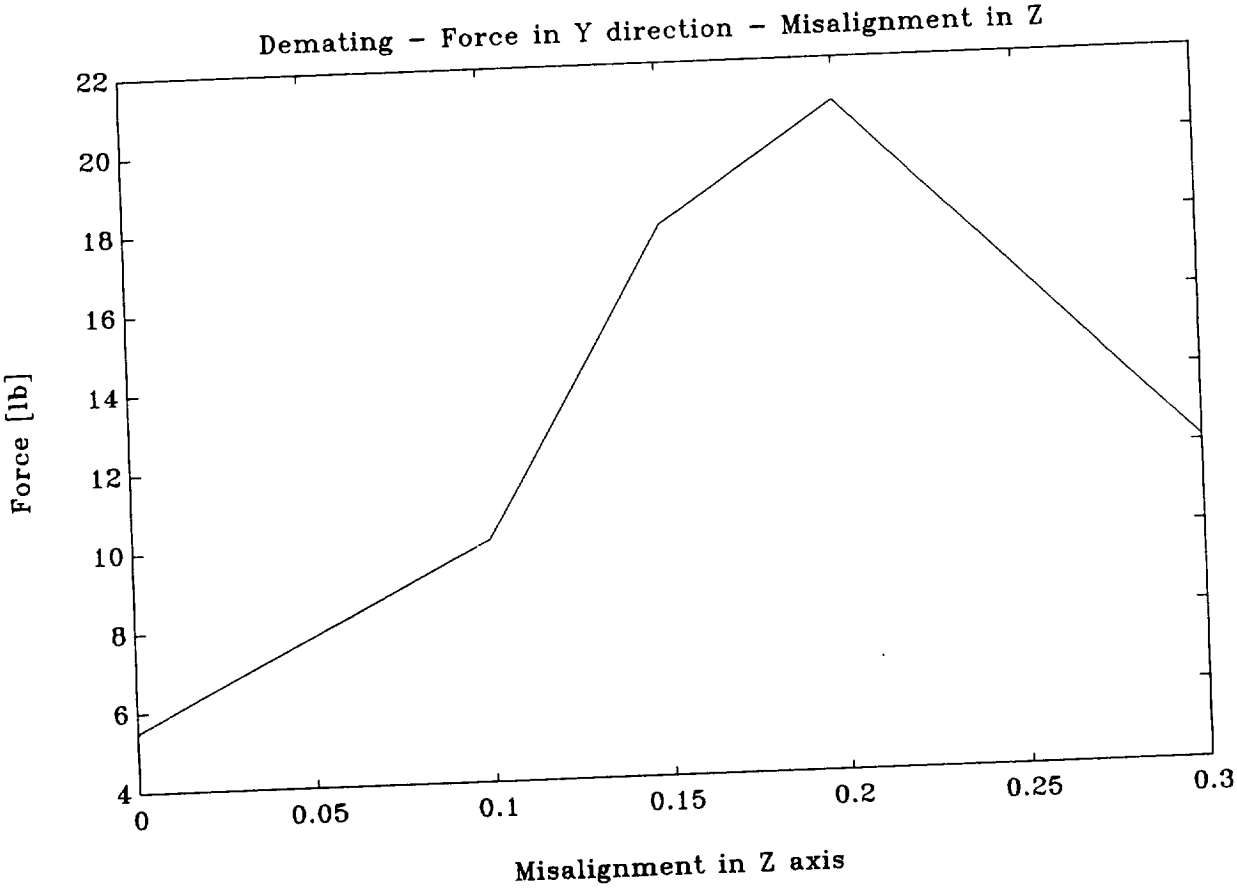

Figure 67

H-Interface
Translational Misalignment

Maximum demating force (in lb) along the Z-axis
versus misalignment (in inches) in the Z-axis

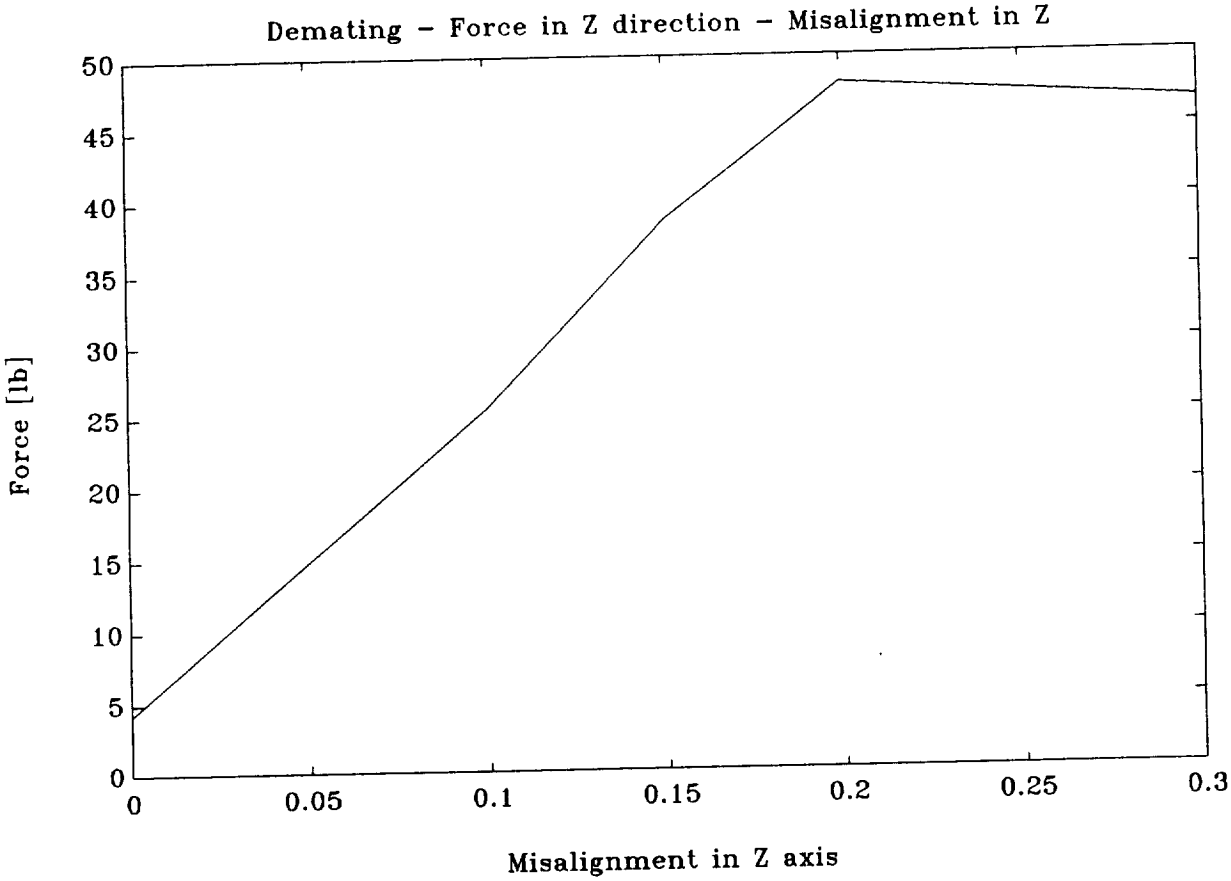

Figure 68

Square-Interface
Force Time History
Translational Misalignment

Force (in lb) along the X-axis
for 0.1 inches misalignment along the Y-axis

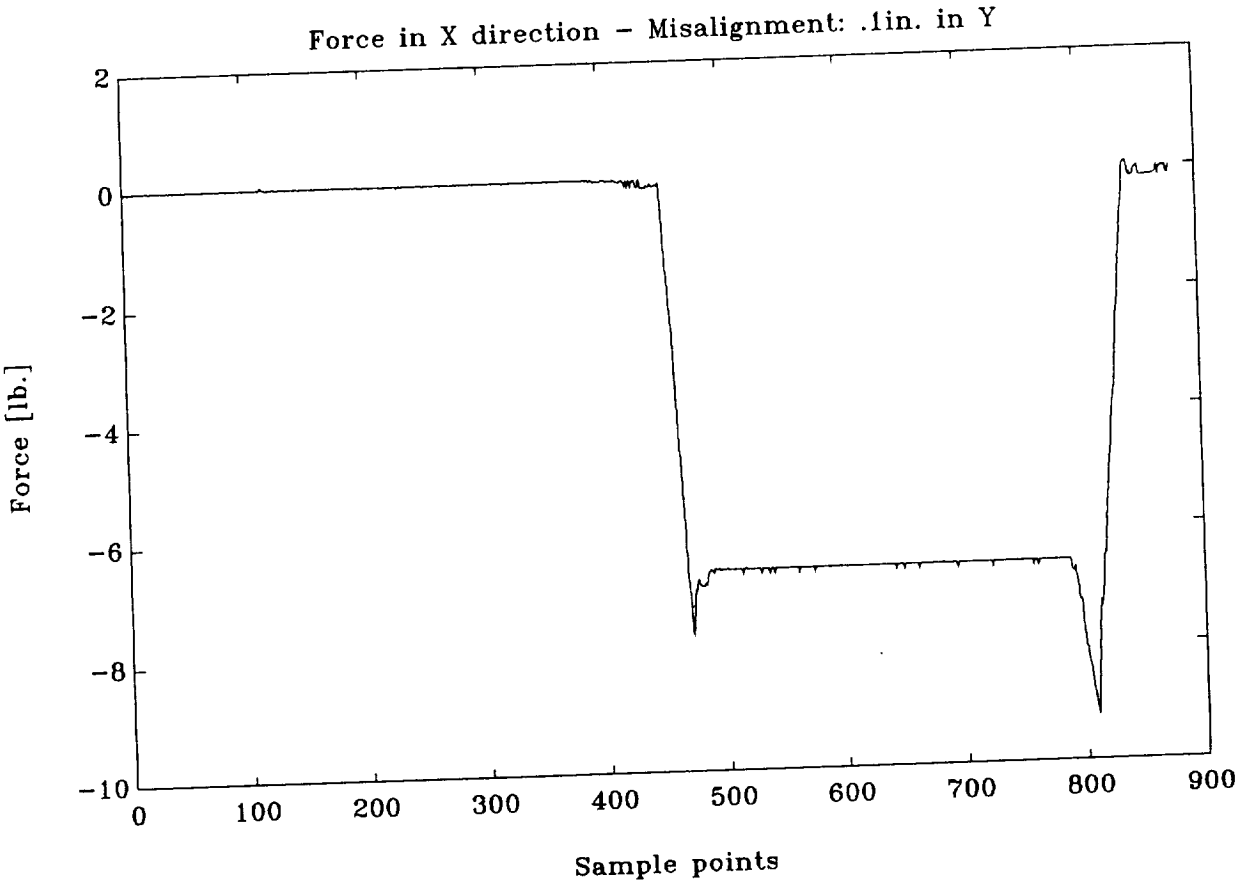

Figure 69

Square-Interface
Force Time History
Translational Misalignment

Force (in lb) along the X-axis
for 0.2 inches misalignment along the Y-axis

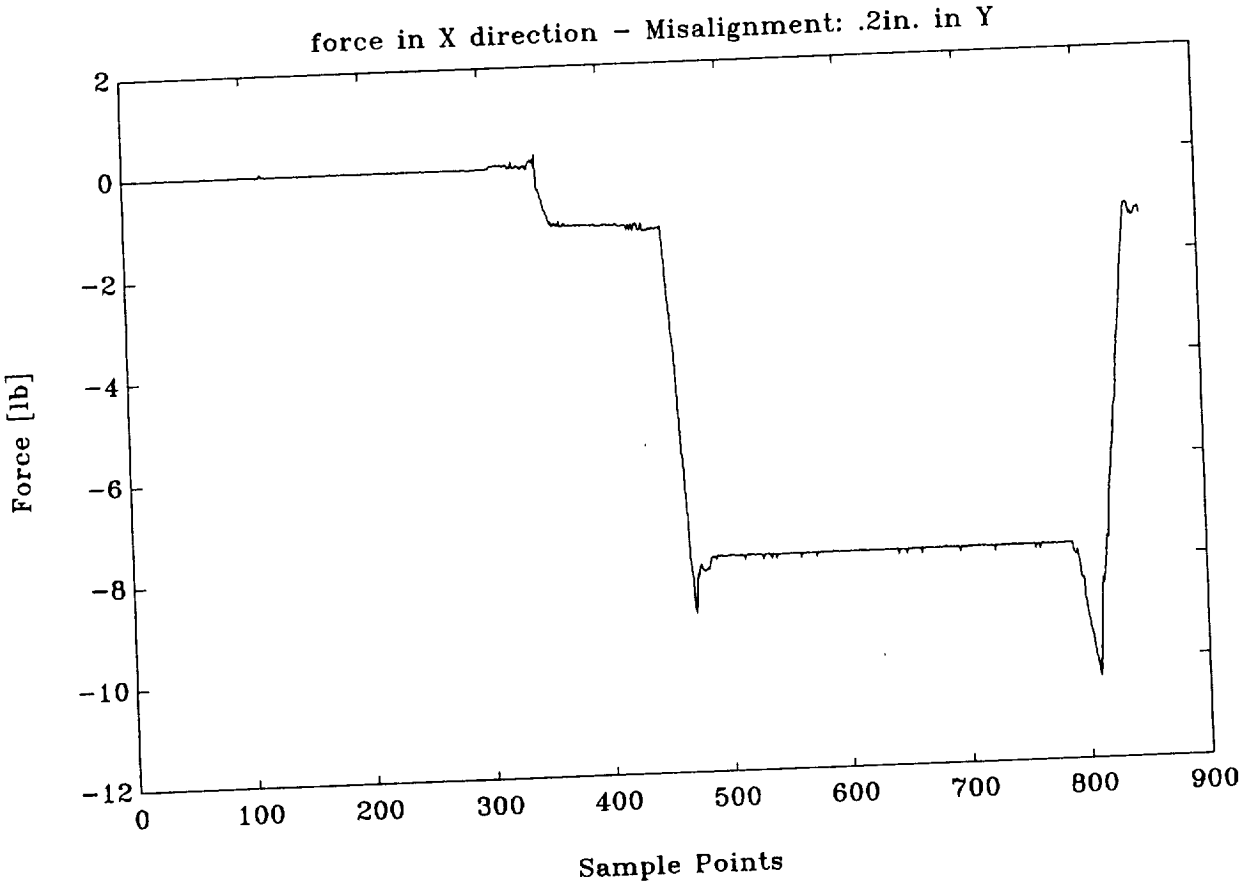

Figure 70

Square-Interface
Force Time History
Translational Misalignment

Force (in lb) along the Y-axis
for 0.1 inches misalignment along the Y-axis

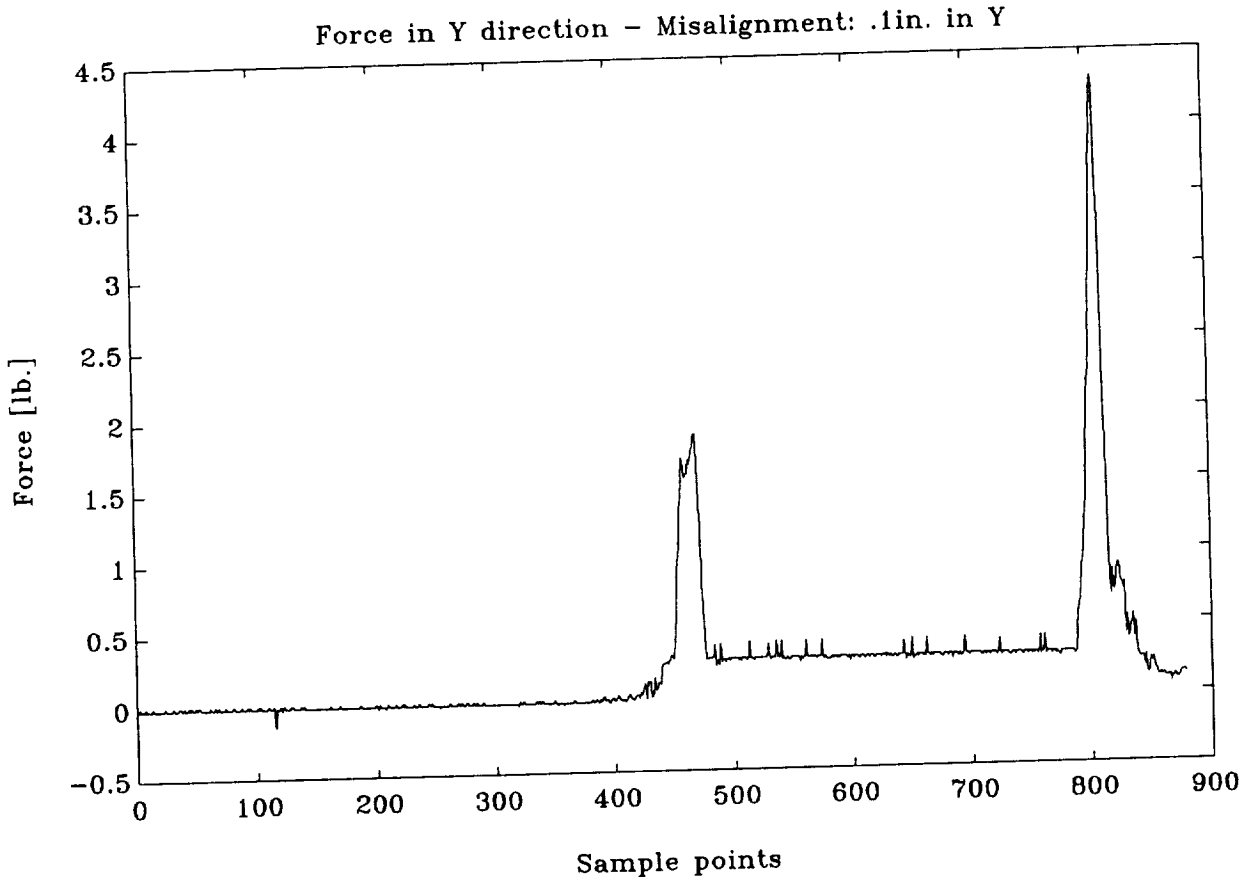

Figure 71

Square-Interface
Force Time History
Translational Misalignment

Force (in lb) along the Y-axis
for 0.2 inches misalignment along the Y-axis

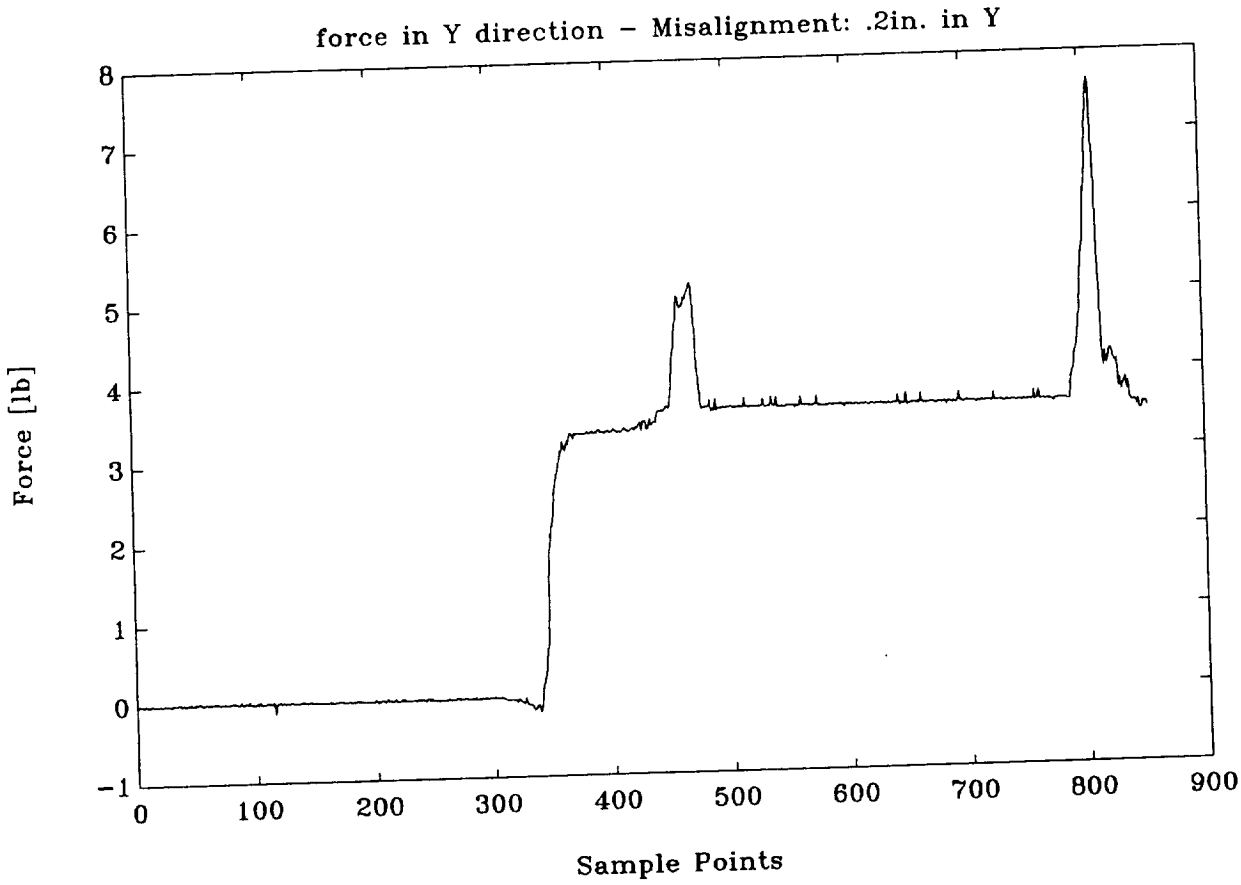

Figure 72

Square-Interface
Force Time History
Translational Misalignment

Force (in lb) along the Z-axis
for 0.1 inches misalignment along the Y-axis

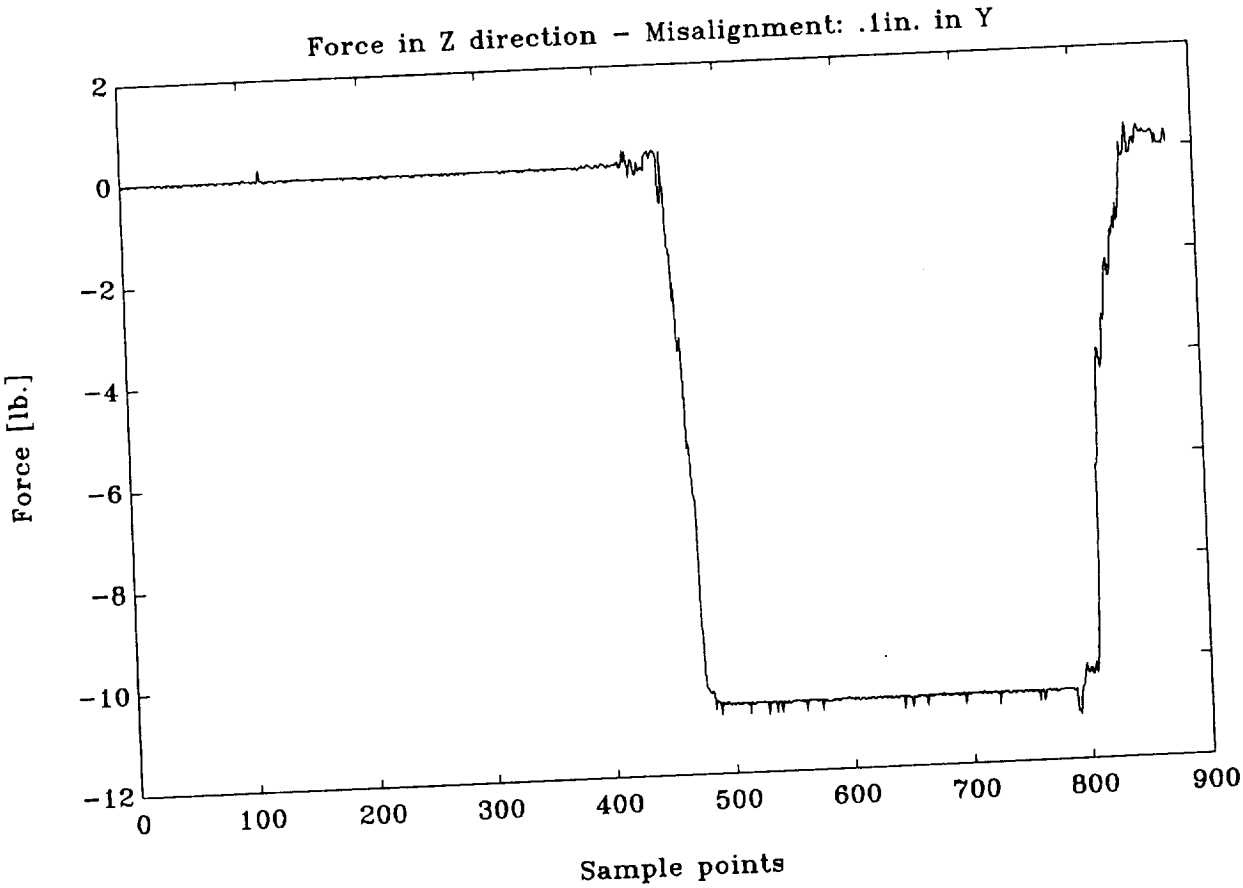

Figure 73

Square-Interface
Force Time History
Translational Misalignment

Force (in lb) along the Z-axis
for 0.2 inches misalignment along the Y-axis

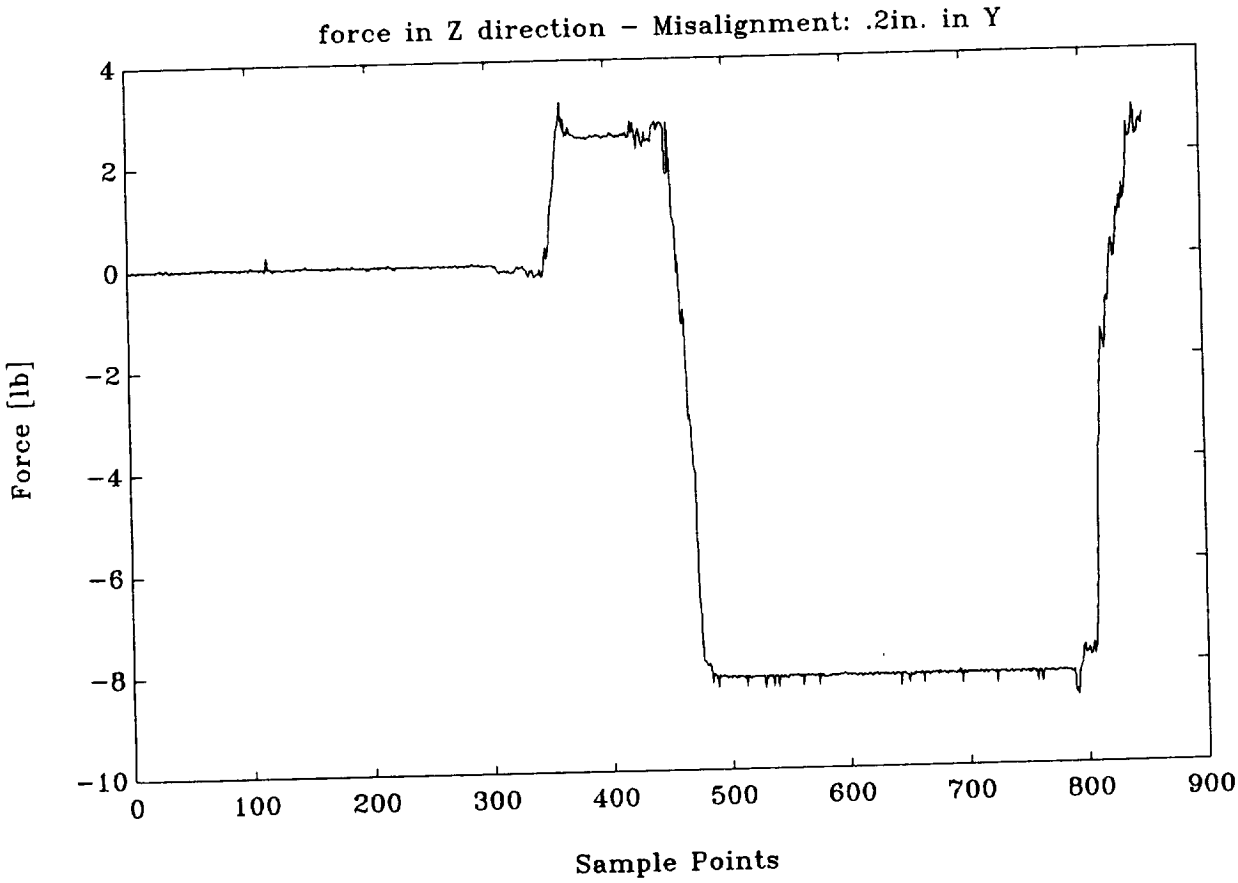

Figure 74